저작자표시-비영리-변경금지 2.0 대한민국

이용자는 아래의 조건을 따르는 경우에 한하여 자유롭게

- 이 저작물을 복제, 배포, 전송, 전시, 공연 및 방송할 수 있습니다.

다음과 같은 조건을 따라야 합니다:

저작자표시. 귀하는 원저작자를 표시하여야 합니다.

비영리. 귀하는 이 저작물을 영리 목적으로 이용할 수 없습니다.

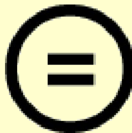
변경금지. 귀하는 이 저작물을 개작, 변형 또는 가공할 수 없습니다.

- 귀하는, 이 저작물의 재이용이나 배포의 경우, 이 저작물에 적용된 이용허락조건을 명확하게 나타내어야 합니다.
- 저작권자로부터 별도의 허가를 받으면 이러한 조건들은 적용되지 않습니다.

저작권법에 따른 이용자의 권리는 위의 내용에 의하여 영향을 받지 않습니다.

이것은 이용허락규약(Legal Code)을 이해하기 쉽게 요약한 것입니다.

Disclaimer

dCollection

A DOCTOR DISSERTATION

Rh-Nb/Zr-Mo Interlayer Coating for First Mirror in Fusion Reactor

Rai Suresh

Department of Nuclear and Energy Engineering
Faculty of Applied Energy System
GRADUATE SCHOOL
JEJU NATIONAL UNIVERSITY
South Korea

제주대학교 중앙도서관
JEJU NATIONAL UNIVERSITY LIBRARY

A DOCTOR DISSERTATION

Rh-Nb/Zr-Mo Interlayer Coating for First Mirror in Fusion Reactor

Rai Suresh

Department of Nuclear and Energy Engineering
Faculty of Applied Energy System

GRADUATE SCHOOL
JEJU NATIONAL UNIVERSITY
South Korea

December, 2019

제주대학교 중앙도서관
JEJU NATIONAL UNIVERSITY LIBRARY

Rh-Nb/Zr-Mo Interlayer Coatings for First Mirror in Fusion Reactor

Rai Suresh

(Supervised by Professor Heon Ju Lee and Professor Sooseok Choi)

A thesis submitted in partial fulfillment of the requirement for the degree of

Doctor of Philosophy

2019.12

The thesis has been examined and approved

Thesis Director

Prof. Heon Ju Lee

Jeju National University ....

Thesis Committee Members

Prof. Sooseok Choi

(Jeju National University) ....

Prof. Young Hun Yu

(Jeju National University) ....

Prof. Kyoung Jae Chung

(Seoul National University) ....

Dr Ji Hun Kim

(National Fusion Research Institute)..

December, 2019

Plasma Application Laboratory

Department of Nuclear and Energy Engineering

Faculty of Applied Energy System

GRADUATE SCHOOL

JEJU NATIONAL UNIVERSITY

제주대학교 중앙도서관
JEJU NATIONAL UNIVERSITY LIBRARY

ACKNOWLEDGMENTS

I would like to express sincere thanks to all who have supported and contributed to complete this doctoral thesis. I am so grateful to the people who have stayed all the time in this tough period of my life to guide and encourage me to help overcome the barriers.

Foremost, I would like to express my sincere and deep gratitude to the beloved research supervisor, Prof Heon Ju Lee. He has not only allowed me to execute the research work but also gave invaluable suggestions, advice, support, and guidance, to extend the period of research work to improve the thesis work. His vision and knowledge towards the practical application, research methodology and motivation much inspired me and will always follow his footsteps.

I am incredibly grateful to my co-supervisor Prof. Sooseok Choi, for his scholarly advice and consistent help during my research period. My sincere thanks to him for the academic support and encouragement especially during the end of the research work.

I want to thank all the thesis committee members; Prof Yong Hun Yu, Prof. Kyuong Jae Chung and Dr. Jin Hun Kim for their valuable time, comments and encouragement. My special thanks to Prof Young Sun Mok and Prof Won Gee Chun for their guidance in my theoretical as well as practical knowledge. They gave me chances to carry out some of my experimental work in their laboratory. Without their permission, this work would not be completed.

I sincerely thank the Brain Korea 21 plus and graduate school of Jeju National University for the full support of research allowances, International conference trip and a stipend during my research period. And also like to thanks to

제주대학교 중앙도서관
JEJU NATIONAL UNIVERSITY LIBRARY

energy department officers to all those documentations processes, constant feeding of information that I needed for my study and research work

I am grateful to have my plasma application laboratory's members who immensely helped and support my personal and professional life at University. This doctoral degree is not all possible without their help and friendly environment. Therefore, I sincerely thank Dr. Ulugbek Shaislamov, Dr. Muhamad Waqar Ahmed, Yang Jong Keun, Saud Shirjana, Dr. Koramy Reda Ahmed Abdul Hafeez and Dr. Lyakhov Konstantin.

My special thanks to brother Dr. Dilli Paudyal and bhauju, Mr. Sorbhyagya Maharjan and bhauju Mrs. Suh Hee Sook who always supported and guided me to live as an ex-pat, making me feel comfortable. I always cherish the beautiful moment we spent together in Jeju Do. Many thanks to Dr. Anil Kumar Khambampati, Dr. Alluri Rao, and other friends, brothers, and sisters from various countries for their support

Heartfelt thanks to Nepalese students in this University, Dr. Pradeep Adhikari, Saud Shirjana, Roshan Mangal Bhattarai, Sunam Kumar Sharma, Maniram Banjade and Krishna Singh Bhandari who made my Jeju life not only easy but also helped to gather lots of unforgettable.

Last but certainly not the least, my heartiest gratitude to my parents, sisters, in-laws for their encouragement and great help at every stage of my personal and academic life. And finally, many thanks to my lovely wife, Mrs. Lakpa Sherpa, bearing all those painful days, care, support, and cheering during this tough journey.

Rai Suresh

December, Jeju National University

제주대학교 중앙도서관
JEJU NATIONAL UNIVERSITY LIBRARY

Table of Contents

ACKNOWLEDGMENTS **3**

List of Figures .... **iv**

List of Tables .... **xi**

NOMENCLATURE .... **xii**

ABSTRACT .... **xiv**

CHAPTER 1 Introduction **1**

1.1. Fusion plasma 1

1.2. Diagnostic mirror in the fusion reactor 7

1.3. Material choice 8

1.4. Deposition techniques 11

1.5. Sputtering method 12

1.5.1 Magnetron sputtering 14

1.5.2 Ion-Beam Sputtering 16

1.6. Motivation and introduction of the thesis 17

CHAPTER 2 Methodology **19**

2.1. Development of experimental setup 19

2.2. Experimental setup 21

2.3. Substrate material and preparation method 25

2.4. Substrate preparation 27

2.5. Thin-film deposition 27

제주대학교 중앙도서관
JEJU NATIONAL UNIVERSITY LIBRARY

2.6. Characterization techniques 32

2.7. Field emission scanning electron microscopy (FESEM) 32

2.8. EDS (Energy-dispersive X-ray Spectroscopy) 33

2.9. Thickness Monitor 33

2.10. X-ray diffraction (XRD) 34

2.11. 3D nano surface profiler 35

2.12. UV-VIS spectrophotometer 36

2.13. Scratch tester and peeling test 37

CHAPTER 3 Deposition and Characterization of a Rh Thin Films with an Nb Interlayer on a Molybdenum Mirror for ITER First-Mirror Application . 39

3.1. Introduction 39

3.2. Experimental Procedure 41

3.2.1. Materials 41

3.2.2. Thin-film deposition 42

3.2.3. Characterizations 44

3.3. Results and Discussion 46

3.4. Conclusion 55

CHAPTER 4 Characterization of Zr Interlayer Coated Mo/Rh Mirror 56

4.1 Introduction 56

4.2 Experimental Procedure 59

4.2.1 Film Deposition 59

4.2.2 Characterization 63

4.3 Results and Discussion 65

제주대학교 중앙도서관
JEJU NATIONAL UNIVERSITY LIBRARY

4.4 Conclusion 78

CHAPTER 5 Ion Assisted Oblique Angle Deposition of Interlayer Coated Metallic Mirror 79

5.1 Introduction 79

5.2 Experimental Setup 82

5.2.1 Film Deposition 83

5.2.2 Characterization 89

5.3 Results and Discussion 91

5.4 Conclusion 108

CHAPTER 6 Summary, Future work and Conclusion 109

6.1 Summary, ... 109

6.2 Conclusion 113

6.3 Future Work 114

REFERENCE 116

제주대학교 중앙도서관
JEJU NATIONAL UNIVERSITY LIBRARY

List of Figures

Figure 1. 1 Chain reaction of hydrogen isotopes to form 4He (Helium) 3

Figure 1. 2 D-T fusion reaction 4

Figure 1. 3 Schematic 3D diagram of a tokamak (courtesy- iter.org) 5

Figure 1. 4 Schematic diagrams showing the magnetron sputtering method 15

Figure 2. 1 Normal incident angle thin film deposition single MS gun experimental setup 20

Figure 2. 2 Re-designed Stainless steel Vacuum Chamber with Dual MS gun at degree oblique angle 20

Figure 2.3 experimental setups (with all components and devices) for thin film deposition by using DC magnetron sputtering with DC ion source 21

Figure 2. 4 Schematic images of water-cooled DC magnetron sputter gun 22

Figure 2. 5 Image of 2" diameter and 1/4th" thick Zr target 22

Figure 2. 6 Hollow cathode ion source 23

Figure 2. 7 commercially purchased silicon wafer (100) 25

Figure 2. 8 Mo mirror manufactured by Cloudray laser technology 26

Figure 2. 9 Specification of Mo mirror by Cloudray Laser technology (curtesy cloudray laser ltd) 27

Figure 2. 10 (a) surface image and (b) schematic diagram of Mo coated mirror. 28

Figure 2. 11 Image of Rh coated Mo/Rh Mirror (a) deteriorated and (b) fine surface 29

Figure 2. 12 Ion current at the different vacuum pressure and power supplies. 31

제주대학교 중앙도서관
JEJU NATIONAL UNIVERSITY LIBRARY

Figure 2. 13 Field emission scanning electron microscopy (FESEM) (TESCAN MIRA 3) 33
Figure 2. 14 Cressington MTM-10 thickness monitor 34
Figure 2. 15 Image of Empyrean Panalytical X-ray Diffraction (XRD) 35
Figure 2. 16 Photographic images of 3D Nano-surface profiler system (Optical surface profiler NV-2400) 36
Figure 2. 17 UV-VIS spectrophotometer (S-3100, SCINCO) 37
Figure 2. 18 Lab-made scratchers (a), ASTM D3359 tape (b), and (c)&(d) are a computer system and mini microscope to capture the magnified images 38
Figure 3. 1. Schematic diagram of the experimental setup for DC magnetron sputtering. 42
Figure 3. 2. Schematic diagram of the lab-made scratch tester. 45
Figure 3. 3 FESEM images and EDS elemental compositions of the Rh/Nb thin films deposited on Mo mirrors via DC magnetron sputtering. Surface (a) and (b) cross-sectional images of the Rh/Nb thin films. EDS spectra of the (c) pristine Mo mirror and the (d) Rh/Nb thin film. 47
Figure 3. 4 XRD patterns of the Rh/Nb thin film deposited on a Mo substrate. 47
Figure 3. 5 FESEM images of the surface morphology of the Rh mirrors (a) before and (b) after heat treatment (c) XRD pattern and (d) grain sizes of Rh thin films before and after heat treatment. 49

제주대학교 중앙도서관
JEJU NATIONAL UNIVERSITY LIBRARY

Figure 3. 6 3D surface images of the mirrors show the surface roughness's (a) pristine Mo mirror and the Rh/Nb-thin-film-coated on the Mo mirrors (b) before and (c) after heat treatment. 50
Figure 3. 7 Reflectivity spectra of the Mo mirror (a) and R/Nb-coated Mo mirror (b) measured before and after the heat treatment. 51
Figure 3 8 Scratch and tape test results for the Rh/Nb/Mo mirrors. Optical microscope image of a surface line scratch under (a) 0.5 N, (b) 1 N, and (c) 1.5 N for the Rh/Nb/Mo mirrors after the heat treatment. (d) Scratch test results of the Rh/Nb/Mo mirrors before the heat treatment. Rh-deposited mirror (e) before, (f) after, and (g) during the tape test, (h) scratch marks on the coated mirror.................... 53
Figure 4. 1 Image of actual Ar plasma deposition of Rh thin film on a Mo-Zr substrate 60
Figure 4. 2 Dual magnetron sputtering used for NAD with a modified substrate holder. 61
Figure 4. 3 Schematic model diagram of dual DCMS guns for OAD........................ 61
Figure 4. 4 Deposition rate graph at 40, 100 and 200 W... 63
Figure 4. 5 EDS and SEM images (a) elemental composition and (b) Rh thin film surface mapping 66
Figure 4. 6 Thickness of the films captured by the SEM, (a) and (c) oblique angle deposition and (b), and (d) normal angle deposition at 40 and 200 W.. 66
Figure 4. 7 XRD spectrum of the thin film Rh-Zr on the Mo substrate. 67
Figure 4. 8 Pristine Mo mirror 3D surface... 68

제주대학교 중앙도서관
JEJU NATIONAL UNIVERSITY LIBRARY

Figure 4. 9 3D images of interlayer coated Mo/Zr/ Rh mirror 1 (a-b) at 40 W and 2 (a-b) at 200 W power supplied 70

Figure 4. 10 UV-VIS reflectivity spectrum of interlayered Mo-Rh mirror coated at 40 W; (1) Zr interlayer Mo-Rh mirror, deposition process of OAD (rotating substrate); (2) films Zr and Rh coated by NAD process and (3) Nb-Rh films deposited using NAD method. 72

Figure 4. 11 Reflectivity graph of Zr interlayered Mo- Rh mirror; (1) deposited by OAD process where substrate rotated and (2) film prepared by NAD method 72

Figure 4. 12 (a) Lab-made scratch tester and (b) pressure-sensitive tape 74

Figure 4. 13.Images of scratch test for the Rh/Zr/Mo mirrors observed by Optical microscope image of a surface scratched under; (a) 0.5 Nb, (b) 1 N, and (c) 2 N for the 40 W power; similarly (d), (e) and (f) for 100 W power and (g), (h) and (i) for 200 W power 76

Figure 4. 14. Photographic images of tape test results of Zr interlayer Rh/Mo mirrors prepared at; (a) 40 W; (b) 100 W and (c)200 W 76

Figure 4. 15 Image of tape test images of thin film deposited on a Mo substrate, stripped off test was performed for five times (a) 40 W and (b) 200 W. 77

Figure 5. 1 IBAD on OAD process 81

Figure 5. 2 Experimental setups for the OAD- ion beam assisted thin film deposition. 83

Figure 5. 3 photographic images of DC hollow cathode ion source, (a) revealing internal parts of the device (b) assemble view 84

제주대학교 중앙도서관
JEJU NATIONAL UNIVERSITY LIBRARY

Figure 5. 4 Schematic diagram of dual DCMS gun sputtered material deposited one at a time by the IA-OAD process. 85
Figure 5. 5 Ion beam assisted deposition with slated substrate holder to have normal angle deposition... 85
Figure 5. 6 Multilayer thin films of Zr and Rh on a Mo substrate.............................. 87
Figure 5. 7 Ion beam current at the different vacuum pressure and power supplies ... 89
Figure 5. 8 Si wafer roughness images deposited by OAD (1a/1b) and IA-OAD (2a/3b) process at 40 W power. 91
Figure 5.9 Si wafer roughness images deposited by OAD (1a/b) and IA-OAD (2a/b) process at 100 W power 92
Figure 5.10 Si wafer roughness images deposited by OAD (1a,b) and IA-OAD (2a,b) process at 200 W power 93
Figure 5.11 3D nano surface roughness thin film deposited by (1-a,b) OAD and (2-a,b) with IA- OAD processes at 40 W 94
Figure 5.12 Images of 3D nano surface roughness (5-a,b)OAD and (6-a,b) with IA-OAD processes at 200 W 95
Figure 5.13 Image XRD pattern of Mo-Zr-Rh thin 96
Figure 5.14 XRD spectrum of 3 different samples (before and after annealing) that prepared by 40, 100, and 200 W power... 97
Figure 5. 15 EDS images of Si substrate (a) and Mo substrate (b)................................ 98
Figure 5. 16 SEM morphology of Rh surface deposited on Mo substrate at 40 W; (a) Mo pristine surface; (b) Zr-Rh thin film surface deposited by NAD; (c) Zr-Rh film deposited with IA-OAD; and (d) Zr-Rh OAD (fixed substrate) 99

제주대학교 중앙도서관
JEJU NATIONAL UNIVERSITY LIBRARY

Figure 5. 17 SEM images of the thin-film OAD process at the power of 40, 100, 200 W. ... 100
Figure 5. 18 Schematic view of OAD film growth; (a) initially few particles reaching at the substrate surface at an angle of α random; (b) nuclei grows with more ions and atoms deposition; (c) columns growth develop as partially shadowing the neighboring columns and suppressing the growth and (d) columns grow with more tilting towards the incident angle and some columns completely stop growth, leaving void between two shadowing columns. ... 101
Figure 5.19 Graph of reflectivity of the Zr-Rh fabricated thin-film coated mirrors at 40 W power; (1) Si substrate coated mirror has the lowest reflectivity (40%) as compared to all other Mo substrate coated mirrors; (2)OAD film has around 50% with tilted columnar structure on the Mo substrate; (3) mirror has nearby 55% of reflectivity due to ion-assisted deposition; (4 and 5) both mirror has highest among all almost 77% of total reflectivity, both were deposited normal angle of deposition ... 103
Figure 5.20 Image of the lab-made scratch tester (a) and pressure-sensitive tape (b) ... 105
Figure 5. 21 Scratch test results of IA-AOD technique thin film surface deposited by three different power (a) ,(b) and (c) by 40 W; (d), (e) and (f) by 100 W; (g), (h) and (i) by 200 W. ... 106

제주대학교 중앙도서관
JEJU NATIONAL UNIVERSITY LIBRARY

Figure 5. 22 photographic image of Zr-Rh coated Mo mirror; Mirror prepared by 40 w (a), 100 W (b) and 200 W (c) power with the Ion beam assisted OAD process 107

제주대학교 중앙도서관
JEJU NATIONAL UNIVERSITY LIBRARY

List of Tables

Table1. 1 Parameters of ITER (courtesy- iter.org) 6

Table1. 2 Classification of thin-film depositions techniques 12

Table 2. 1 Deposition parameters during thin film coating 29

Table 3. 1 Parameters used during the DC magnetron sputtering 43

Table 4. 1 Parameter for the DCMS 62

Table 4. 2 Deposition rate of Nb, Zr, and Rh at parameter mentioned in table 4.1.... 63

Table 5. 1 Experimental parameter for IA-OAD 87

List of Equations

Eqn 1.1 2

Eqn 2.1 34

Eqn 3.1 49

Eqn 4.1 69

제주대학교 중앙도서관
JEJU NATIONAL UNIVERSITY LIBRARY

NOMENCLATURE

3D	3 Dimensional
AC	Alternating current
ASTM	The American society for testing and materials
BSE	Backscattering electrons
BT	Toroidal field
CVD	Chemical vapor deposition
CXN	Charged exchange neutrons
DC	Direct current
DCMS	Direct current magnetron sputtering
DI	De-ionized
D-T	Deuterium-Tritium
EDS	Energy dispersive X-ray spectroscopy
FC	Faraday cup
FESEM	Field emission secondary electron microscopy
FM	First mirror
FWHM	Full width half maximum
HIPIMS/HiPIMS	High power impulse magnetron sputtering
IA-OAD/ IBAD	Ion assisted-oblique angle deposition/ion beam deposition
ITER	International thermonuclear experimental reactor
JCPDF	The joint committee on powder diffraction standard
mA	milli-Ampere
Mo	Molybdenum

제주대학교 중앙도서관
JEJU NATIONAL UNIVERSITY LIBRARY

MS	Magnetron sputtering
mTorr	milli-Torr
NAD	Normal angle deposition
Nb	Niobium
Nb-Rh	Niobium-Rhodium
OAD	Oblique angle deposition
PFC	Plasma facing component
PVD	Physical vapor deposition
RF	Radio frequency
RFMS	Radio frequency magnetron sputtering
Rh-Nb-Mo	Rhodium-Niobium-Molybdenum
Rh	Rhodium
Rh-Zr-Mo	Rhodium-Zirconium-Molybdenum
Si	Silicon
Tokamak	Toroidal chamber with magnetic coils
TMP	Turbo-molecular pump
UV-VIS	Ultraviolet-visible spectrophotometer
XRD	X-ray diffraction
Zr	Zirconium
Zr-Rh	Zirconium-Rhodium
μA	micro-Ampere
μTorr	micro-Torr

제주대학교 중앙도서관
JEJU NATIONAL UNIVERSITY LIBRARY

ABSTRACT

The nuclear fusion reactor is a very hot temperature chamber where light atoms are made to collide each other forming heavier atoms by releasing energy. In this process, most of the particles are ionized and form a burning plasma. Hence, it is necessary to know the phenomena involved in the burning plasma to control and protect the devices and components for the efficient and effective performance of the fusion reactor. There are several diagnostic systems which help to understand the physics behind the plasma reaction in the reactor. One of the diagnostic systems is the optical diagnostic system. It is an essential technique to understand the plasma physics involved in burning plasma, which helps the further study of the plasma phenomena. Metallic mirrors are used in fusion reactors like the International Thermonuclear Experiment Reactor (ITER) for optical plasma diagnostics and imaging systems. Plasma diagnostic systems are necessary tools for the future success of the ITER for a better understanding of magnetically confined burning plasma and its other phenomena inside the tokamak (Toroidal Chamber with Magnetic Coil). The closest mirrors to the plasma environment for the optical diagnostic is First Mirror (FM).

In the harsh environment of fusion plasma, the FMs need to survive and perform to reflect the light signals to the analyzing system through the complicated arrangement. Meanwhile, the FMs surface will gradually change their properties due to adverse effects of erosion and redeposition of impurities owing to high energetic charge exchange neutral (CXN) particles, UVs, X-rays, and gamma radiations. Moreover, the most critical problem is the reduction of optical reflectance. Any changes in the reflectivity of the FM will affect the reliability of the signals. Despite these extreme conditions, the reliability of the diagnostic system and the plasma-facing components

제주대학교 중앙도서관
JEJU NATIONAL UNIVERSITY LIBRARY

have to maintain the required optical properties for a better understanding of hot nuclear fusion plasma. To minimize the reduction of optical properties of the FMs, choice of material plays essential roles, like having low sputter yield, resistance to a chemical reaction, high thermal conductivity & resistance, high reflectance, and surface quality sustainability for an extended period of time under the plasma environment.

In search of new inventions or continuous progress of technology to have expected optical properties of the FMs around the world, different laboratories are researching on various possible FM's materials and fabrication techniques. So far, some materials show matching features to some extent, like; copper (Cu), stainless steel (SS), tungsten (W), molybdenum (Mo), and rhodium (Rh). However, Mo and Rh are the most attractive and preferred choice. Both metals can have stability and reliability to withstand the harsh condition of the plasma environment and have better reflectivity among all the metals. Among two metals, the monocrystal mirror of Rh shows better optical properties. However, due to the expensive Rh material cost as well as a technological limitation for the production (limited size), the Rh thin-film coating on the bulk Mo is considered. Still, the thin-film surface is consumed into the plasma environment in the long run as it gets eroded on the mirror's surface due to the bombardment of high energy charged particles. Thin films might get detached from the substrate surface due to the stress that occurs between the two materials (Mo-Rh) when there is a difference in the thermal coefficient of material and lattice.

The main focus of this thesis work is to provide an experimental study and fabrication of the thin interlayer coating FMs for the fusion reactor, keeping an acceptable level of reflectivity and adhesion strength of the coated films.

제주대학교 중앙도서관
JEJU NATIONAL UNIVERSITY LIBRARY

For the experiment, we choose the DC magnetron sputtering systems to deposit a thin film of Rh metal on the bulk Mo substrate. Thin interlayer materials niobium (Nb) and zirconium (Zr) are chosen as their thermal expansion coefficient falls between Mo and Rh. We expected to bridge the thermal expansion coefficient of materials that would respond to thermal expansion reasonably, and coated films will remain attached to the surface.

In this study, Si (100) wafers are used extensively for checking surface morphology, deposition rates and thicknesses of the deposited films of Nb, Zr, and Rh at different parameters. The reflectivity (before and after high-temperature exposure), scratch and adhesion tests performed on commercially purchased Mo mirrors throughout the experiment. All substrates were ultrasonicated in acetone and ethanol followed by rinsing in distilled water (DI) and finally, dried with pure nitrogen gas (N2). Prior to the deposition, all substrates were heated to 100°C for an hour to remove residual impurities and to reduce the surface stress

In DCMS, all the target materials of 99.95% purity (50.8 mm diameters, and 6.35 mm thicknesses) were used. A base pressure of 10-12 μTorr, the working pressure of 5 mTorr, and process gas (Ar) 30 SCCM were kept constant for entire experimental processes. For the characterization of thin film deposition, FE-SEM, EDS, XRD, 3D nano-system, and UV-VIS spectrometer was used. Lab-made scratch tester was used for testing scratch strength of the thin films along with adhesive tape test for adhesion strength.

To date, extensive fabrication methods and their results have been presented in many articles to develop FMs as per the requirement of the fusion reactor (ITER). Most of the Mo-Rh thin-film FMs fabricated for the ITER show 70-80% of reflectivity

제주대학교 중앙도서관
JEJU NATIONAL UNIVERSITY LIBRARY

[1] in the visible wavelength. Our experimental results of the fabricated mirror (Rh-Nb/Zr-Mo) also match with the many articles published in a different journal [1]–[3]. The reflectivity of the mirrors was 70-75% (in the visible wavelength) after high-temperature exposure. Both the scratch tests on the surface of the mirrors (film thickness:190 nm thick) with a load of 0.5-2.0 N at the rate of 37 mm/sec for 10-20mm of scratch length and the pressure-sensitive tape showed great adhesion strengths. Mirror fabricated at low power showed better reflectivity as well as better adhesion strength. Thin films coated at 40 W has a better scratch and adhesion strength than films coated at 200 W. On the other hand, Ion assisted-oblique angle deposition (IA-OAD) has good film density, but reflectivity of the mirror was lower than the normal angle deposition (NAD) processed films.

This thesis has six chapters; chapter 1 composed of essential background to give information about nuclear fusion, optical diagnostics, and the importance of first mirrors. This chapter also briefly explains the deposition techniques and motivation for the research. Chapter 2 discusses the experimental method and brief descriptions about the instruments and components used in the experiment, the sample preparation process, and characterization techniques implemented to find out the results of the work.

In our study, we applied three different methods for the deposition of thin-layer films (Rh-Nb/Zr) on the Mo substrate. In chapter 3, the NAD technique was used, where surfaces of the target and the substrate are parallel to each other or particle flux direction are perpendicular (normal- 90°) to the substrate's surface. Nb was the material used as interlayer between the Mo substrate and Rh film. Different powers were supplied (40, 100, 200W) to deposit the films in various time to attain the same film thickness of Nb (40 nm) and Rh (140 nm) in all samples. Moreover, the comparison

제주대학교 중앙도서관
JEJU NATIONAL UNIVERSITY LIBRARY

between the results with and without interlayer coated mirrors was made. High temperature (200℃ for 6 hrs) exposed mirror has a reduction of reflectivity by 10-15%. The low power deposition showed better adhesion than a high power deposition process. Note that, interlayer coated Rh-Nb-Mo mirror is installed in NFRI/KSTAR for testing its reliability and reflectivity.

Chapter 4 explains the interlayer Zr films deposited by NAD and OAD (oblique angle deposition) techniques to fabricate Rh-Zr-Mo FMs. The thickness of the thin-films was the same, as mentioned in the previous chapter. The NAD process showed better reflectivity of surface than the OAD process. In chapter 5, the experiment uses the IA-OAD technique to fabricate FMs. The thin film deposited by the IA-OAD process displayed better adhesion strength than the previous two deposition techniques but exhibited low surface reflectivity. The analysis showed a reflectivity of 60%. However, the film thickness of 2 μm on Mo substrate was successfully deposited by this technique without any blister or peeling off signs. This advantage can be used to increase the reflectivity of the film by polishing technique. Chapter 6 is about the summary of this thesis, the importance of this research work, significant findings, scope, and future work for the application of FMs to accomplish the requirement of the fusion reactor application to realize the fusion energy in the near future.

제주대학교 중앙도서관
JEJU NATIONAL UNIVERSITY LIBRARY

CHAPTER 1
Introduction

1.1. Fusion plasma

Plasma is a hot ionized gas where electrons are split away from the atoms. Plasma comprises over 99% of the visible universe [1]–[3]. Plasma can be seen in the form of stars, nebulas, and auroras glow above the north and south poles in the night sky. The lightning branch that cracks in the sky, so are the neon signs along our city streets, are plasma, and so is our Sun that makes life on earth possible [4], [5].

Along with the solid, liquid, and gas, plasma is called "the fourth state of matter," Solid changes into the liquid, as a liquid boils, changes into a gas when energy is added, heating a gas will form the plasma. Plasma is a mixture of electrically neutral, positive (ions), and negative (electrons) particles. It shows collective behavior because of the attraction and repulsion of electric forces. Moving charged particles generate an electric current within a magnetic field, and any movement of a charged plasma particle affects and is affected by the fields created by the other.

Albert Einstein's famous formula, $E=mc^2$, provides the basis for understanding fusion. Einstein's theory that mass can be converted into energy was further explored to discover two practical methods for achieving this energy conversion. Fission is the one method in which heavy atoms, such as uranium, are split, releasing the internal energy that holds the atom together. The other method is fusion, fused, or joined. Nuclear fusion is the process in which two or more light atomic nuclei come very close and collide at a very high speed to form a new type of heavier atom. During this process, tremendous amounts of energy are released, and that energy is what we see as light.

제주대학교 중앙도서관
JEJU NATIONAL UNIVERSITY LIBRARY

The basic idea of fusion research is to reproduce hotter temperatures than in the core of the Sun to have nuclear fusion and to produce clean energy. The nuclear fusion reaction in the Sun produces an enormous amount of helium (^{4}He) and release energy. We can produce ^{4}He in the laboratory with a different combination of reactions between hydrogen isotopes. Below are some of the reaction combinations.[6]

Reaction	Eqn
$^{2}D + ^{1}p \rightarrow ^{3}He + \gamma$ (+4.98 MeV)	
$^{3}He + ^{3}He \rightarrow ^{4}He + 2\,^{1}p$ (+12.86 MeV)	
$^{2}D + ^{3}He \rightarrow ^{4}He + ^{1}p$ (+18.354 MeV)	1.1
$^{2}D + ^{2}D \rightarrow ^{3}He + ^{1}n$ (+3.268 MeV)	
$^{2}D + ^{2}D \rightarrow ^{3}T + ^{1}p$ (+4.032 MeV)	
$^{2}D + ^{3}T \rightarrow He^{4} + ^{1}n$ (+17.571 MeV)	

Eqn 1. 1 D-T reaction

제주대학교 중앙도서관
JEJU NATIONAL UNIVERSITY LIBRARY

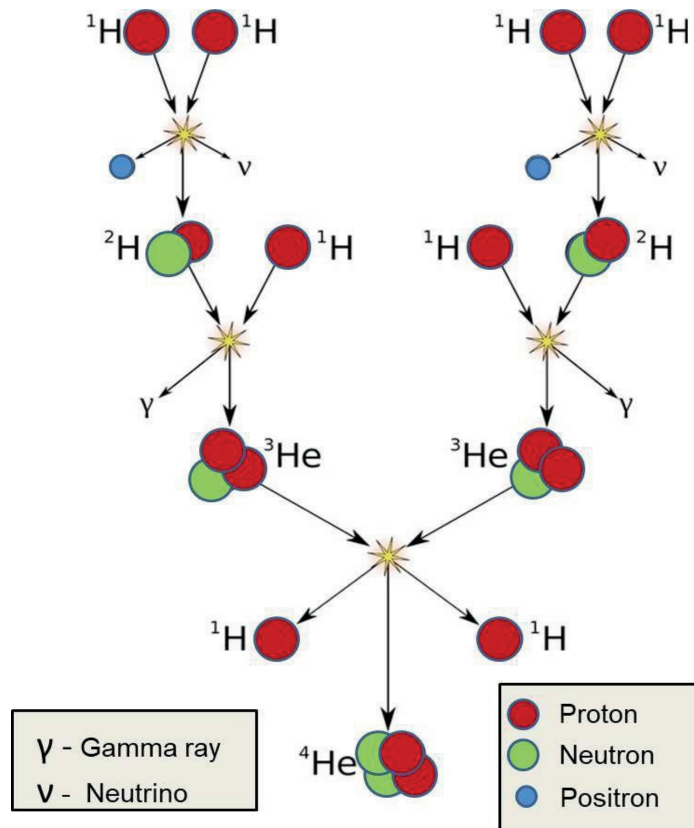

Figure 1. 1 Chain reaction of hydrogen isotopes to form ^{4}He (Helium) [7]

Figures 1.1, 1.2, and Eqn 1.1 show the chain fusion reaction of the hydrogen isotopes, which form into helium atom releasing high energy. The most efficient fusion reaction between two hydrogen isotopes deuterium (D) and tritium (T) produces the highest energy at the lowest operating temperatures (about 10 keV) and form helium [8]. In this D-T fusion occurs at very high temperature and mixture gas is fully ionized[6]. The neutralized electrostatic charge of the nuclear ions by the presence of an equal number of electrons and the resulting quasi-neutral gas form plasma. The neutrons produced by the plasma reactions leave the plasma without interactions. In contrast, the charged α particles (He^{2+}), which transfer their 3.5 MeV energy to the plasma through collisions and thus contribute to the heating of the plasma[6],[9].

제주대학교 중앙도서관
JEJU NATIONAL UNIVERSITY LIBRARY

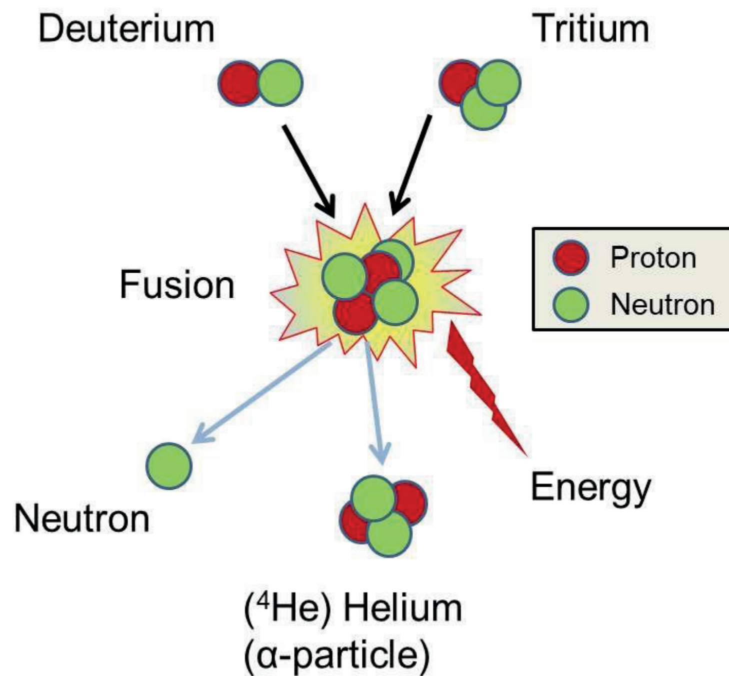

Figure 1. 2 D-T fusion reaction

The helium nucleus carries an electric charge; however, the neutron is not charged and can be absorbed by the walls of the reactor if they are coated with neutron-absorbing materials. Since the neutrons carry 80% of the energy produced in this reaction as kinetic energy, when the walls absorb them, this energy is transformed into heat[7]. Just like other conventional power plants, a fusion power plant will use this heat [10], [11] to boil water to produce steam, which drives a turbine that generates electrical energy.

Higher the temperature, the faster the atoms move, and when they collide at high speed. With that high speed of the collision, atoms overcome the Coulomb force, and the nuclei fuse with realizing energy. In order to produce fusion energy for practical use to generate electricity, the deuterium-tritium fuel must be heated to about 100 million

제주대학교 중앙도서관
JEJU NATIONAL UNIVERSITY LIBRARY

degrees Celsius (°C) for a long enough time so that more energy can be released through fusion reaction. The high-temperature inside the reactor is achieved by confining plasma in a vacuum chamber in a doughnut-shaped reactor called a tokamak. The term "tokamak" comes from Russia, which stands for "toroidal chamber with magnetic coils"[12].

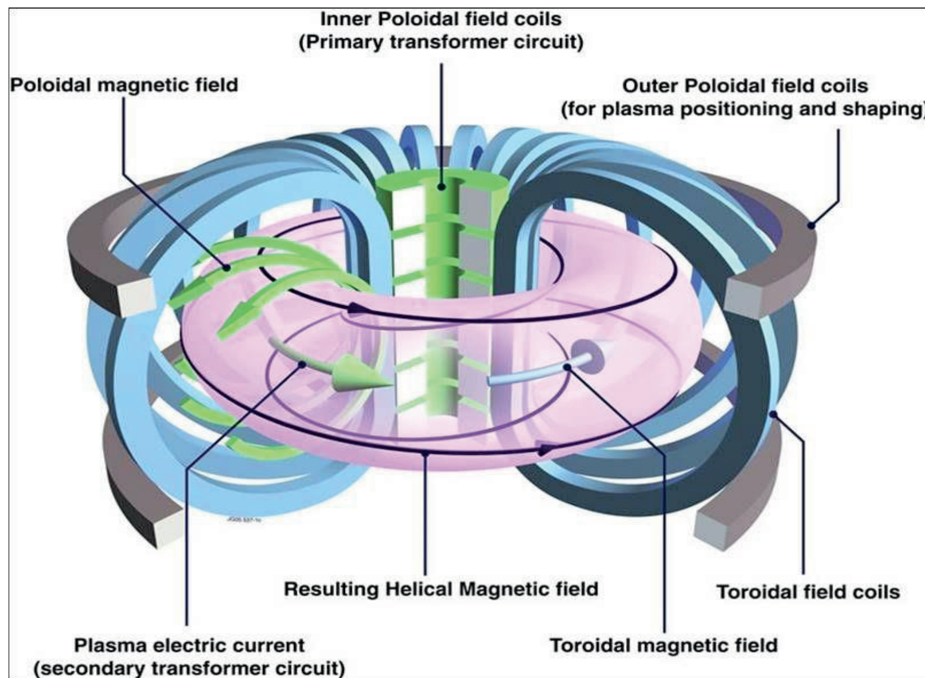

Figure 1. 3 Schematic 3D diagram of a tokamak (courtesy- iter.org)

The tokamak consists of a toroidal vacuum vessel inside which a strong toroidal magnetic field is generated by external poloidally wound magnetic coils (figure. 1.3). But, this field alone is insufficient to confine the plasma as the toroidal geometry of the toroidal field (B_T) is not uniform inside the chamber within the major radius (R) of the tokamak ($B_T \propto R^{-1}$) [6].

The resulting $E \times B$ drift separates ions and electrons that make the plasma unstable thus

제주대학교 중앙도서관
JEJU NATIONAL UNIVERSITY LIBRARY

to prevent this drift; the magnetic fields are made in helical to the toroidal field a poloidal magnetic field produced by the plasma current.

The ITER (International Thermonuclear Experimental Reactor) tokamak is the largest and most powerful fusion device in the world, which has millions of components and parts. ITER is one of the most ambitious mega projects in the world. And ITER will be the first fusion device to test the integrated technologies, materials, and physics regimes necessary for the commercial production of fusion-based electricity[10].

ITER is designed for much higher fusion power gain, or Q ≥ 10, ten-fold of 50 MW that injected heating power will produce 500 MW of fusion power for long pulses of 400 to 600 seconds. ITER will not capture the power it produces as electricity, but as the first of all fusion experiments in history to produce energy [10], [13].

Table1. 1 Parameters of ITER (courtesy- iter.org)

Total fusion power output	500 MW
Q- fusion power	≥ 10
Stored magnetic energy	51 GJ
Magnet temperature	4 K
Plasma temperature	150-300 million ºC
Plasma volume	840 m^3
Plasma major radius (R)	6.2 m
Plasma minor radius (a)	2.0 m
Blanket maximum thermal load	736 MW

제주대학교 중앙도서관
JEJU NATIONAL UNIVERSITY LIBRARY

interior vacuum chamber volume	1400 m^3
Magnetic field (peak toroidal field)	11.8 T
Magnetic field (peak poloidal field)	6 T
Plasma burn time	≥ 400 s
Plasma current (I_p)	15 MA
Plasma surface	678 m^2
Auxiliary current drive/heating power	73 MW
Machine weight	23000 ton

1.2. Diagnostic mirror in the fusion reactor

It is necessary to know the phenomena involve in the burning plasma to control and protect the devices and components for the efficient and effective performance of the fusion reactor. Inside the hot plasma, a high level of radiation and neutrons is expected and it needs to control and to protect the PFCs from the adverse effect of the hot plasma. There are several diagnostic systems which help to understand the physics behind the plasma reaction in the reactor. One of the diagnostic systems is the optical diagnostic system that uses different shapes and sizes of metallic mirrors. ITER itself uses more than 80 metallic mirrors [14] for the optical diagnostics depending on the locations in the vacuum vessel and diagnostic requirement. The main purpose of metallic mirrors is to transmit all the light signals to diagnostics through an intricated (labyrinthine) path in the shielding block.

A mirror is an object or surface that reflects the light in some wavelength range. The reflected light can acquire the detail physical characteristic of the source of the light. The reflectivity of the mirror is measured in the percentage of reflected light per total of

제주대학교 중앙도서관
JEJU NATIONAL UNIVERSITY LIBRARY

incident light and the reflectivity may vary with the wavelength of the light

The metallic mirror installed for diagnostic systems in the fusion reactor that face the hot confined plasma is called "First Mirrors."(FMs). Being the closest element to the plasma, FMs suffer from intense radiation, from bombardment by CXN particles, UVs, X-rays, and gamma radiations. FMs also subjected to erosion, redeposition of impurities on the surface [15] And the most critical problem is the gradual reduction of reflectance. Despite these extreme conditions, the reliability of the diagnostic system and the plasma-facing components have to maintain the required optical properties for a better understanding of hot plasma nuclear fusion. Thus, any changes in the reflectivity of the first mirror will affect their liability of the transmitted signal to the diagnostic system. As per the design of the ITER spectroscopic systems, the interest wavelength range is from 0.05-1000 nm [16] but generally, FMs operation wavelength ranges from 5 nm to 118μm [17]. Depending on the locations, mirrors will be exposed to different levels of particle fluxes, so the quality of the mirrors varies with the requirements and location. Therefore, the choice of the first mirror material, size, and thickness are made by considering the interest wavelength range, location where it is being used for the chosen system. Since wavelength range is fixed by the system to be used, and the resistance of the material to the degradation mechanisms to be encountered.

1.3. Material choice

According to the location and quality requirements, metallic mirrors are made into various shapes and sizes. FMs subjected to high radiation, CXN particles, erosion, and redeposition on the surface [15] and occurs gradual decrease of optical properties. Therefore, there has been developed various methods and techniques to fabricate the

제주대학교 중앙도서관
JEJU NATIONAL UNIVERSITY LIBRARY

FMs according to the requirement and material choice.

FM must satisfy some important requirements to be used in the fusion reactor;

- It should high reflectivity as possible
- Reflectivity should not depend too much on the wavelength in the operating spectral range.
- Resistance to physical and chemical reactivity
- High thermal conductivity and resistance to high temperature.
- Low sputter yield.
- Fit for the in-situ cleaning

Materials like; copper (Cu), stainless steel (SS), tungsten (W), molybdenum (Mo), and rhodium (Rh) [8] show matching features to some extent. However, among all, molybdenum (Mo) and rhodium (Rh) are chosen for the preferred choice of materials as they can withstand the harsh conditions of the plasma environment and retain better reflectivity [18]. Both (Rh and Mo) tend to resist chemical and high temperatures and low sputter yield. Most of the materials lost their optical properties by erosion and redeposition of contaminants during operation. An SC (single crystal) Mo/Rh (bulk) has the highest quality of optical properties maintaining expected requirements for the fusion plasma application. But due to manufacturing technological difficulties and high cost of SC Rh material limits its use as a single material in the FM of larger size mirrors (e.g. diameter 350 mm [6] and large up to the diameter of 500 mm [19]); as a result, it is considered to coat thin layer of highly reflective material on to the bulk substrate of having similar characteristics.

제주대학교 중앙도서관
JEJU NATIONAL UNIVERSITY LIBRARY

The thin-film coating of Rh on the metallic substrate has many advantages on a single or bulk material mirror. It gives wider possibilities of choosing substrate material from many metals, can be fabricated in any size and shape with the minimum possible cost. The film thickness can be chosen according to the requirement of optical qualities. The coating of thin-film can be made with high adhesion strength so it can last for a long period of operation time.

However, the FM thin-film surface is consumed as it gets erode, corrode, etch on the mirrors' reflective surface due to the bombardment of CXN particles and contaminants the plasma environment. Thin-film might be detached from the substrate surface due to the thermal stresses developed between the two different materials (bulk substrate and thin-film coated materials). Thermal stresses occur with the difference in the thermal coefficient of the materials and lattice mismatch between them. It weakens the bonding of two materials at the interface and forms blister and eventually peeled off the thin layer. This material removed from the surface of the mirror will contaminate the plasma and will redeposit into the same surface and gradually reduced the optical properties of the mirror.

Hence it is necessary to minimize such kind of problem and to maintain high reflectivity in the fusion reactor; we considered introducing thin interlayer material (Niobium or Zirconium) reducing thermal stresses on the interface of the two material (Mo/Rh).

Here in this research work, we used Mo as a bulk substrate and Rh as top layer coating to fabricate First Mirror. Thin-film of Nb and Zr deposited as interlayer material to bridge between the Mo surface and the thin layer of Rh by DC magnetron sputtering

제주대학교 중앙도서관
JEJU NATIONAL UNIVERSITY LIBRARY

technique, which can have high reflectivity as well as better adhesive property to withstand harsh condition of plasma environment.

1.4. Deposition techniques

Deposition techniques, processes, and equipment for thin film deposition is regarded as the primary components since the semiconductor and microelectronic device. It is essential to understand and optimize the deposition procedure to grow good quality thin films. Therefore, process parameters and equipment are upgraded to meet the demands of improved quality and economic viability. Another reason for the rapid growth of deposition technology is due to the more understanding of the physics and chemistry of films, surfaces, interfaces, and microstructures of different materials.

There are many depositions methods for growing layers [20]–[22] in the various thickness from few nanometers to tens of micrometers. Thin-film deposition technologies are classified as either purely physical (physical vapor depositions, PVD) or purely chemical (chemical vapor deposition, CVD) techniques [23]. Sometimes both physical and chemical processes combine to deposit thin films such is called physical-chemical methods or hybrid process, such as

- Magnetron sputtering and e-beam evaporation
- Magnetron sputtering and filtered cathodic arc deposition
- E-beam evaporation and filtered cathodic arc deposition
- PVD, polymer flash evaporation, and magnetron sputtering/evaporation.

제주대학교 중앙도서관
JEJU NATIONAL UNIVERSITY LIBRARY

Primary thin film deposition techniques are tabulated in Table 1.2

Table1. 2 Classification of thin-film depositions techniques

Depositions techniques for thin-film growth	
PVD (Physical Vapor Deposition)	Chemical vapour deposition (CVD
Thermal PVD	Atmospheric pressure CVD
Electron beam PVD	Laser-induced CVD (PCVD)
Reactive PVD	Electron-enhanced CVD
Sputtering (DC-diode, RF, Magnetron)	CVD epitaxy

1.5. Sputtering method

The very basic and well-known PVD process is the sputtering [9], [22], [26], where the atoms are ejected from an electrode surface by momentum transfer from bombarding ions to surface. This deposition is called Sputter deposition as a common name.

When a surface is bombarded with high energy, positive ions, it causes to eject the surface atoms by overcoming the internal bonding force (Coulomb force). This process of ejecting atoms from the surface by a bombardment of positive ions (usually inert gas ions) by the momentum transfer process between the sputter gas and target atoms is commonly known as sputtering (cathode sputtering) [27], [28]. Ar (argon) is usually used as the sputtering gas as it is inert gas and does not interact with any other materials. The ejected atoms will deposit or condense to form a thin film on a substrate at some distance. With the neutral atoms, charged atoms and electrons are also emitted from the surface. The sputtering yield (number of atoms ejected from the surface of the

제주대학교 중앙도서관
JEJU NATIONAL UNIVERSITY LIBRARY

target per incident ion) depends on the target size, material composition, binding energy, base vacuum pressure, process gas pressure, and flow rate, and the experimental geometry. It also depends on the applied voltage and sputters power at which sputtering takes place [29]. Sputtering takes place when the kinetic energy of the bombarding particles is much higher than average thermal energies in the plasma environment. This can allow a much more pure and precise thin film deposition on the atomic level [30].

In the sputtering process, the entire target surface is the source, unlike the evaporation process, where a point on the target is the source. The source surface implies a higher coverage area during deposition as compared to other evaporation techniques. The deposition process in sputtering is not purely ballistic. The high kinetic energy of the sputtered particles (~ tens of eV) gives rise to better adhesion to the substrate as well as dense film growth. The high KE of particles will impinge the substrate surface and act like the stitching of atoms on to the surface to form a layer. The sputtering deposition of a thin film causes re-distribution of atoms on the substrate, leading to (a) high uniformity, density and interface adhesion of the deposited film (b) deposition over the large surface area [19]. Usually, the target is water-cooled, and by cooling provision in sputtering, higher melting point elements can be deposited. Sputtering processes become versatile methods for preparing high-quality thin films with a better understanding of the techniques. Commercially available, a wide variety of cathodes and targets, including various options for magnet strength, also made sputtering widely used technique for thin-film coating

제주대학교 중앙도서관
JEJU NATIONAL UNIVERSITY LIBRARY

1.5.1 Magnetron sputtering

Sputtering sources generally employ magnetrons that utilize strong magnetic fields to confine charged plasma particles near the surface of the sputter target in order to increase the sputter yield. In the magnetic field, electrons follow helical paths around magnetic field lines [31]. This movement causes an increase in more ionizing collisions with gaseous neutrals near the target surface [32]. The sputtered neutral particles are much heavier and are unaffected by the magnetic field. The sputter gas usually is an inert gas such as Ar. The Ar ions created by collisions with electrons and lead to a higher deposition rate. So, it also means that the plasma can be sustained at a lower Ar pressure.

A schematic diagram showing the target and magnetron sputtering arrangement is shown in Fig 1.4. The E×B drift path in the figure, shows the electrons are confined to increase the sputter yield generated by the magnets installed behind the target. An electron ejected by the target is affected by the component of the magnetic field bending towards the target surface (magnetron component) and finally returns, after completion of the magnetic circuit [33], [34]. As the target material is removed due to sputtering, an annular erosion profile may appear on the surface of the target like the race track.

제주대학교 중앙도서관
JEJU NATIONAL UNIVERSITY LIBRARY

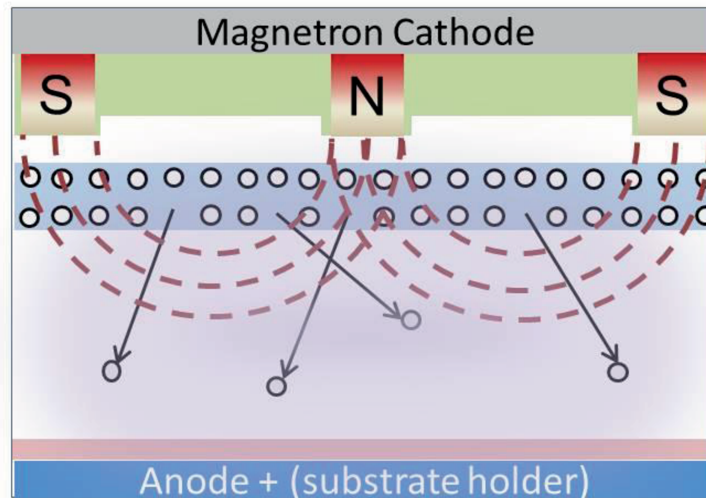

Figure 1. 4 Schematic diagrams showing the magnetron sputtering method

Various types of power supply methods can be used in magnetron sputtering (MS). Commonly used are (direct current) DC MS, (radio frequency) RF MS, pulse DC, and recently (high-power impulse) HIPIMS [35], [36].

DCMS is the simplest and less expensive way to operate the magnetron sputtering using a DC power supply. There are special powers supplies for sputter deposition that have been manufactured to suppress the arc to occur during the reactive sputter deposition. The main advantage of MS configuration is that a dense plasma can be formed near the cathode at low pressures so that ions can accelerate from the plasma to the cathode or substrate without loss of energy due to charge exchange collisions of particles. Disadvantages are target material utilization is non-uniform, only about 30% [37] of whole target material being used, hence to improve the utilization recycle of the target is being done. Some target designer uses a magnetic pole that extends above the target surface for improving maximum material utilization.

제주대학교 중앙도서관
JEJU NATIONAL UNIVERSITY LIBRARY

DCMS is an economical solution for many types of metal coatings. However, its limitation is that non-conducting dielectric insulating materials may arc or cause poisoning the target with the charge due to localization of charge over time and might completely cease the sputtering process [30].

There some methods developed to overcome these limitations of DC Sputtering, such as Radio Frequency (RF) Sputtering and High-Power Impulse Magnetron Sputtering (HIPIMS). RF Sputtering alternates the electrical polarity at Radio Frequency and prevents a charge buildup on the target or coating material, and self-sustained discharge is maintained. A typical RFMS employed frequency in the range from 5 to 30 MHz. However, 13.56 MHz is the most common frequency used for RFMS [38], [39]

HIPIMS uses a very high voltage, short-duration burst of energy focused on the target coating material to generate high-density plasma that results in a high degree of ionization of the coating material in the plasma [40].

1.5.2 Ion-Beam Sputtering

It is a process where ion beams generated from the ion beam source through glow discharges in a high vacuum system. For the scientific investigation, sputtering is useful as effective film-deposition systems for unique materials on relatively small substrate areas [32]. The ion source comprises the cathode and the anode, which are concentrically aligned. An electrostatic field is developed inside the ion source with the application of a high voltage field when Ar gas supplied into that high electric field. An electric field causes the gas to ionize which results in creating plasma inside the ion source region with sufficient energy gain, ions are accelerated from the anode region to the cathode region [41], [42]. The ion beam can be used either, impinges on a target material and sputter the surface of the sputter towards the substrate or used to assist the

제주대학교 중앙도서관
JEJU NATIONAL UNIVERSITY LIBRARY

deposition (ion beam assisted deposition-IBAD) by bombarding the film grown by Ar ions to change the structure and properties. There are several advantages of ion-beam sputter deposition. IBAD can improve the adhesion, density of the film growth, control the stoichiometry, and low optical absorption (short wavelengths) in the thin films [42], [43]. Glow plasma discharge also results in higher-purity films.

Here in this study, the hollow cathode ion source is used to bombard the ions on the surface of the substrate, and simultaneously DC magnetron gun will sputter the target material to grow the film on the substrate

1.6. Motivation and introduction of the thesis

As technology advancement, most of the experimental analysis has become more comfortable and better to understand. Similarly, the scientific inventions' physical and chemical properties of the materials and other phenomena have become easier to understand. Fabrication of first mirrors development has been made significantly from the several bulk materials to thin layer coating of amorphous to the high-performance nanocrystalline structure. Furthermore, it is proving reliability in the harsh plasma environment. But still, thin-film stability and reliability have been the crucial performance for the fusion reactor. According to the locations and requirements set up for the fusion reactor, FMs are fabricated into various shapes and sizes by using different materials and technologies. With the available number of choices of materials and depositions techniques; an improvement in the FMs lifetime and reflectivity has found promising results in the different laboratories research articles.

In particular, several new developments have been made based on the progress of detector, component fabrication technologies, data acquisition electronics, and

제주대학교 중앙도서관
JEJU NATIONAL UNIVERSITY LIBRARY

analysis methods. This has made simple and easy for the diagnostics and the understanding of fusion physics [44], [45]. The influenced of new devices and promising results, which in turn encourage and motivate us to do further research to improve the performance of FM with the thin interlayer coating by using the DCMS method. We expect with the introduction of the thin layer of the coating decreases the thermal coefficient between the two material and reduces the thermal distortion and increases the adhesion of thin-film with the bulk substrate

This thesis aims to fabricate the Mo-Rh first mirror introducing two different types of materials (Nb and Zr) between Mo and Rh as an interlayer and to compare the results. This might optimize the optical performance in the hot plasma by retaining reflectivity and adhesion of the thin-films and extends the lifetime. Other research works have shown that rhodium material coated on the bulk molybdenum has a significant improvement in the overall performance, compare to thin layer coating of Cu, SS, Al, Ag, Mo, Ta, W, and some alloys like ZrO2 [1], [44]–[46]. However, durability and the reliability of FMs in the environment of plasma is still needed to be improved as thin-films is being consumed onto the harsh plasma environment due to erosion and detachment from the surface of the substrate. The deposition of thin-films is to be performed by applying different techniques with and without ion-assisted deposition, normal and oblique angle deposition. Furthermore, is to characterized and compare the results of optical properties and adhesion strengths of the thin films

제주대학교 중앙도서관
JEJU NATIONAL UNIVERSITY LIBRARY

CHAPTER 2
Methodology

This chapter describes an experimental procedure, the components used, development of the vacuum reactor, and brief about the characterization techniques that apply for the thin film fabricated mirror.

2.1. Development of experimental setup

The experimental reactor has been modified from time to time as per the requirement of our research. Small components like substrate holder inside the vacuum chamber, substrate holder for handling outside the chamber prior, and after the deposition, some small flanges, fixtures, etc. have been designed, fabricated, and manufactured in the laboratory. Some larger parts have been fabricated in the fabrication company. Most of the measuring devices and complicated parts were purchased from various manufacturers around the world.

Earlier our experimental setup was normal incidence angle (target and surface of the substrate) for deposition, as shown in figure 2.1. But later, the vacuum chamber was redesigned and fabricated to have dual MS guns where both target Nb/Zr and Rh (interlayer material and top coating material) can be used simultaneously to deposit multilayer thin films on a Mo substrate. The re-designed chamber is shown in figure 2.2. For designing purposes, mechanical designing software, Solidworks, and AutoCAD were used.

제주대학교 중앙도서관
JEJU NATIONAL UNIVERSITY LIBRARY

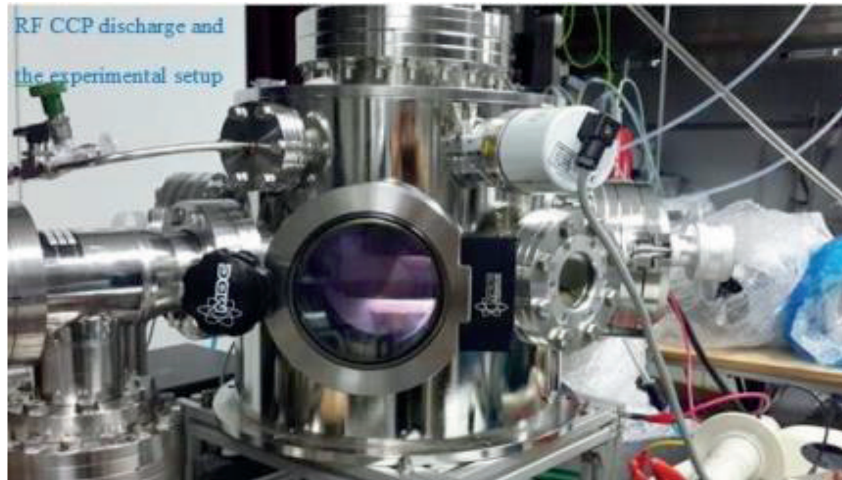

Figure 2. 1 Normal incident angle thin film deposition single MS gun experimental setup

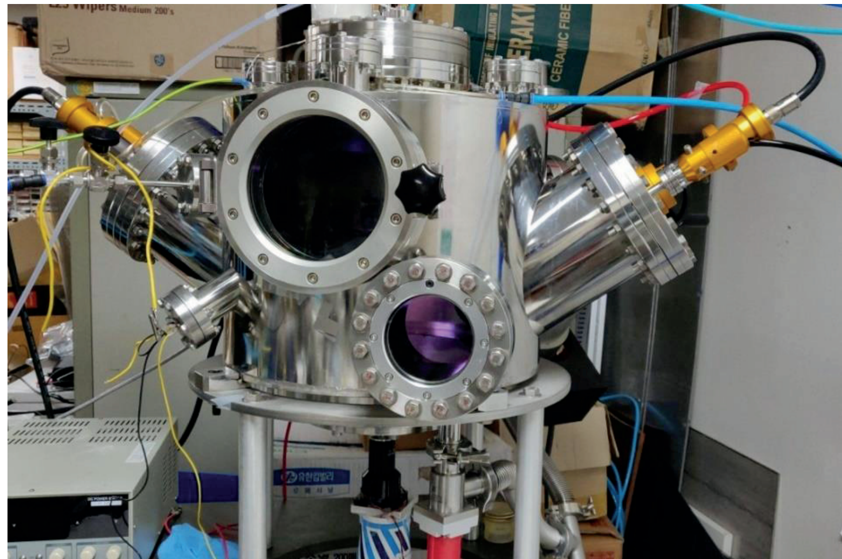

Figure 2. 2 Re-designed Stainless steel Vacuum Chamber with Dual MS gun at degree oblique angle

제주대학교 중앙도서관
JEJU NATIONAL UNIVERSITY LIBRARY

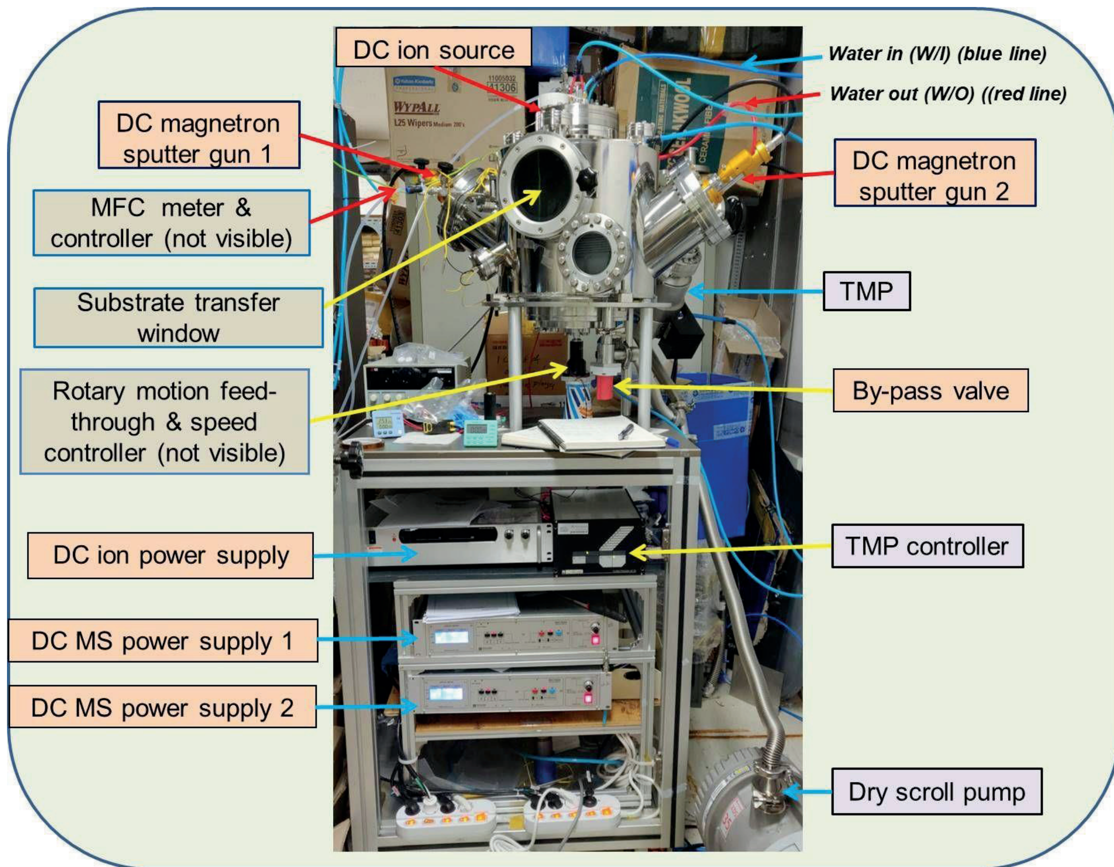

Figure 2. 3 Experimental setups (with all components and devices) for thin film deposition by using DC magnetron sputtering with DC ion source

2.2. Experimental setup

Thin-film was fabricated on the Mo substrate by a sputter deposition method. It was performed in a high vacuum chamber (both single and dual MS gun deposition) by using a DC magnetron sputtering source (magnetron sputter source, Korea Vacuum Technology, as shown in Figure 2.4). Complete experimental setup (dual MS gun type) with all the components and devices attached to it, is shown in Figure 2.3. To achieve a high vacuum, the turbo-molecular pump (controller NT20; Turbo vac 361, Leybold

제주대학교 중앙도서관
JEJU NATIONAL UNIVERSITY LIBRARY

Vacuum GmbH, Germany) and dry scroll vacuum pump (XDS 35i, Edwards) were used.

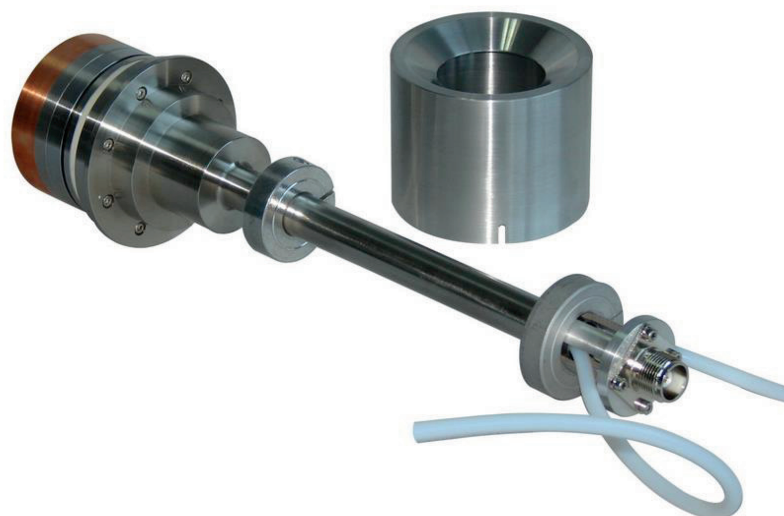

Figure 2. 4 Schematic images of water-cooled DC magnetron sputter gun

Figure 2. 5 Image of 2" diameter and 1/4th" thick Zr target

제주대학교 중앙도서관
JEJU NATIONAL UNIVERSITY LIBRARY

In our experiment, we kept a base pressure of 10-12 µTorr and a working pressure of 5 mTorr for the Ar gas. The distance between the interlayer (Nb/Zr) target and the substrate was 120 mm, and the Rh target to the substrate was 70mm. All the target materials had 99.95% purity, with 50.8 mm diameters and 6.35 mm thicknesses (4science.net, South Korea, as in figure 2.5). Dual DC magnetron sputter guns (as in figure 2.4) were ignited one at a time with a different power rating (e.g., 40 W, 100 W, and 200 W) by using a power supply (SDC1022A, 2 KW psplasma, South Korea).

DC hollow cathode ion sources, as shown in figure 2.6, were used to assist the DCMS during deposition. Figure 2.6 (a) is the view of the inside structure, and (b) is the image from the top of the ion source used in the experiment. Dc power to the ion source is supplied by Matsusada Precision (AU Series 600 W) throughout the ion-assisted deposition, 10 SCCM Ar gas was supplied through the MFC and control valve.

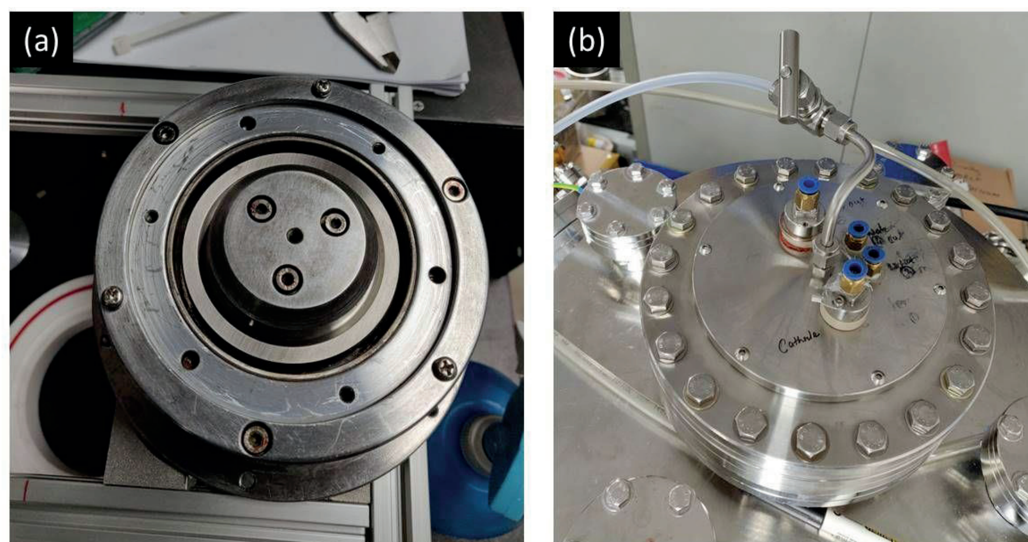

Figure 2. 6 Hollow cathode ion source

In our study, we applied three different methods for the deposition of thin-layer films (Rh-Nb-Zr) on the Mo substrate. At first normal angle deposition (NAD)

제주대학교 중앙도서관
JEJU NATIONAL UNIVERSITY LIBRARY

technique is used, where surfaces of the target and substrate are parallel to each other or particle flux direction is perpendicular (90° angle) to the substrate's surface. The second method of deposition is to deposit a thin film by oblique angle deposition (OAD). Here incoming particles incident angle is 54° with the vertical plane and third deposition process is done by ion-assisted oblique angle deposition (IA-OAD). In all experiments, the substrate base kept fixed or rotated at a constant speed of 20-25 RPM through a rotary motion feed-through (MVF-106A, Huntington Vacuum Products, USA)

In the experimental setup fan and water-cooling systems were employed to cool the devices and instruments. The heat developed on the sputter gun and ion source during the deposition were cooled by using chiller (refrigerated bath circulation, RC-10V, JEIO TECH, South Korea) by circulating cold water around the target area. This heat was converted from electrical energy from the power supply through the target to thermal energy. For better heat transfer, the chiller temperature was kept at 20 ℃ and a flow rate of about 5.5 L/min. The temperature of TMP and dry scroll pump was controlled by supplying direct tap water during the operation.

Parameters such as the target-to-substrate distance, the working pressure of the Ar gas, and the flow rate (total flow rate30 SCCM) was kept constant throughout the procedures. The LineTech Korea MFC (M3030V) and the readout control unit (FM 30VP) were used to manage the gas flow rate. Vacuum valves and vacuum pressure gauges type were the product of Pfeiffer Vacuum GmbH, Germany.

Fabricated interlayered Mo/Rh mirrors were heat-treated in a vacuum oven (10 Torr, JSVO-30T, jSR, South Korea) on 200 ℃ for 4 to 6 hours, at a heating rate of

제주대학교 중앙도서관
JEJU NATIONAL UNIVERSITY LIBRARY

1 °C/minute, and allowed them to cool naturally to room temperature (RT). This heat treatment allows the reduced str on the coated films, which were developed during the deposition. With the results of the heat treatment, we can analyze the thermal effect on the surface of the mirrors

2.3. Substrate material and preparation method

Substrate materials used for the experiment were Si (100) wafers (Silicon Technology Corporation) and Mo mirrors (Cloudray Laser Solution, China) on which target materials were deposited, as shown in figure 2.7 and 2.8. The Si wafers, however, were used only for thickness measurements.

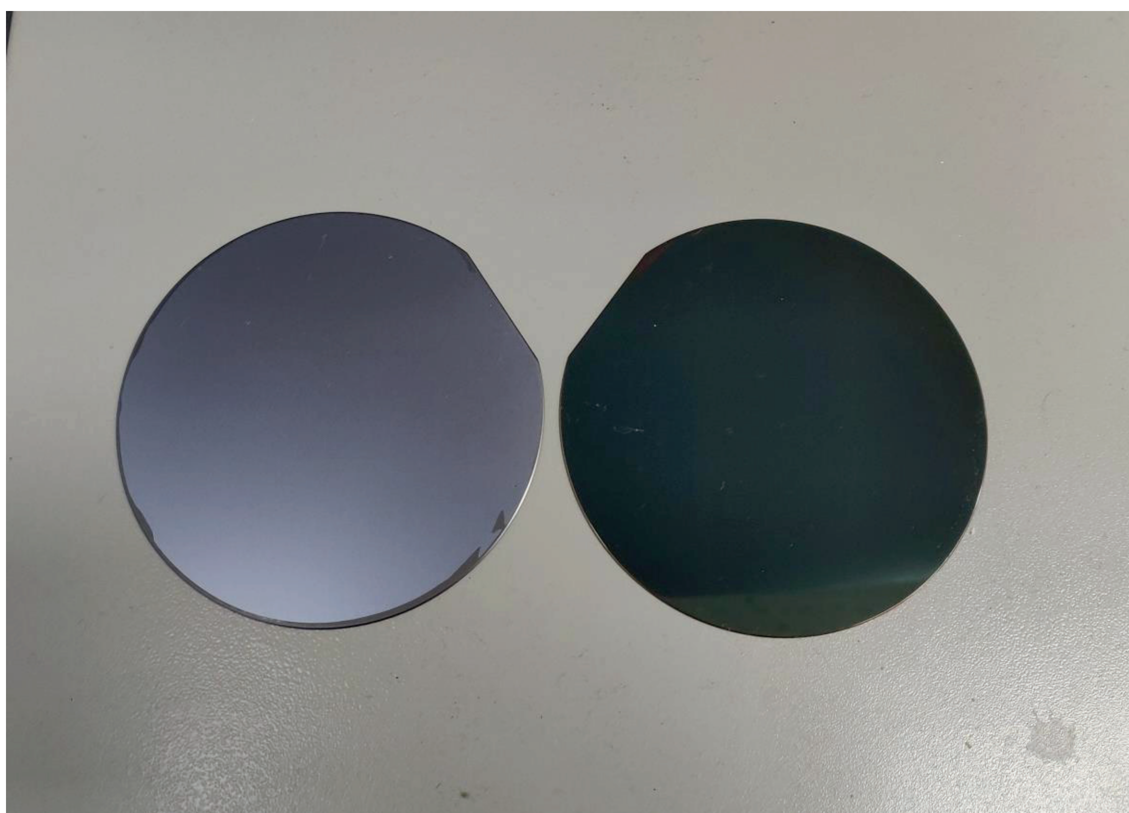

Figure 2. 7 commercially purchased silicon wafer (100)

제주대학교 중앙도서관
JEJU NATIONAL UNIVERSITY LIBRARY

Commercially available Mo mirrors with 20 mm diameters and 3 mm thicknesses were used as the base materials throughout the experiment. The surfaces of the Mo mirrors were mechanically polished to achieve an average roughness of 6-10 nm. The specification of the Mo mirror is shown in figure 2.9.

Figure 2. 8 Mo mirror manufactured by Cloudray laser technology

제주대학교 중앙도서관
JEJU NATIONAL UNIVERSITY LIBRARY

Specifications

Figure 2. 9 Specification of Mo mirror by Cloudray Laser technology (curtesy cloudray laser ltd)

2.4. Substrate preparation

The Si (100) wafer and Mo mirror substrates were cleaned using an ultrasonic cleaner (2300, Chosun Scientific Co., South Korea). Substrates were sonicated in acetone for 10 minutes and in ethanol for 5 minutes. They were then rinsed in deionized (DI) water and dried with N_2 gas. Before the deposition, the cleaned samples were heated for an hour at 100°C to remove residual impurities to reduce the surface stress to improve the adhesion of the deposited layers. Our Mo substrate sizes of diameter 20 mm and 3 mm thickness were used.

2.5. Thin-film deposition

A thin film of niobium (Nb), zirconium (Zr), and rhodium (Rh) was deposited on a Mo substrate in a controlled environment. In all thin-film fabricated samples,

제주대학교 중앙도서관
JEJU NATIONAL UNIVERSITY LIBRARY

approximately 190 nm total thickness was maintained (as in figure 2.10) to control the blister formation and to bulge off the film from the surface. The thin interlayers were 40 nm, and Rh thin film for the top layer was 150 nm thick. We choose the small thickness of films as the minimum thickness of film 150 nm to several microns was used for the FMs [24] During the experiment, it is noticed that ambient temperature, air quality, and humidity affect the quality of the deposited film and deteriorate almost immediately. So handling the substrate before and after the deposition is crucial. But after the vacuum heat treatment of the substrate at 200 ℃ for 4 to 6 hrs (as shown in figure 2.11), deterioration of film did not appear for a very long time.

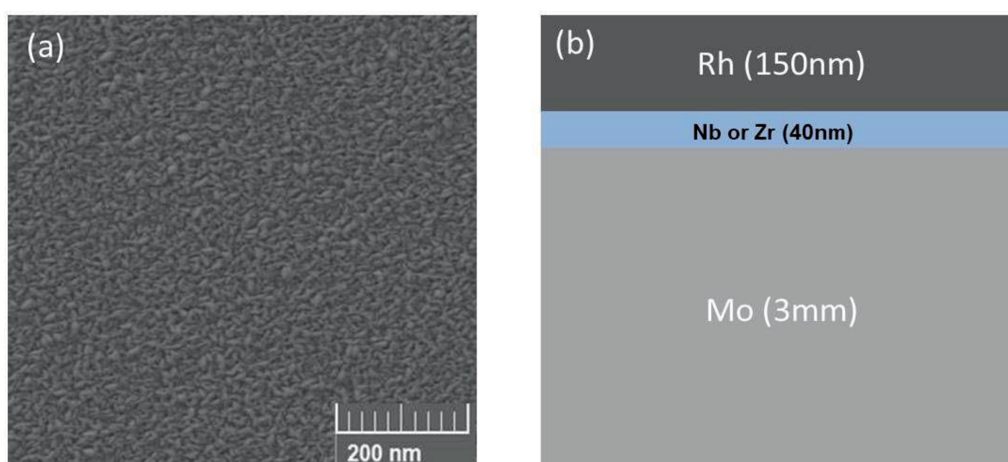

Figure 2. 10 (a) surface image and (b) schematic diagram of Mo coated mirror.

제주대학교 중앙도서관
JEJU NATIONAL UNIVERSITY LIBRARY

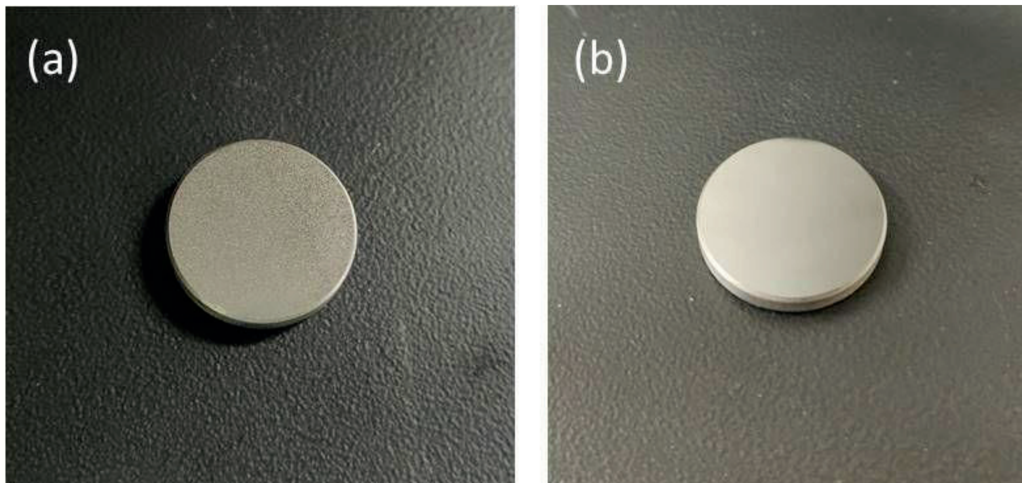

Figure 2. 11 Image of Rh coated Mo/Rh Mirror (a) deteriorated and (b) fine surface

Distance between the substrate surface and target or work distance (WD) and power supplied during the thin film fabrication time affect the deposition rate. Substantial iterations of work have been done to get optimum parameters for better deposition rate as well as working Ar gas pressure and power for our purpose of work. Table 2.1 highlights the deposition rates of the different targets at different WD and incidence angle of deposition at 40 W power supplies. The Si wafers were used to check the film thickness and adhesion at the beginning, as they are cheaper, readily available, and easy to handle. It is seen that substrate preparation quality directly affects the deposition of the film. Therefore, we carefully adopted a proper substrate preparation procedure.

Table 2. 1 Deposition parameters during thin-film coating

Parameters	**Values**
Base pressure	10-12 μTorr
Working pressure	5 mTorr

제주대학교 중앙도서관
JEJU NATIONAL UNIVERSITY LIBRARY

Ar gas flow rate	30 SCCM
Discharge power of the dual magnetron sputtering gun	40 W,100 W, 200W
Target-substrate distance (Normal angle deposition)	60 mm
Target-substrate distance (Oblique angle deposition)	70 mm and 120 mm
Film thickness	Approx. 40 nm (Nb) – approx. 150 nm (Rh)
Target-substrate incidence angle at OAD	54° (vertical)
Normal incidence angle	90° (with the surface of the substrate)
Target dimensions	50.8 mm diameter, 6.25 mm thickness
Substrate temperature	Room temperature
Substrate rotation (revolving)	0 and 25 rpm
Vacuum chamber inner dimensions	320 mm cylindrical height, 370 mm diameter

Later in the study, we also used the ion-assisted deposition to check the quality of the deposited film, assuming better adhesion and reflectivity. The hollow cathode ion

제주대학교 중앙도서관
JEJU NATIONAL UNIVERSITY LIBRARY

source was kept 330mm apart from the surface of the substrate. Simple (lab-made) faraday cup was used to measure ion current from the source. Figure 2.12 shows the ion current measured from the FC in different power supplied at different working pressure. For our purpose, we used 200mA current and 280 V DC supply at 5 mTorr vacuum pressure, the voltage and current were stable. The 5 mTorr pressure was also a working Ar pressure during the operation period of all the experiments.

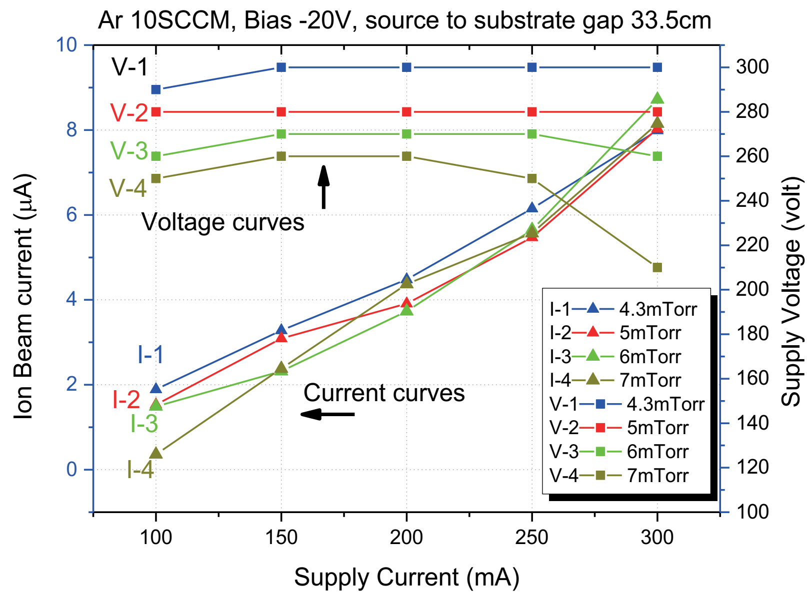

Figure 2. 12 Ion current at the different vacuum pressure and power supplies.

제주대학교 중앙도서관
JEJU NATIONAL UNIVERSITY LIBRARY

2.6. Characterization techniques

Thin-film coating industries are grown dramatically. Films are grown or coated by various materials by using different processes that necessarily requires characterizing to determine properties of the coating. Several analytical techniques have been used to provide information about the characteristics as the chemical composition, amount of trace impurities, or the physical structure. This information is vital to the researchers or manufacturers in order to understand the material and to verify the product. Some of the major instruments used for the characterization of this study were briefly explained below.

2.7. Field emission scanning electron microscopy (FESEM)

TESCAN MIRA 3, FESEM employs electron beams in order to get information from a sample at the nanoscale level. The main types of singles that are detected are the backscattered electrons (BSE) and secondary electrons (SE) which generate an image of the samples at a very high magnification where 5 to 15 kV acceleration voltage was used. In the earlier phase of this study FESEM, JOEL (JSM-6700F) was also used for surface characterization.

.

제주대학교 중앙도서관
JEJU NATIONAL UNIVERSITY LIBRARY

Figure 2. 13 Field emission scanning electron microscopy (FESEM) (TESCAN MIRA 3)

2.8. EDS (Energy-dispersive X-ray Spectroscopy)

EDS is a standard method for identifying and quantifying elemental composition in a sample. The EDS analysis was done along with the FESEM (TESCAN), Energy-dispersive X-ray Spectroscopy analysis has now become standard practice of the surface morphology, and it is an essential part of an SEM.

2.9. Thickness Monitor

To measure the thin film thickness deposited by DCMS, the Cressington MTM-10 thickness monitor was used, which gives the flexibility to approximate the thickness of the films. Quartz crystal sensor is used to measure the thickness of the material at which rate it is being deposited. Most of the time, deposited material on the substrate and

제주대학교 중앙도서관
JEJU NATIONAL UNIVERSITY LIBRARY

reading on the monitor sensor might not be the same. Therefore, thickness monitors use the tooling factor to compare the amount of material deposited.

$$F_m = F_i\ (T_m/T_i) \qquad (2.1)$$

where F_i is the initial tooling factor, T_i is the measured film thickness by the instrument, and T_m is the actual thickness deposited film.

Figure 2. 14 Cressington MTM-10 thickness monitor

2.10. X-ray diffraction (XRD)

XRD is the most widely accepted non-destructive analytical technique to identify the crystalline structure of the materials sample purity. Here Empyrean, Malvern Panalytical UK, XRD was used to obtain crystalline phase information, which operates at 40 kV and 40 mA current using Cu-Kα radiation at room temperature. The calculation made on the Bragg's equation, a detector records and processes the x-ray signal, which in turn converts into a count rate and the reflected X-ray peaks obtain on each atomic plane in the crystal lattice. In the X-ray diffractometer sample rotates in the

제주대학교 중앙도서관
JEJU NATIONAL UNIVERSITY LIBRARY

path of the collimated X-ray beam at an angle θ and the goniometer rotates at an angle of 2θ, while the detector is mounted on the arm to collect the diffracted X-rays and

Figure 2. 15 Image of Empyrean Panalytical X-ray Diffraction (XRD)

2.11. 3D nano surface profiler

It is the non-contact, non-destructive micro or nanoscale surface measurement and characterization device. The roughness of the films was measured by using a 3D Nano-surface profiler system (Optical surface profiler NV-2400, Nanosystem, South Korea). Micro/Nanoscale images were captured by using an i50x objective lens in high accuracy mode on the area of 50 μm^2.

제주대학교 중앙도서관
JEJU NATIONAL UNIVERSITY LIBRARY

Figure 2. 16 Photographic images of 3D Nano-surface profiler system (Optical surface profiler NV-2400)

2.12. UV-VIS spectrophotometer

An ultraviolet-visible spectrophotometer (UV-VIS) is the instrument that measures the wavelength and intensity of absorption or reflectance of near-ultraviolet and visible light. The light source is usually a deuterium lamp for the UV range measurement and tungsten for visible measurements. The prism separates the wavelengths of this continuous light source, and spectra are obtained by scanning the wavelength at a single wavelength. Here UV-VIS spectrophotometer (S-3100, SCINCO Co. Ltd. South Korea) was used for measuring the reflectivity of the fabricated mirror.

제주대학교 중앙도서관
JEJU NATIONAL UNIVERSITY LIBRARY

Figure 2. 17 UV-VIS spectrophotometer (S-3100, SCINCO)

2.13. Scratch tester and peeling test

For basic mechanical (contact test) characterization, scratch and tape tests were used to check the adhesion strength of the films. The lab-made mini scratcher was used to perform scratch on the mirror surface, as shown in figure 2.16 (a). A pressure-sensitive adhesive tape (ASTM D3359, Elcometer, USA) (as in figure 2.16 (b)), is pressed with a good enough pressure onto the film and rapidly stripped off. The lab-made scratch tester motor can pull till the approximately scratch length was up to10-20 mm along the surface of the mirror. The wear tracks were observed with an optical microscope (2MP, 20x - 400x, 8 LED, USB Digital Microscope, China). Figure 2.16 (c) and (d) show the PC and mini microscope setup, which gives real-time imaging on PC via USB interface and the help of software.

제주대학교 중앙도서관
JEJU NATIONAL UNIVERSITY LIBRARY

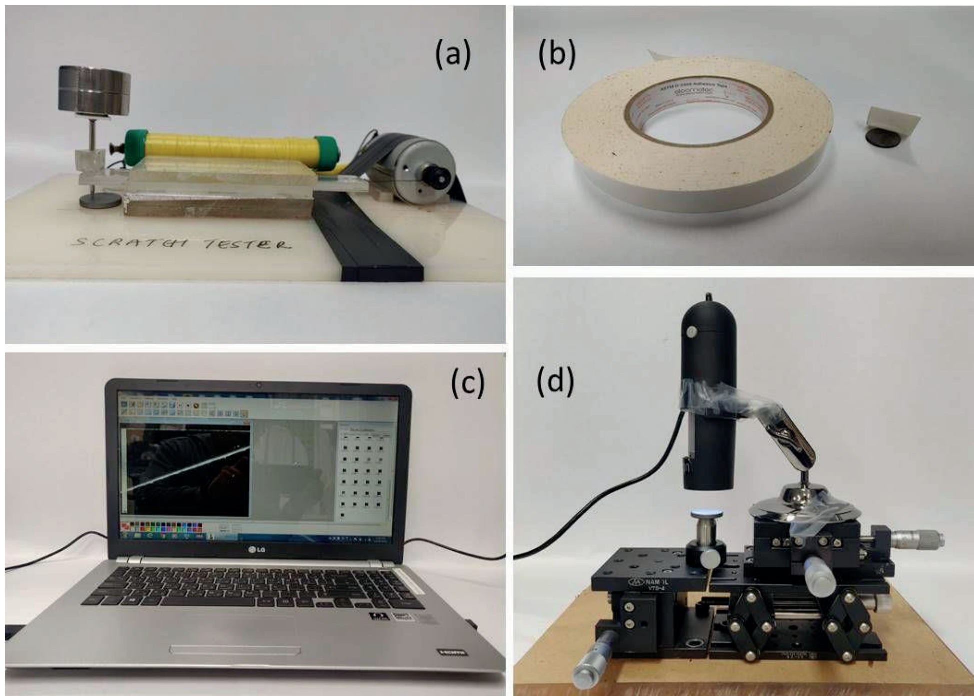

Figure 2. 18 Lab-made scratchers (a), ASTM D3359 tape (b), and (c)&(d) are a computer system and mini microscope to capture the magnified images

제주대학교 중앙도서관
JEJU NATIONAL UNIVERSITY LIBRARY

CHAPTER 3

Deposition and Characterization of a Rh Thin Films with an Nb Interlayer on a Molybdenum Mirror for ITER First-Mirror Application

3.1. Introduction

All the essential optical and imaging systems require high performance for plasma diagnostics. Most plasma-facing components (PFCs) use metallic mirrors for optical diagnostics. In particular, reflectivity influences the quality and reliability of the performance of mirrors. Plasma-facing mirrors have lower-quality reflection due to erosion owing either to the high energetic charge exchange neutral particles as well as UV, X-ray and gamma radiation, or impurities deposited on the mirror's surface by the materials eroded from the in-vessel components of ITER. Many research laboratories are investigating the diagnostic mirrors of high-quality, reliable, and cost-effective [25] that can withstand the plasma environment. The main impact on the optical and the polarization characteristics are believed to be from the erosion processes caused by the fast-moving charge exchange neutrals (CXNs) and the mirror's location in the main chamber. Different locations of the FM have different heat flux intensity and have a different rate of degradation of optical properties. The mirror surface which faces the plasma directly will likely be eroded, and degraded faster. Many researchers have found that single-crystal (SC) [26] mirrors have better quality as they can maintain their optical and morphological properties under Ar ion sputtering [27]. SC Mo and Rh-coated mirrors are reported to be under consideration as the most promising metallic mirror materials for ITER. The technology for producing Rh-coated mirrors is presently being developed in several laboratories [28].

제주대학교 중앙도서관
JEJU NATIONAL UNIVERSITY LIBRARY

Neither of the two mirrors mentioned above, however, can significantly preserve its reflectivity after exposure to the high temperature [29]. The minimization of thermal distortions in the mirror's thin layered surface by keeping the thermal stresses at an acceptable level is an essential structural issue for all mirrors, especially those under ITER conditions. Hence thin layers were made up of different combined materials, like Mo and Rh [30]. Mo is considered as a first mirror (FM) due to its excellent advantages under the sputtering condition, such as its low sputtering yield [31], cost-effectiveness, corrosion, and heat resistance. Rh thin film can be deposited on the Mo mirror to enhance the performance in the ITER environment as it has high reflectivity in the visible range and high thermal resistance properties[32]–[34]. Rh also prevents oxide and carbide formation as it has low chemical reactivity [2]. Due to the differences in thermal expansion coefficients and the lattice mismatch between two materials, surface adhesion of thin films become weaker and are prone to get damaged easily in the plasma environment. Therefore, to prevent such type of problems, interlayers are introduced between the thin films. Here, we considered niobium (Nb) as a suitable interlayer material between Rh and Mo because of its intermediate thermal expansion coefficient and lattice parameter (Mo: 4.8 μm/m-K, 3.15 Å; Nb: 7.3x μm/m-K, 3.30 Å; Rh: 8.2 μm/m-K, 3.8 Å at RT) [11].

Instead of high power, we supplied a low deposition power of 40 W, which leads to a lower deposition rate and a smooth deposition. Ions and electrons of low kinetic energy at the low supplied power will not damage the surface of the substrate and will keep the substrate temperature close to room temperature. Higher power means a higher deposition rate. Higher deposition rates at low temperatures might affect the single crystal growth [12] and degrade the surface orientation [13]. The thin film will

제주대학교 중앙도서관
JEJU NATIONAL UNIVERSITY LIBRARY

be porous in the microstructure and challenging to control the film's thickness.

In this work, the properties of the Rh thin film on a Mo mirror with a thin Nb interlayer were studied. The Rh thin films were deposited via DC magnetron sputtering, and their properties (reflectivity, morphology, and stability) were investigated. The optical property and the stability of the deposited films before and after the heat treatment process were also investigated to ensure their longevity in the plasma environment.

3.2. Experimental Procedure

3.2.1. Materials

Si (100) wafers (Silicon Technology Corporation) and Mo mirrors (Cloudray Laser Solution, China) were used as substrates on which target materials were deposited. The Si wafers, however, were used only for thickness measurements. Industrially prepared Mo mirrors with 20 mm diameters and 3 mm thicknesses were used as the base materials throughout the experiment. The surfaces of the Mo mirrors were mechanically polished to achieve an average roughness of 6-10 nm.

The Mo mirror substrates were cleaned using an ultrasonic cleaner (2300, Chosun Scientific Co., South Korea). Substrates were sonicated in acetone for 10 minutes and in ethanol for 5 minutes. They were then rinsed in deionized (DI) water and dried with N_2 gas. Before the deposition, the cleaned samples were heated for an hour at 100 °C to remove residual impurities to reduce the surface stress and to improve the adhesion of the deposited layers.

제주대학교 중앙도서관
JEJU NATIONAL UNIVERSITY LIBRARY

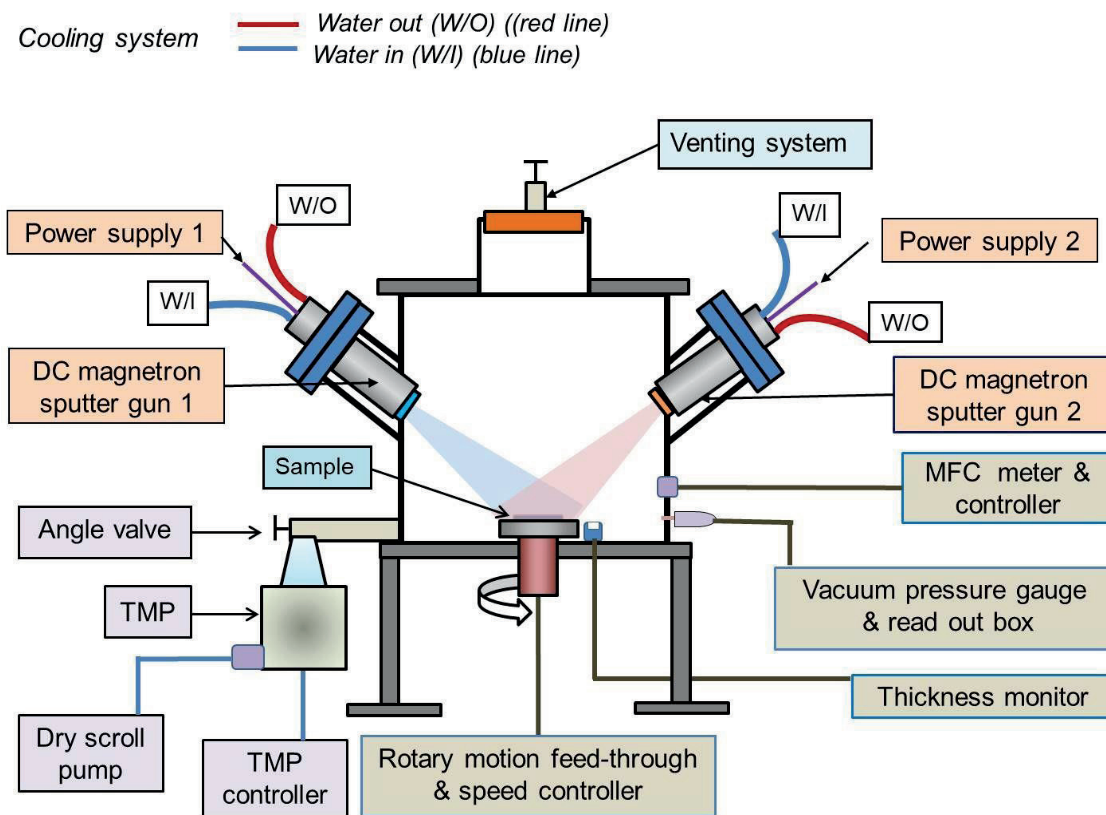

Figure 3. 1. Schematic diagram of the experimental setup for DC magnetron sputtering.

3.2.2. Thin-film deposition

Depositions of the thin film were performed in a high-vacuum chamber by using a DC magnetron sputtering source (magnetron sputter source, Korea Vacuum Technology), as shown in Fig. 3.1. The turbo-molecular pump (controller NT20; Turbo vac 361, Leybold Vacuum GmbH, Germany) and dry scroll vacuum pump (XDS 35i, Edwards) were used to achieve a base pressure of 12 μTorr and a working pressure of 5 mTorr for the Ar gas. The distance between the target and the substrate was kept at 120 mm. All the target materials had 99.95% purity, with 50.8 mm diameters and 6.35 mm thicknesses (4science.net, South Korea). Dual DC magnetron sputter guns were ignited one at a time with a power rating of 40 W by using a power supply (SDC1022A,

제주대학교 중앙도서관
JEJU NATIONAL UNIVERSITY LIBRARY

2 KW psplasma, South Korea), while the sample holder was rotated through a rotary motion feed-through (M/N: MVF-106A, Huntington Vacuum Products, USA). Much of the electrical energy from the power supply through the target was converted to thermal energy to heat which was cooled by using chiller (refrigerated bath circulation, RC-10V, JEIO TECH, South Korea) by circulating cold water around the target area. For better heat transfer, the chiller temperature was kept at 20 °C and a flow rate was set about 5.5 L/min. Parameters such as the target-to-substrate distance, the working pressure of the Ar gas, and the flow rate were kept constant throughout the processes. The other deposition parameters were summarised in Table 1. To study the thermal effect, we heat treated the as-prepared mirrors in a vacuum oven (10 Torr, JSVO-30T, jSR, South Korea) on 200 °C for 6 hours, at a heating rate of 1°C/minute, and allowed them to cool naturally to room temperature (RT).

Table 3. 1 Parameters used during the DC magnetron sputtering

Parameters	**Values**
Base pressure	12 μTorr
Working pressure	5 mTorr
Ar gas flow rate	30 SCCM
Discharge power of the dual magnetron sputtering gun	40 W
Target-substrate distance	120 mm

제주대학교 중앙도서관
JEJU NATIONAL UNIVERSITY LIBRARY

Film thickness	Approx. 40 nm (Nb) – approx. 150 nm (Rh)
Target-substrate incidence angle	36° (horizontally)
Deposition rate	8 nm (+/- 3 nm)/min (Nb) 12 nm (+/- 3 nm)/min (Rh)
Target dimensions	50.8 mm diameter, 6.25 mm thickness
Substrate temperature	Room temperature
Substrate spinning (revolving)	25 rpm
Vacuum chamber inner dimensions	320 mm cylindrical height, 370 mm diameter

3.2.3. Characterizations

To validate the results of this study, we used various methods and instruments to characterize all the mirrors. The surface morphologies were observed via field emission scanning electron microscopy (FESEM; JSM-6700F, Joel, Japan). Film thickness measurements were done by using FESEM and Cressington MTM-10 (UK). The film's crystallinity and microstructure were recorded via X-ray diffraction (XRD; Empyrean, Malvern Panalytical, UK). The roughness of the films was measured by using a 3D Nano-profiler system (Optical surface profiler NV-2400, Nanosystem, South Korea). The images were captured by using an objective lens on the area of 50 μm^2. The reflectivity of the deposited films was measured with a UV-VIS spectrophotometer

제주대학교 중앙도서관
JEJU NATIONAL UNIVERSITY LIBRARY

(S-3100, SCINCO Co. Ltd., South Korea).

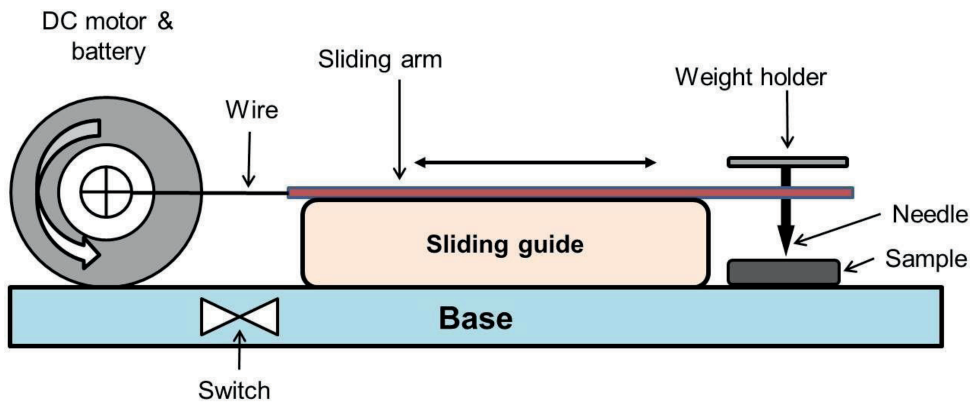

Figure 3. 2. Schematic diagram of the lab-made scratch tester.

The adhesions of the deposited films on the substrates were tested using two well-known tests: the tape and the scratch tests. The tape test was completed by using adhesive tape (ASTM D3359, Elcometer, USA) while the scratch test was performed using a lab-made scratch tester, as schematically shown in Fig. 3.2. The main components of the scratch tester were a DC motor, which drove the tungsten-carbide needle (tip radius: 250 μm) [38] across the surfaces of the mirrors to create a scratch with predetermined vertical loads. The needle holder, which was connected to the driving shaft of the motor via a piece of yarn, was guided by using a sliding guide that traveled back and forth in the horizontal direction. The testing mirror was positioned below the tip of the needle and was attached using double-sided tape to prevent its movement during scratching. The tip of the needle was cleaned with ethanol and a lint-free wiper before and after the scratch test. The scratching speed of the tip was set to 37 mm/s, and the length of the scratch was approximately 10 - 20 mm along the surface of the mirror. A normal load in the range of 0.5 - 1.5 N was applied on the

제주대학교 중앙도서관
JEJU NATIONAL UNIVERSITY LIBRARY

surface to make a scratch mark under a constant rate. The wear tracks were observed with an optical microscope (2MP, 20x - 400x, 8 LED, USB Digital Microscope, China).

3.3. Results and Discussion

FESEM, in conjunction with energy-dispersive X-ray spectroscopy (EDS), was used to investigate the surface morphology and elemental composition of the deposited surface layers. Figure 3.3(a) and (b) show the surface profile and the cross-sectional SEM images of the Rh/Nb thin film deposited at 40 W. The surface image shows that the film has dense and uniform grains with an average size of ~15 nm. The thicknesses of the Nb and Rh interlayers were determined by the cross-sectional FESEM image as shown in Fig. 3(b). Under the given deposition conditions, the thicknesses of the Rh thin film and the Nb interlayer were 150 nm and 40 nm, respectively. In the experiment, we kept the film thicknesses approximately 190 nm because, beyond that thickness, the deposited thin films appeared to form blisters and peel off due to thermal expansion and mismatch of lattice parameters [12]. The deposited films were seen to have dense, columnar structure [8] along the growth direction. The formation of well-defined columnar structures in the thin film was due to the high surface diffusion of adatoms and periodically nucleated on the surface of the growing crystals [13]. EDS images ensure the presence of the Mo material in the pristine form (Fig 3(c)), and fig. 3(d) confirms the presence of Rh as a major element alongside Nb and Mo, in the Rh/Nb thin-film sample. Minimal traces of impurities, like carbon, were detected as contaminants on the sample surface.

제주대학교 중앙도서관
JEJU NATIONAL UNIVERSITY LIBRARY

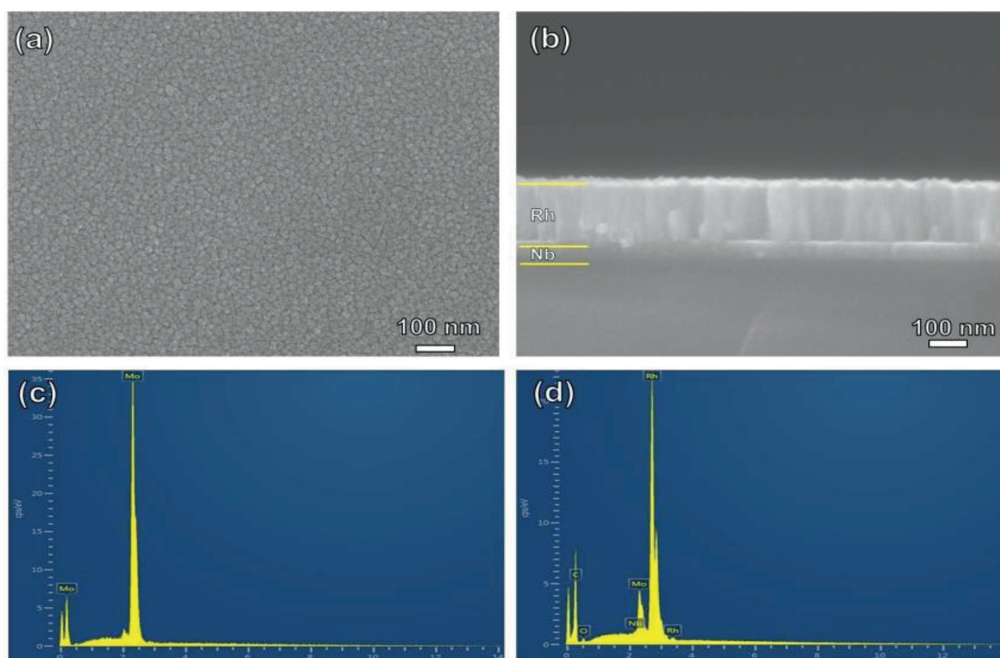

Figure 3. 3 FESEM images and EDS elemental compositions of the Rh/Nb thin films deposited on Mo mirrors via DC magnetron sputtering. Surface (a) and (b) cross-sectional images of the Rh/Nb thin films. EDS spectra of the (c) pristine Mo mirror and the (d) Rh/Nb thin film

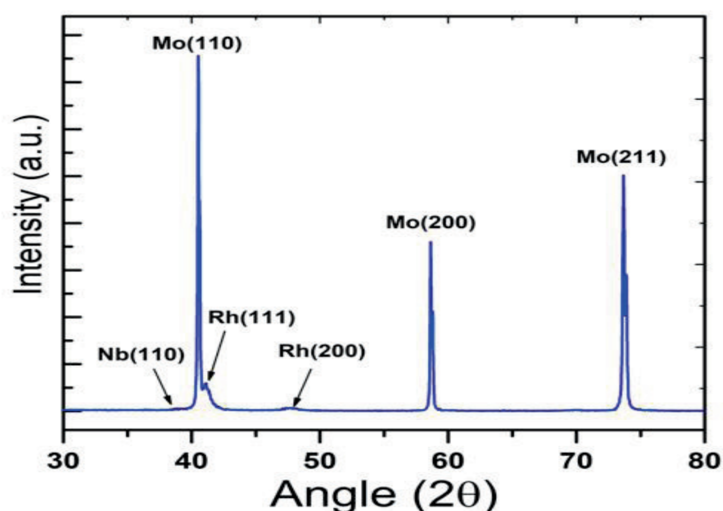

Figure 3. 4Figure 3. 5 XRD patterns of the Rh/Nb thin film deposited on a Mo substrate.

제주대학교 중앙도서관
JEJU NATIONAL UNIVERSITY LIBRARY

The microstructures of the deposited film were further characterized by using XRD, as shown in Fig. 3.4. The XRD image shows sharp diffraction peaks at 2θ - 40.52°, 58.64° and 73.67°corresponding to the (110), (200) and (211) reflection planes of the body-centered cubic Mo substrate (JCPDF #00-042-1120), respectively. The Rh top layer shows distinct reflection peaks at 2θ - 41.12° and 47.759°, corresponding to the (111) and (200) planes, respectively (JCPDF #00-005-0685). The Nb interlayer shows a very weak diffraction peak at 2θ - 38.59°, corresponding to the (110) plane. We observed from the XRD results that there were no diffraction peaks of other impurities. The multilayers films of high crystalline purity were deposited with Rh major elements.

Further, the as-fabricated multilayer Rh/Nb/Mo mirrors were subjected to heat treatment to study the effect of thermal stress on the microstructures and performances of the mirrors. The mirrors were heat-treated in a vacuum oven at 200 ℃ for 6 hours in a 10 Torr vacuum environment and were cooled naturally to room temperature before analysis. FESEM images in Figures 3.5(a) and (b) show the surface morphologies of the Rh/Nb/Mo mirrors before and after the heat treatment. Results revealed that after the heat treatment, the average grain size of Rh increased from 10-15 to 28-35 nm. Furthermore, the effects of the heat treatment on the film's microstructure and grain size were investigated via XRD. Fig. 3.5(c) shows the high-resolution XRD patterns of the Rh/Nb/Mo mirror before and after the heat treatment, where the Rh (111) peak was analyzed. It is shown that after the heat treatment, the full width at half maximum (FWHM) of the Rh (110) peak was modified and could be obtained through Scherer's relation (1) to access the crystalline size.

제주대학교 중앙도서관
JEJU NATIONAL UNIVERSITY LIBRARY

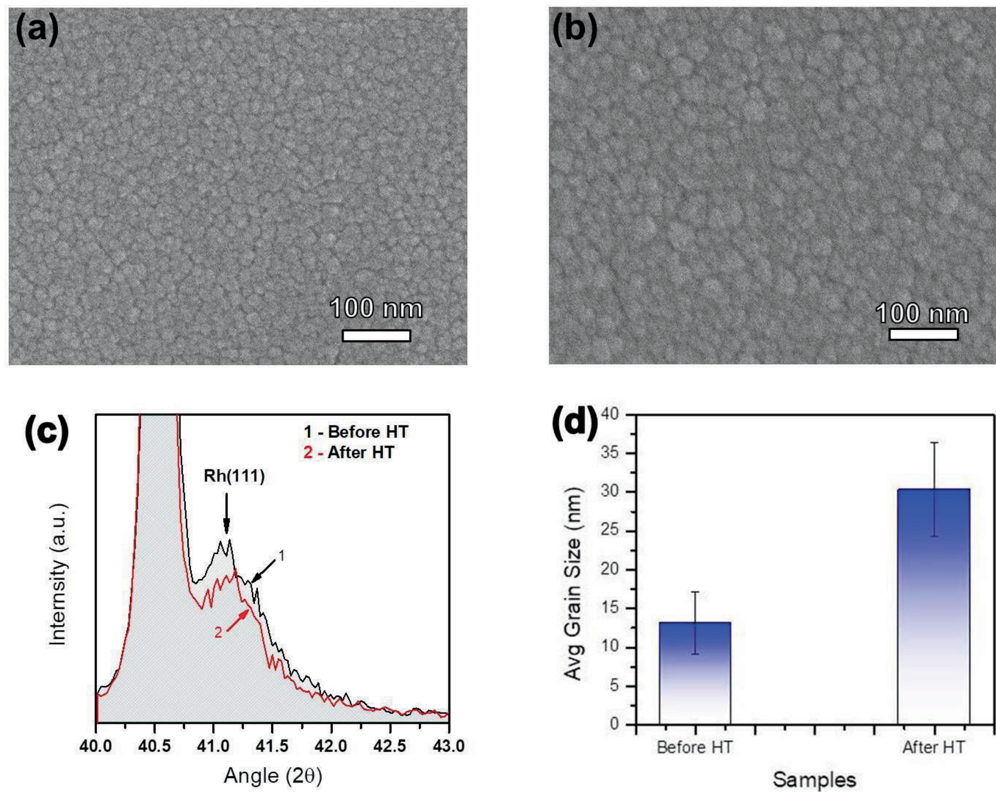

Figure 3. 6 FESEM images of the surface morphology of the Rh mirrors (a) before and (b) after heat treatment (c) XRD pattern and (d) grain sizes of Rh thin films before and after heat treatment.

$$D = k\lambda/\beta\cos\theta, \qquad (3.1)$$

Where k was the shape factor 0.9, the X-ray wavelength was λ (0.15406 nm), β was the FWHM of the peak, and θ was the Bragg diffraction angle ($2\theta/2$). As could be seen in Fig. 5(d), the average crystallite sizes (grains) of the Rh thin film had increased from 13.21 nm before, to 30.37 nm after the heat treatment, which was in good agreement with the SEM result shown in figures 3.5(a) and (b). Consequently, we concluded that high-temperature heat exposure induces the growth of the crystalline size and film density [37], [39]–[41], which in turn would affect the optical properties of the

제주대학교 중앙도서관
JEJU NATIONAL UNIVERSITY LIBRARY

films (to be discussed in the next section).

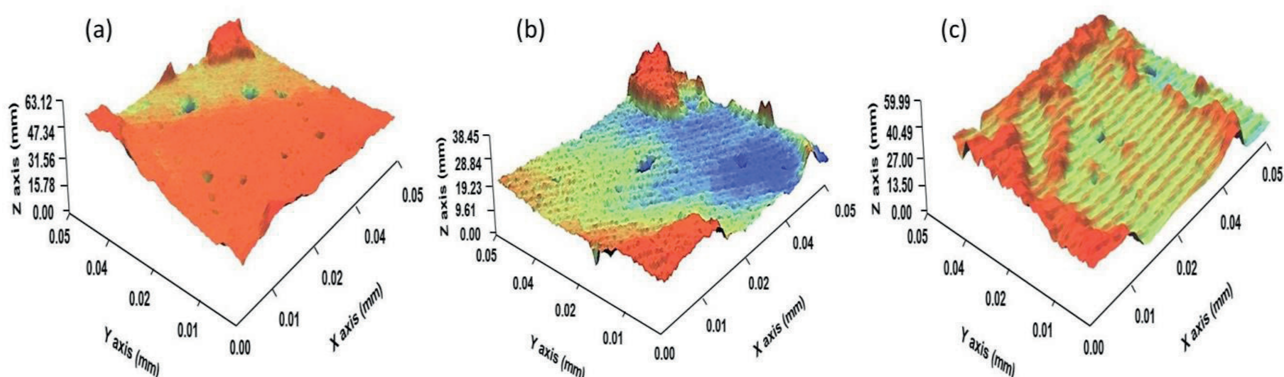

Figure 3. 7 3D surface images of the mirrors show the surface roughness's (a) pristine Mo mirror and the Rh/Nb-thin-film-coated on the Mo mirrors (b) before and (c) after heat treatment.

The surface roughness of the FM is a critical parameter as it directly affects the reflectance of the mirror and its performance in the ITER environment. The roughness levels of the Rh/Nb/Mo multi-layered mirror before and after the heat treatment were measured using a 3D nano-profiler, and the results were compared with the roughness levels of the pristine Mo mirror's surface. Fig.3.6 (a) shows a 3D image of an industrially manufactured pristine Mo surface, which has an average roughness (Ra) of 8.12 nm. We could see there were many pinholes and tiny hillocks with an average depth of 400 nm. Figures 3.6 (b) and (c) present the surface of the Rh thin films in this study, on which the Mo surface with an Nb interlayer was coated, before and after the heat treatment, respectively. The average surface roughness of the film before the heat treatment was about Ra 3.89 nm. The number of pinholes decreased, and the surface became much smoother after the deposition of Rh/Nb films on the surface of the Mo mirrors. Fig. 3.6 (c) shows the surface profile of the Rh/Nb-film-coated Mo mirror

제주대학교 중앙도서관
JEJU NATIONAL UNIVERSITY LIBRARY

after heat treatment. The Rh thin film's roughness was observed to increase from 3.89 to 6.69 nm, probably due to the grain growth of the Rh top layer during the heat treatment. Heat treatment at elevated temperature promotes the growth of grains, which led to the closure of the voids between the grains of the columnar structure and increased the grain density [42]. Due to recrystallization, some grains had lower film surface tension, and the film-substrate interface tension grew at the expense of the other grains. The surviving grains might have (in-plane) diameters much larger than the film's thickness and the surfaces tend to become rougher [43].

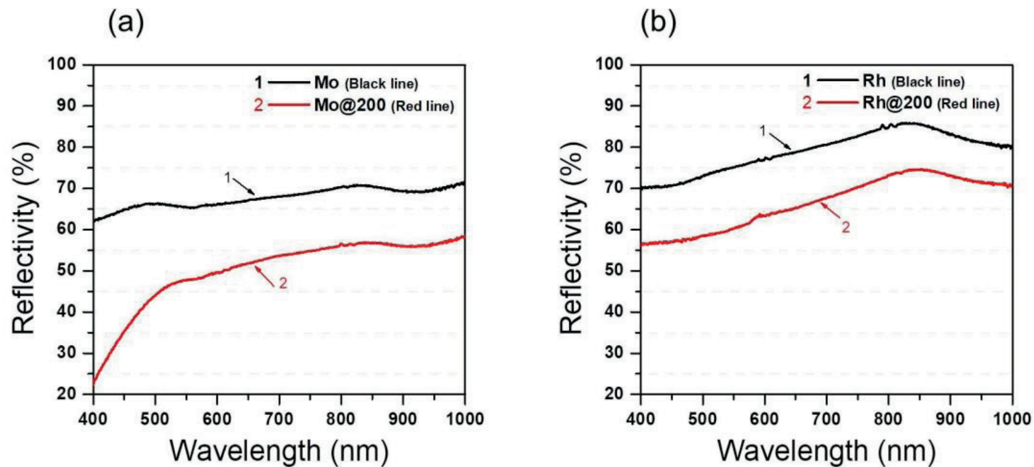

Figure 3. 8 Reflectivity spectra of the Mo mirror (a) and R/Nb-coated Mo mirror (b) measured before and after the heat treatment.

The reflectivity of the FM's surface, the major characteristic for the optical diagnostics in ITER, was measured via UV-VIS spectroscopy, and the results were presented in Fig. 3.7. Figure 3.7(a) shows the reflectivity of the pristine Mo mirror before and after the heat treatment. The reflectivity of the Mo mirror before heat treatment can be seen around 60-70% in the UV-vis range but decreased drastically to 20-45% after the heat treatment. Figure 3.7(b) shows the reflectivity of the Rh/Nb-coated Mo mirror. Initially, the reflectivity of the Rh thin film was higher than

제주대학교 중앙도서관
JEJU NATIONAL UNIVERSITY LIBRARY

that of the pure Mo mirror (70-80% in the UV-vis range, more than 85% at 840 nm). Similarly, the reflectivity of the Rh surface declined after the heat treatment, but the decline was not as dramatic as in the case of Mo mirror (Fig. 3.7a). The reflectivity of the Rh coated surface after the heat treatment was found to have decreased about 10-15% (i.e., it retained reflectivity up to 75%). The effects of the heat treatment process on the drop in reflectivity had been extensively discussed elsewhere [44].

Mirror surface exposed to high temperature for a considerable time would change the surface morphology and the optical characteristic. Rh/Nb coated Mo mirrors were exposed to the high temperature, and we found that their microstructures were modified with the increase in the grain sizes [as shown in Figures 3.4(c) and (d)] and surface roughness (Fig. 3.6) due to recrystallization. We could conclude that the increase in the grain sizes and roughness parameters reduced the reflectivity of the mirror [45].

제주대학교 중앙도서관
JEJU NATIONAL UNIVERSITY LIBRARY

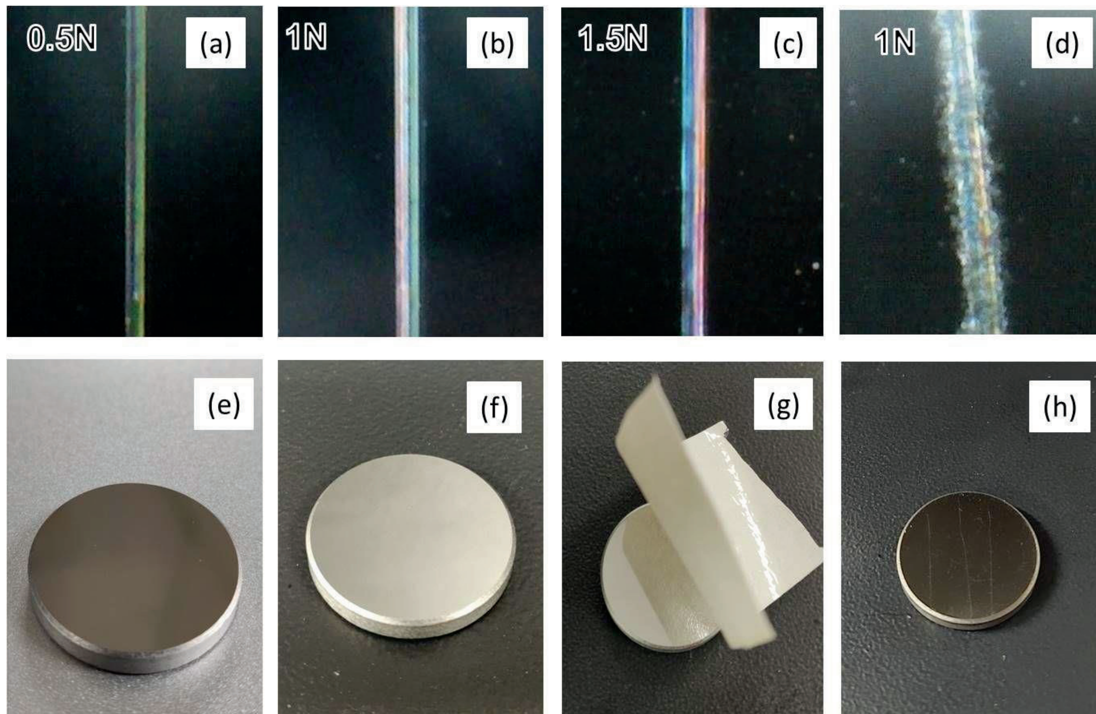

Figure 3. 9 Scratch and tape test results for the Rh/Nb/Mo mirrors. Optical microscope image of a surface line scratch under (a) 0.5 N, (b) 1 N, and (c) 1.5 N for the Rh/Nb/Mo mirrors after the heat treatment. (d) Scratch test results of the Rh/Nb/Mo mirrors before the heat treatment. Rh-deposited mirror (e) before, (f) after, and (g) during the tape test, (h) scratch marks on the coated mirror.

The adhesion strength of the thin film on the substrate mirror is critical as it confirms the stability and longevity of the FM. Therefore, the stability and the adhesion of the deposited Rh/Nb films in this study were confirmed through two well-known techniques: the tape and the scratch tests. A scratch test was performed using a lab-made scratch tester, as described in the experimental section. This test was done at a constant film thickness of 190 nm of the Rh/Nb after heating of the samples at 200 ℃ for 6 hours. The weight of the needle and holder was 3.5 gm. (0.035 N), the

제주대학교 중앙도서관
JEJU NATIONAL UNIVERSITY LIBRARY

minimum force that could be applied to the Rh/Nb/Mo samples. Figures 3.8(a)-(c) show the results of the scratch test performed under the applied loads of 0.5, 1, and 1.5 N on the heat-treated samples. No apparent damage or unusual wear on the Rh/Nb-interlayered thin-film surface was observed. The result of the scratch test that was performed on the surface of the Rh thin film directly deposited on the Mo mirror without any interlayer was shown in Fig 3.8(d). The edges of the scratch line were not smooth and had considerable damage marks, indicating weak adhesion between the Rh thin film and the Mo substrate. The above evidence shows that the depositions of the Nb interlayer between Rh and Mo were essential for ensuring the strong adhesion of the Rh thin films.

Moreover, an additional heat treatment process caused the grains of the thin film to become denser and more compact[42], which increases the hardness and promotes better adhesion strength. Total film thicknesses were kept under 190 nm as a coating with higher film thickness would be more brittle [46]. We speculate that the use of the dual sputtering system for the deposition of both the Nb and the Rh films might be another reason for the better adhesion as that allowed the immediate deposition of the subsequent layers, preventing surface oxidation and contamination. In this study, heating at high temperature was seen to reduce the formation of the crack on the film's surface [41] and strengthen the thin film, but at the expense of the reflectivity.

The tape test results are shown in Figures 8(e)-(g) further confirm the stable adhesion of the deposited films without any blisters. The pressing force given to the tape against the coated surface was approximately 20 N (pressure load was measured on the weighing machine for approximation), which is sufficient to stick the tape properly onto the surface. The scratch and the tape tests show excellent adhesion between Mo

제주대학교 중앙도서관
JEJU NATIONAL UNIVERSITY LIBRARY

and the Rh thin film with the thin Nb interlayer. The introduction of the Nb layer with suitable and matching parameters (e.g., lattice constant and thermal expansion coefficient) between the Rh and Mo played a crucial role in reducing the surface tension during contraction and expansion.

3.4. Conclusion

In conclusion, a new technique for fabricating a rhodium (Rh)-coated molybdenum (Mo) mirror with a niobium (Nb) thin interlayer was demonstrated with promising results. The thin-film-coated mirror can withstand high temperatures and has excellent adhesion quality and acceptable reflectivity. The thermal heating at 200 ℃ for 6 hours increased the grain size and roughness while reducing the reflectivity by 10-15%. The interlayer apparently reduced the problem of thermal expansion between the thin-film layers. Also, the adhesion property increased with increasing substrate hardness. Therefore, using Nb as a thin interlayer can increase the adhesion between Mo and the Rh thin-film layer. Such Mo/Nb/Rh mirrors with better adhesion and high reflectivity can withstand high temperatures for a longer time and can reduce the formation of the blisters involved in the deuterium implantation in the ITER first mirror (FM) for the plasma diagnostic application.

제주대학교 중앙도서관
JEJU NATIONAL UNIVERSITY LIBRARY

CHAPTER 4
Characterization of Zr Interlayer Coated Mo/Rh Mirror

4.1 Introduction

In the experimental fusion reactor plasma viewing or optical diagnostics elements, mirrors are used. Mirrors are used to guide plasma radiation towards the detecting systems in optical and laser-based (International Thermonuclear Experiment Reactor) ITER plasma diagnostics system. The mirror which directly faces the plasma environment called First Mirror. Most plasma-facing components (PFCs) use metallic mirrors for optical and laser-based diagnostics for their high reflectivity and reliability in the harsh plasma environment. According to the recent studies, Plasma-facing mirrors suffer from sputtering the high energetic charge exchange neutral particles as well as UV, X-ray and gamma radiation and redeposition of plasma impurities onto the mirror's surface [26] by the materials eroded from the in-vessel components of ITER and deteriorate the performance and affect the entire optical diagnostic performance.

Reflectivity, durability, and longevity of the first mirror are crucial in the harsh plasma environment. To address crucial properties, various organizations investigating the diagnostic mirrors and are reporting positive results[47]

On the previous chapter proved that using low power DC magnetron sputtering high-quality mirrors can be fabricated by introducing a thin layer of Nb. Here we are characterizing Zr coated mirror as well as comparing it with Nb interlayer coated FMs. The significant impact on the optical and the polarization characteristics are believed to be affected by the erosion processes caused by the fast-moving charge exchange neutrals (CXNs) and the mirror's location in the main chamber. The mirror surface that

제주대학교 중앙도서관
JEJU NATIONAL UNIVERSITY LIBRARY

faces the plasma directly will likely be eroded, and thus it degraded faster. Research articles proved that a mirror composed of crystallites with nano-size guarantees a more uniform erosion during fusion reactor operation [48]. The surface relief pattern would remain small with respect to the wavelength of the reflected light, thus ensuring a low diffuse reflectivity and, ultimately, a more reliable diagnostic. It is also found that crystalline structured [26][8] mirrors have better quality as they can maintain their optical and morphological properties under Ar ion sputtering [27].

Still, at the harsh condition of plasma, to preserve higher reflectivity of mirrors is a major challenge for the actual use of mirrors on the fusion reactor after the exposure to the high temperature [29].

The maximum estimated erosion rate is about 100 nm/year for a single crystal molybdenum mirror. The maximum deposition rate in the worst-case scenario is about ~900 nm/year [49][47]. Hence, it is also the major problem for the redisposition of contaminants and erosion of the mirror surface, and to cleaning the redeposited contaminants, there has been installing the cleaning system and to recover the possible degradation of first mirror reflectivity. Also, there are a lot of studies on the mitigation of deposition on FM surface

Here in this study, we tried to minimize the thermal distortions in the mirror's thin layered surface by keeping the thermal stresses at an acceptable level, it is an essential structural issue for all mirrors, especially those under ITER conditions. Hence thin layers were made up of different combined materials, like Mo and Rh [30]. Mo is considered as a first mirror (FM) due to its excellent advantages under the plasma sputtering condition [31].

제주대학교 중앙도서관
JEJU NATIONAL UNIVERSITY LIBRARY

The cost-effectiveness, corrosion, and heat resistant characteristic. SC materials have proven good optical performance under plasma sputtering conditions, and now they are a primary material for the first mirrors[25]. Rh thin film can be deposited on the Mo mirror to enhance the performance in the fusion plasma environment as it has high reflectivity in the visible range and high thermal resistance properties[27],[48],[54].

Furthermore, the Rh crystal structure is more compact and prevents oxide and carbide formation as it has low chemical reactivity. However, due to the differences in thermal expansion coefficients and the lattice mismatch between two materials, surface adhesion of thin films become weaker and are prone to get damaged easily in the plasma environment. Thus, to prevent such type of problems, interlayers are introduced between the thin films. Here, we considered Zirconium (Zr) as a suitable interlayer material between Rh and Mo because of its intermediate thermal expansion coefficient and lattice parameters (Mo: 4.8 μm/m-K, bcc, 3.15 Å; Zr: 5.7 μm/m-K, hcp = a-3.23, b- 3.23 and c- 5.14 Å; Rh: 8.2 μm/m-K, ccp, 3.8 Å at RT)[36].

Here thin film deposition was accomplished by the various power of 40, 100, and 200 W. The lower the deposition power, the lower the deposition rate and a smooth deposition but longer time to deposit the thicker films [18]. Low K.E of ion and electrons will have a lesser impact on the substrate, and energy transfer will be lower, which in turn keeps substrate temperature close to room temperature. Higher deposition rates at low temperatures might affect the single crystal growth[37] and degrade the surface orientation[51].

In this work, the Zr sandwich between the bulk Mo substrate and Rh film as an

제주대학교 중앙도서관
JEJU NATIONAL UNIVERSITY LIBRARY

interlayer has been deposited to study the adhesion and reflective properties of the Mo/Rh mirror. DCMS was used to deposit the films by both normal and oblique angled deposition techniques and characterized to analyze the optical property and the stability of the deposited films.

4.2 Experimental Procedure

Substrate material for the experiment was used as Si (100) wafers (Silicon Technology Corporation) and Mo mirrors (Cloudray Laser Solution, China) on which target materials were deposited, as shown in the figures 2.7 and 2.8.

The Mo mirror substrates were cleaned using an ultrasonic cleaner. Substrates were sonicated in acetone for 10 minutes and in ethanol for 5 minutes. They were then rinsed in deionized (DI) water and dried with N_2 gas. To remove residual impurities and surface stress build on while handling, samples were heated for an hour at 100 ℃ before placing into the plasma environment to deposit thin film.

4.2.1 Film Deposition

Prior to the actual film deposition on the substrate surface. The vacuum chamber was thoroughly cleaned and pumped down to vacuum pressure of 10 μm as a base pressure to evacuate the residual gases as much as possible. The high vacuum provides a long mean free path for the collision of particles during the sputtering and deposition process [52]. Thin films were fabricated at a working gas pressure of 5 mTorr. Both normal and oblique angle deposition was adopted to deposit the thin film on the substrate.

제주대학교 중앙도서관
JEJU NATIONAL UNIVERSITY LIBRARY

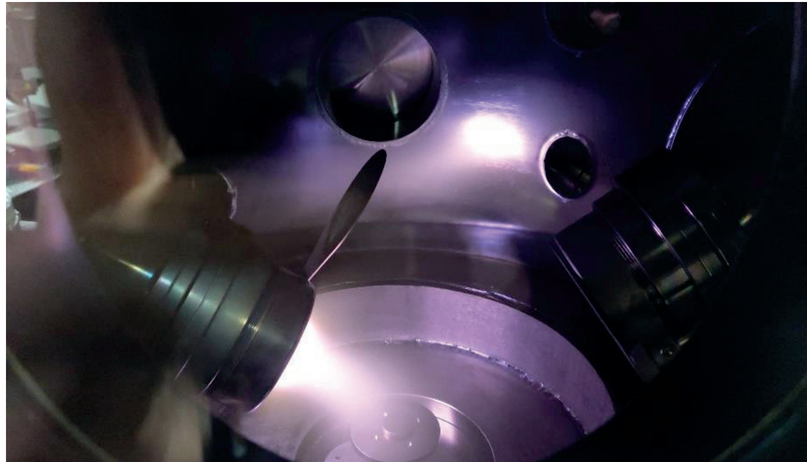

Figure 4. 1Image of actual Ar plasma deposition of Rh thin film on a Mo-Zr substrate

Figure 4.1 shows the actual Rh target sputtered by DC magnetron gun at 54º degree oblique angle of deposition (OAD) and figure 4.2 shows the normal angle of deposition (NAD) where substrate holder is modified in such a way that incidence angle of sputtered particles is 90° degree or normal to the substrate surface. The model of the plasma sputtering process and orientation of sputtering guns are shown in figure 4.3. The parameters that used for deposition of Zr and Rh are shown in table 4.1.

제주대학교 중앙도서관
JEJU NATIONAL UNIVERSITY LIBRARY

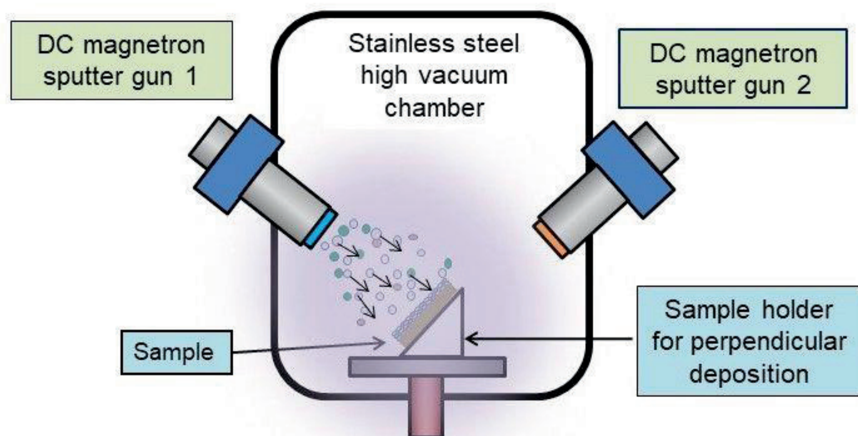

Figure 4. 2 Dual magnetron sputtering used for NAD with a modified substrate holder.

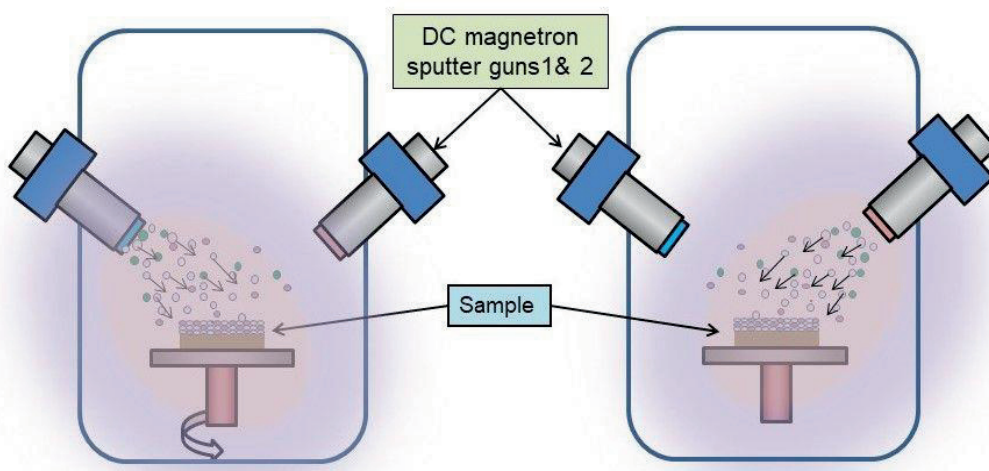

Figure 4. 3 Schematic model diagram of dual DCMS guns for OAD

제주대학교 중앙도서관
JEJU NATIONAL UNIVERSITY LIBRARY

Table 4. 1 Parameter for the DCMS

Parameters	Values
Base pressure	10μTorr
Working pressure	5 mTorr
Ar gas flow rate	30 SCCM
Discharge power of the dual magnetron sputtering gun	40 W, 100 W, 200 W
Target-substrate distance	60 mm and 120 mm
Film thickness	Approx. 40 nm (Zr) – approx. 150 nm (Rh)
Target-substrate incidence angle	90° (NAD), 54°(OAD)
Deposition rate	As in table 4.2
Target dimensions	50.8 mm diameter, 6.25 mm thickness
Substrate temperature	Room temperature
Substrate spinning (revolving)	0, 25 RPM
Vacuum chamber inner dimensions	320 mm cylindrical height, 370 mm diameter

제주대학교 중앙도서관
JEJU NATIONAL UNIVERSITY LIBRARY

Table 4. 2 Deposition rate of Nb, Zr, and Rh at parameter mentioned in table 4.1

Power supply (W)	Deposition rate (nm/min; ±3)					
	Nb (NAD)	Zr (NAD)	Rh (NAD)	Nb (OAD	Zr (OAD)	Rh (OAD)
40	6	8	17	4	5	12
100	18	22	40	12	16	27
200	32	43	87	22	33	48

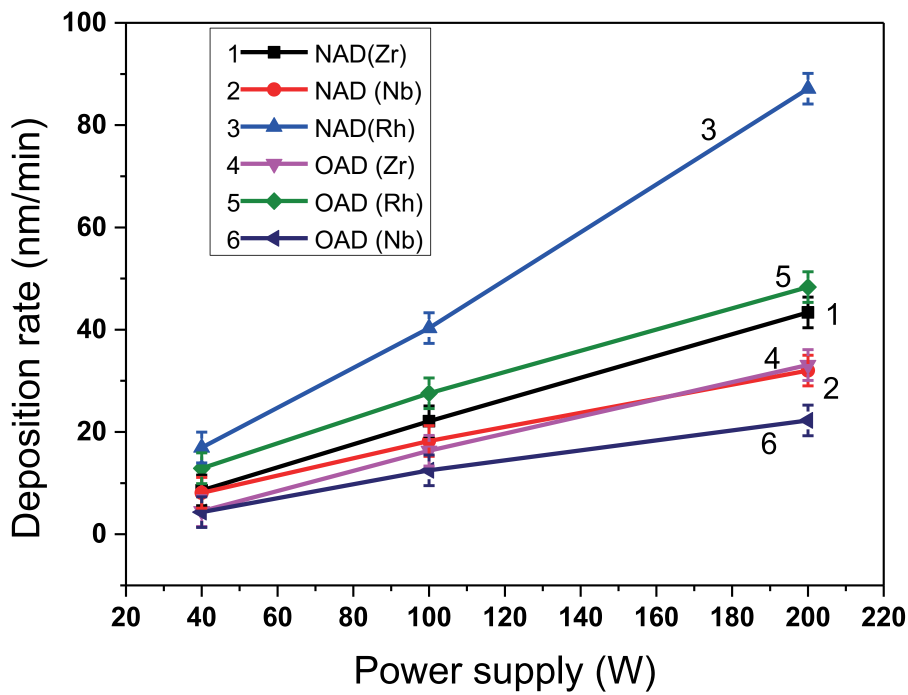

Figure 4. 4 Deposition rate graph at 40, 100 and 200 W

4.2.2 Characterization

The Rh and Zr coated mirrors were characterized by using various methods and instruments. As explained in chapter 2, the surface morphology of the deposited films

제주대학교 중앙도서관
JEJU NATIONAL UNIVERSITY LIBRARY

was measured by using field emission scanning electron microscopy (FESEM). The chemical composition of Rh, Zr coated molybdenum mirror was confirmed by the energy-dispersive X-ray spectroscopy (EDS). EDS was used in conjunction with FESEM. Film thickness measurements were measured and cross-checked using FESEM and thickness monitor. The crystalline structure was recorded with XRD and A 3D Nano-profiler system was used to measure the roughness of the films' surfaces of the interlayer coated mirrors. The reflectivity of the deposited films was measured with a UV-VIS spectrophotometer Reflectance was the mode of measurement and measured in the visible range of 400- 1000nm (most effective range of the reflectance measured for the optical diagnostic in the fusion reactor [8]) of the optical wavelength. The LapPro Plus computer software converts the reflected optical intensity at each wavelength, and plotting all the single value gives the line spectrum of the measured reflectance of the surface.

Contact characterization of the film deposited on the substrates was done by two methods, namely, the tape and the scratch tests. These two old and conventional are still used to check the adhesion strength of the films. The adhesive tape (described in chapter 2) test was done by sticking pressure-sensitive tape on a surface of the fabricated mirror, and the scratch test was performed using a lab-made scratch tester, as schematically shown in fig. 2.16. A DC motor used to pull the tungsten-carbide needle tip with a radius of 250 μm [38] across the surfaces of the mirrors to create a scratch with predetermined vertical loads. The needle holder, which was connected to the driving shaft of the motor via a piece of yarn, was guided by using a sliding guide that traveled back and forth in the horizontal direction. The substrate was positioned below the tip of the needle. The tip of the needle was cleaned with ethanol and a lint-free

제주대학교 중앙도서관
JEJU NATIONAL UNIVERSITY LIBRARY

wiper before and after the scratch test. The scratching speed of the tip was set to 37 mm/s; load was applied until the lab-made scratch tester motor can pull till an approximate scratch length was 10-20 mm along the surface of the mirror. Normal load in the range of 0.5 - 2 N was applied on the surface to make a scratch mark under a constant rate. The wear tracks were observed with an optical microscope 2MP, 20x - 400x, 8 LED, USB Digital Microscope.

4.3 Results and Discussion

EDS was used in conjunction with FESEM to investigate the surface morphology and elemental composition of the deposited surface layers. Fig. 4.5 (a) shows EDS images that give the confirmation of surface elemental composition i.e., Rh, Zr on the Mo substrate material along with small traces of impurities carbon and oxygen. Figure (b) shows a single element of the surface, and that also confirmed that the top of the film was composed of only one type of material (i.e., Rhodium). Rh is the outermost coated layer, and the analysis result shows major elements that present were, Rh- 61.96 wt%, Mo-27.68 wt%, C-8.69 wt%, and Zr- 1.67 wt%.

The thickness of the deposited film was measured by a cross-sectional analysis by FESEM. We have seen that normal angle deposition (NAD) for both 40 W and 200 W are smoother and dense film growth as compare to the oblique angle deposition (OAD) as shown in figure 4.6 (b) and (d) NAD; (a) and (c) OAD. In OAD substrate was rotated at 25 RPM to give the uniform deposition on the surface of the substrate. As in the figures, columnar structures were perpendicular to the substrate, and NAD materials were larger than that material deposited by OAD by magnetron sputtering. Average grain sizes after the heat treatment were increased[39].

제주대학교 중앙도서관
JEJU NATIONAL UNIVERSITY LIBRARY

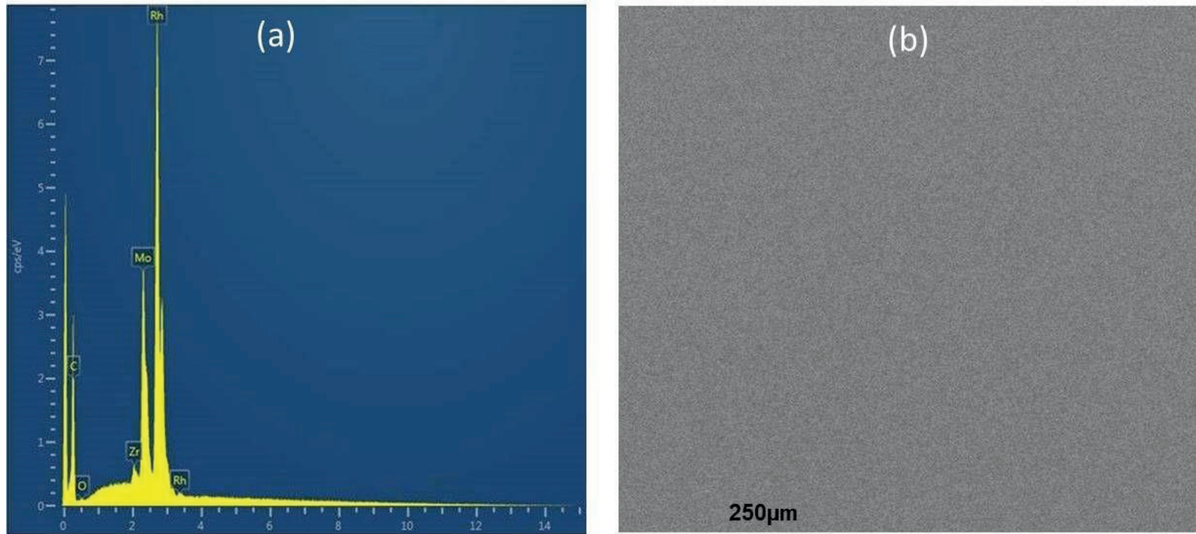

Figure 4. 5 EDS and SEM images (a) elemental composition and (b) Rh thin film surface mapping

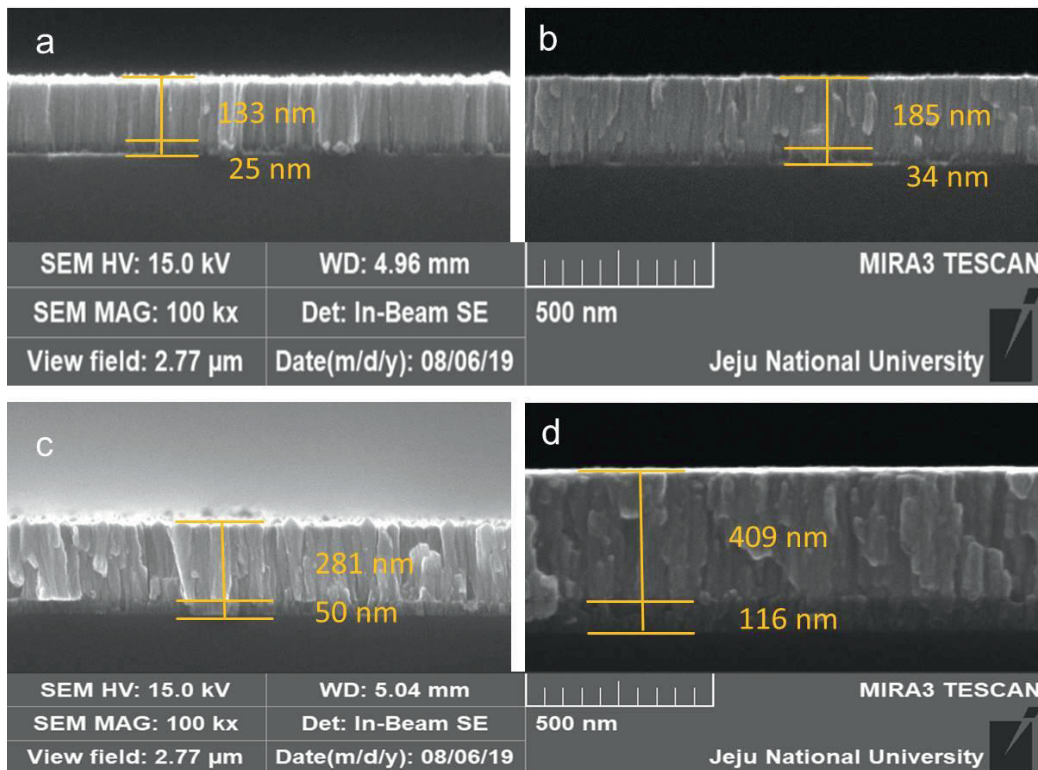

Figure 4. 6 Thickness of the films captured by the SEM, (a) and (c) oblique angle deposition and (b), and (d) normal angle deposition at 40 and 200 W.

제주대학교 중앙도서관
JEJU NATIONAL UNIVERSITY LIBRARY

Under the given deposition conditions, the thicknesses of the Rh thin film and the Zr interlayer were 150 nm and 40 nm, respectively. In the experiment, we kept the film thicknesses approximately 190 nm. High film thickness with high the power showed that surface appeared to form blisters and peel off due to thermal expansion and mismatch of lattice parameters[53] of the Mo, Zr, and Rh material when the substrate was around RT.

The deposited films were seen to have the dense, columnar structure[54] along the growth direction (almost perpendicular to the surface of the substrate). The formation of well-defined columnar structures in the thin film was due to the high surface diffusion of adatoms periodically nucleated on the surface of the growing crystals [40]. The columnar configuration is due to low surface mobility of continuous deposition of the material [55] on the top of each growing grains in the same direction.

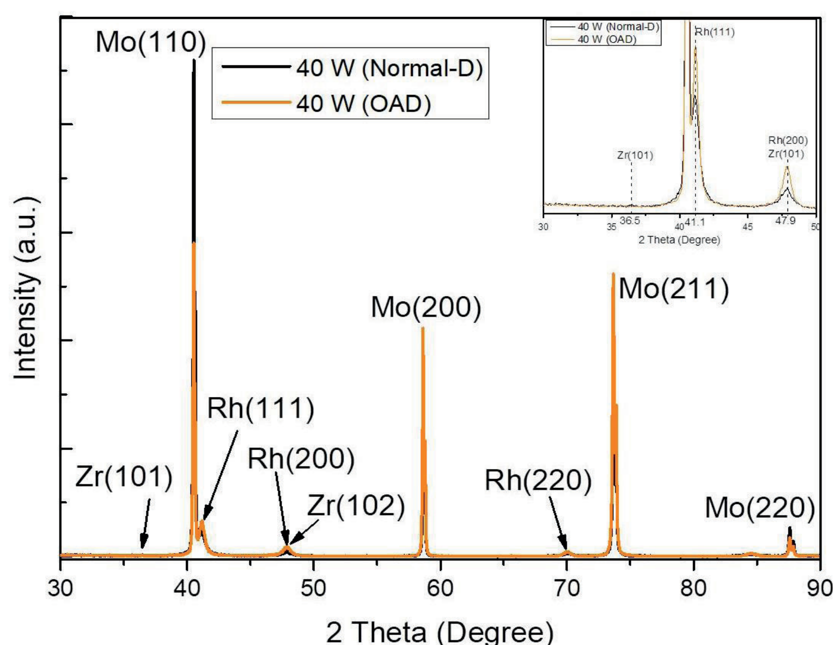

Figure 4. 7 XRD spectrum of the thin film Rh-Zr on the Mo substrate.

제주대학교 중앙도서관
JEJU NATIONAL UNIVERSITY LIBRARY

Fig. 4.7 shows the high-resolution XRD diffraction patterns of the Rh/Zr/Mo mirror where peaks are at 2θ - 40.51°, 58.76° and 73.66° corresponding to the (110), (200) and (211) reflection planes of the body-centered cubic Mo substrate (JCPDF #00-004-0809). The Zr interlayer shows a very weak diffraction peak at 2θ - 36.511° and 47.99° (JCPDF #00-005-0665), corresponding to the (101) and (102) planes. The Rh top layer shows distinct reflection peaks at 2θ - 41.12° and 47.96°, corresponding to the (111) and (200) planes, respectively (JCPDF #00-005-0685). Moreover, the absence of extra peaks suggests the high purity of the prepared sample. The XRD peak of Rh (111) shows the high crystalline structure and it shows polycrystalline thin film deposition.

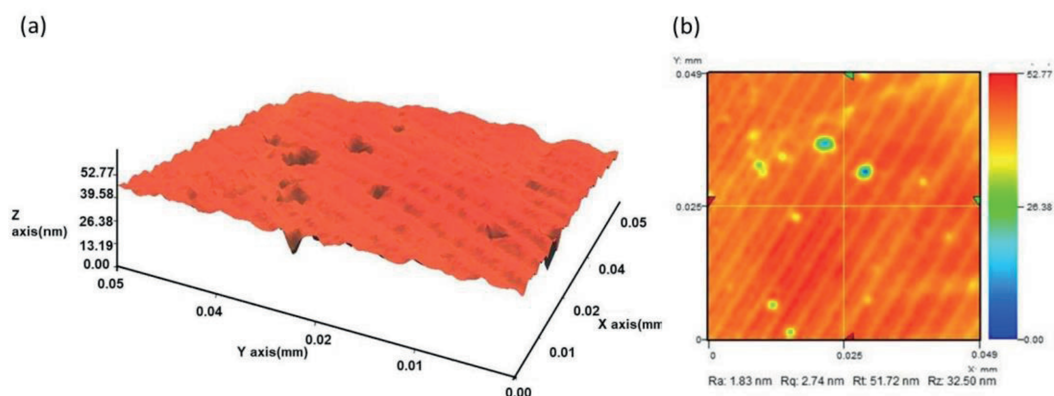

Figure 4. 8 Pristine Mo mirror 3D surface

The fabricated all multilayer Rh/Zr/Mo mirrors were subjected to heat treatment to reduce the thermal stress on the microstructures, which intact the films firmly to each other hence better adhesion but slightly in the reduction of mirrors' reflectivity [18], [56]. The mirrors were heat-treated in a vacuum oven at 200 °C for 4-6 hours in a 10 Torr vacuum environment and were cooled naturally to room temperature before analysis. Here, all the characterized results were obtained after the heat-treatment of

제주대학교 중앙도서관
JEJU NATIONAL UNIVERSITY LIBRARY

the prepared mirrors. Crystalline sizes were calculated by the Scherer's relation (Equation 4.1).

$$D = k\lambda/\beta\cos\theta, \qquad 4.1$$

Where k was the shape factor 0.9, the X-ray wavelength was λ (0.15406 nm), β was the FWHM of the peak, and θ was the Bragg diffraction angle ($2\theta/2$). The result shows that crystallite became larger after exposure to high temperature. The average crystallite sizes (grains) of the Rh thin films with Nb and Zr interlayer have almost similar (approximately grain size increased by 10 nm) for all samples, but higher the deposition rate larger the grain size and lower the roughness [18], [57].

제주대학교 중앙도서관
JEJU NATIONAL UNIVERSITY LIBRARY

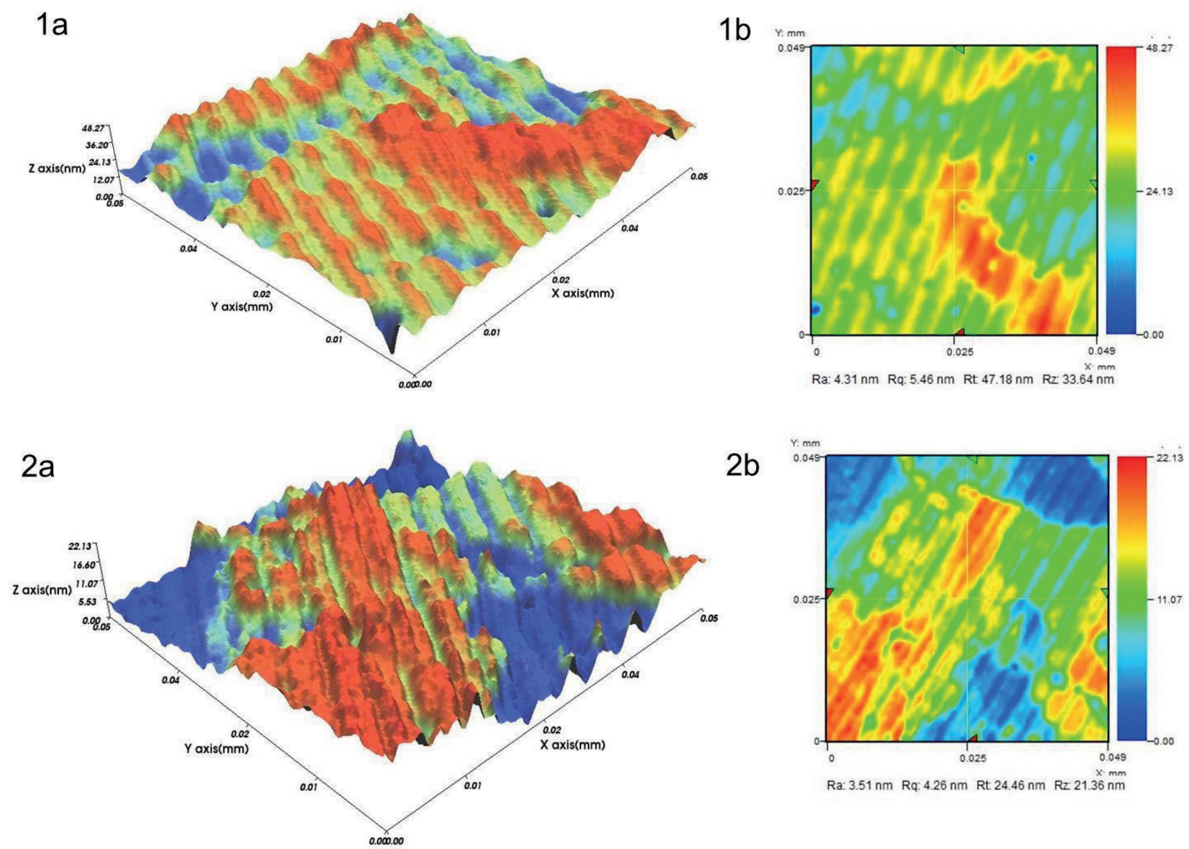

Figure 4. 9 3D images of interlayer coated Mo/Zr/ Rh mirror 1 (a-b) at 40 W and 2 (a-b) at 200 W power supplied

The roughness of the surface directly affects the reflectivity of the mirror and its performance in the fusion plasma environment. The roughness of the Rh/Zr/Mo inter-layered mirror was measured using a 3D nano-profiler Fig. 4.8 shows a 3D image of commercially available pristine Mo surface, which has an average roughness (Ra) of 4 ± 2 nm (avg of 5 spot measured images). We can see there are many pinholes and tiny hillocks with depth and width somewhere 100- 400 nm. Figure 4.9 shows the surface profile of the Rh/Zr-film-coated Mo mirror after heat treatment. Fig 4.9 (a) and (b) represents the film-coated at 40 W power and 200 W respectively, where the

제주대학교 중앙도서관
JEJU NATIONAL UNIVERSITY LIBRARY

roughness of the Rh thin film’s got smoother with the increase of power, probably an elevated temperature promotes the growth of grains and that led to the closure of the voids between the grains of the columnar microstructure and increased grain density [42].

제주대학교 중앙도서관
JEJU NATIONAL UNIVERSITY LIBRARY

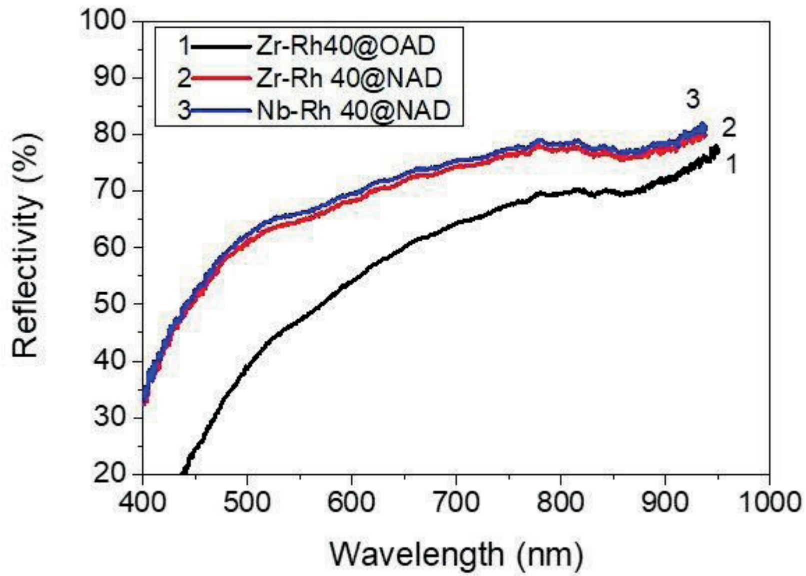

Figure 4. 10 UV-VIS reflectivity spectrum of interlayered Mo-Rh mirror coated at 40 W; (1) Zr interlayer Mo-Rh mirror, deposition process of OAD (rotating substrate); (2) films Zr and Rh coated by NAD process and (3) Nb-Rh films deposited using NAD method.

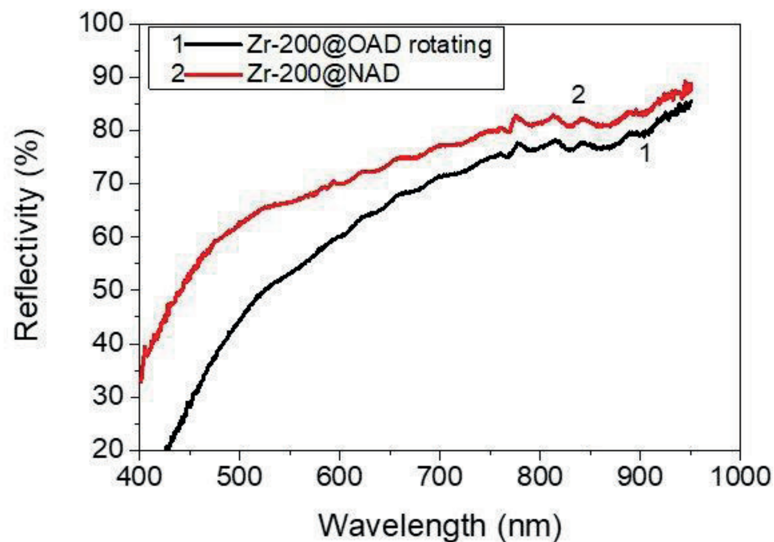

Figure 4. 11 Reflectivity graph of Zr interlayered Mo- Rh mirror; (1) deposited by OAD process where substrate rotated and (2) film prepared by NAD method.

제주대학교 중앙도서관
JEJU NATIONAL UNIVERSITY LIBRARY

The reflectivity property of the FM's surface is a crucial parameter for the optical diagnostics in the fusion reactor, which collects the scattered light and sends it to the detector for diagnostics. The reflectivity was measured via UV-VIS spectroscopy, and the results were presented in figure 4.10 and 11. The reflectivity pattern of the mirror with thin films fabricated by 40 and 200 W is shown. The mirror prepared by the 40 W (NAD) power has lesser reflectivity than that of 200 W (NAD) deposited mirrors. Comparing the reflectivity with Nb and Zr interlayered mirrors (both are deposited at 40 W NAD), we could not exactly separate which one is better, because they look identical in the reflectance value. In both power (40 and 200 W) thin-film mirror fabricated by oblique angle deposition (rotating substrate at 25 RPM) has lower reflectivity, as in figure 4.10 and 4.11. Reflectivity can be seen around 65-75% (at 840 nm (i.e., NAD deposited mirror retained reflectivity up to 75%). The Rh deposited with 200 W (NAD) has slightly higher reflectivity.

But with the experiment, we found that higher power deposited films have weaker surface adhesion. The blister formation, cracks and peeling off the coating were noticed on the surface. We concluded that because of variation in temperature at the Mo surface and deposited film layers (Zr and Rh materials) experiences internal thermal stresses [58] because of different thermal coefficient values and build up internal stress and strain between the films layers in higher power deposition for the more extended time [59].

제주대학교 중앙도서관
JEJU NATIONAL UNIVERSITY LIBRARY

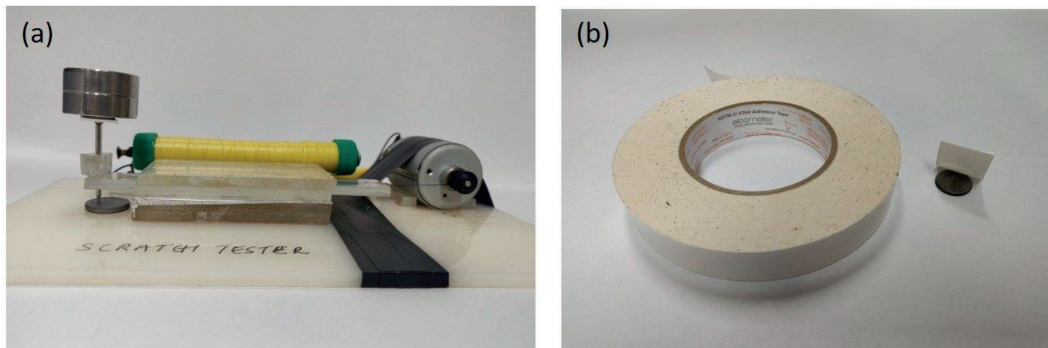

Figure 4. 12 (a) Lab-made scratch tester and (b) pressure-sensitive tape

The adhesion strength of the film confirms the better stability and the longevity of the FMs. Here we checked the stability and the adhesion of the deposited Rh/Zr films by old but convenient two well-known methods: (1) Scratch test and (2) tape test. A scratch test was performed using a lab-made scratch tester, as described in the experimental section (as in figure 4.10). The weight of the needle and holder was 3.5 gm. (0.035 N), the minimum force that could be applied to the Rh/Zr/Mo samples (similar to the Nb interlayer mirror). Figure 4.13 shows the results of the scratch test performed under the applied loads of 0.5, 1, and 2 N on the power of 40, 100, and 200 W deposited samples. As shown in figure table 4.13, no apparent damage or unusual wear on the Rh/Zr-interlayered thin-film surface was observed until the 1 N applied the load at the speed of 37 mm/sec. Comparison is shown on table 4.3; direct comparison might not be the fair because, the tests were done with the different devices and with different applied load process. Our device might give an only approximation of the result but still results show as par with the result found in the previous article [8], [46] Scratch test for the Zr coated interlayer mirrors also has similar scratch resistance as Nb coated interlayer mirror. The evidence shows that the depositions of the Zr interlayer

제주대학교 중앙도서관
JEJU NATIONAL UNIVERSITY LIBRARY

are as strong as the Nb interlayer coated mirror between Rh and Mo mirror.

Table 4. 3 Scratch test result compared with the previous results of published articles

Parameters	Our test results	Previous results from the article [8], [46]
Tip materail	Tungsten carbide	Diamond stylus
Spherical tip radius	250 μm	200 μm
Scratch speed	37mm/sec	10 N/min (progressive load)
Load application	Dead load 0.5, 1, 2 N	Progressive load 0-20N
Scratch length	10-20 mm	10 mm
Scratch appearance	After 1 N	After 1 N
Critical load	Not calculated	12.9 N

Moreover, an additional heat treatment process caused the grains of the thin film to become denser and more compact [42], which increases the hardness and promotes better adhesion strength. We also can say that the use of the dual sputtering system for the deposition of both the Nb and the Rh films might have another reason for the better adhesion as that allowed the immediate deposition of the subsequent layers. In this study, heating at high temperature was seen to reduce the formation of the crack on the film's surface [41] and strengthen the thin film, but at the expense of the reflectivity.

제주대학교 중앙도서관
JEJU NATIONAL UNIVERSITY LIBRARY

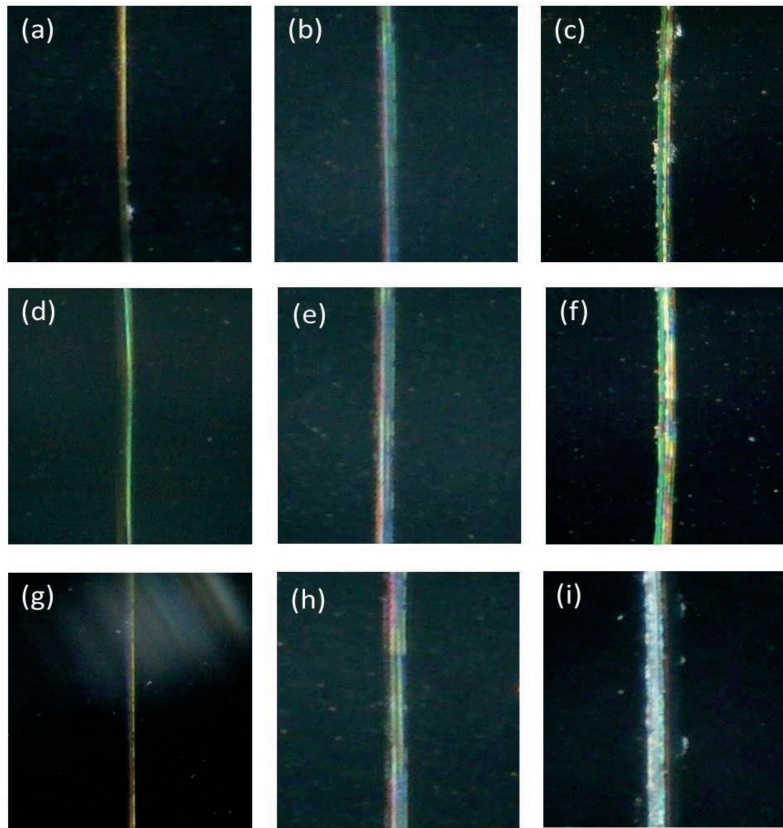

Figure 4. 13. Images of scratch test for the Rh/Zr/Mo mirrors observed by Optical microscope image of a surface scratched under; (a) 0.5 Nb, (b) 1 N, and (c) 2 N for the 40 W power; similarly (d), (e) and (f) for 100 W power and (g), (h) and (i) for 200 W power

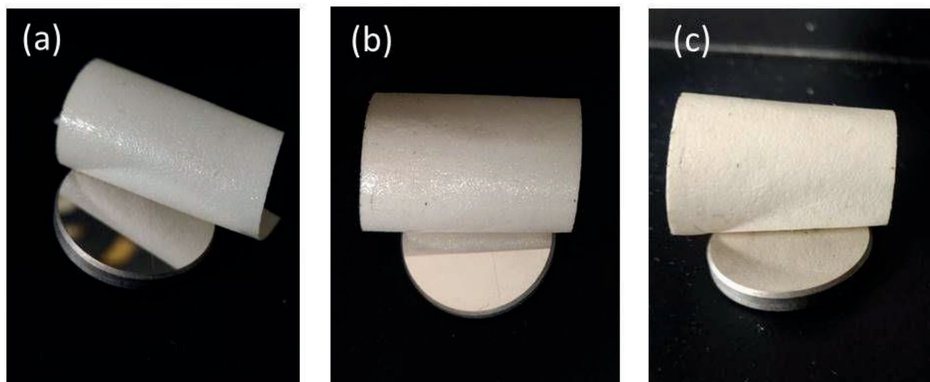

Figure 4. 14. Photographic images of tape test results of Zr interlayer Rh/Mo mirrors prepared at; (a) 40 W; (b) 100 W and (c)200 W

제주대학교 중앙도서관
JEJU NATIONAL UNIVERSITY LIBRARY

Pressure-sensitive tape test result further confirmed the stable adhesion of the deposited films without any blisters. The pressing force given to the tape against the coated surface was approximately 20 N, which is sufficient to stick the tape properly onto the surface. The scratch and the tape tests show excellent adhesion between Mo and the Rh thin film with the thin Zr interlayer, as shown in figure 4.14. Figure (a), (b), and (c) are the mirrors fabricated by the power of 40, 100 and 200 W. All the scratch tests and tape tests show excellent adhesion of the films. However, with repeating tape test on the same mirror for several times (more than 5 times) shows some films material stick on the tape from the surface the prepared with the power of 200 W as shown in figure 4.15 (b), but for the film deposited on 40 W has film intact firmly on the substrate. Therefore, our study shows (in our available laboratory environment) that low power of deposition makes slow and uniform deposition, and the temperature of the substrate and deposited layers remains low to adjust the thermal expansion more safely. Hence the introduction of the Zr layer with suitable and matching parameters can play a crucial role in reducing the surface tension during contraction and expansion.

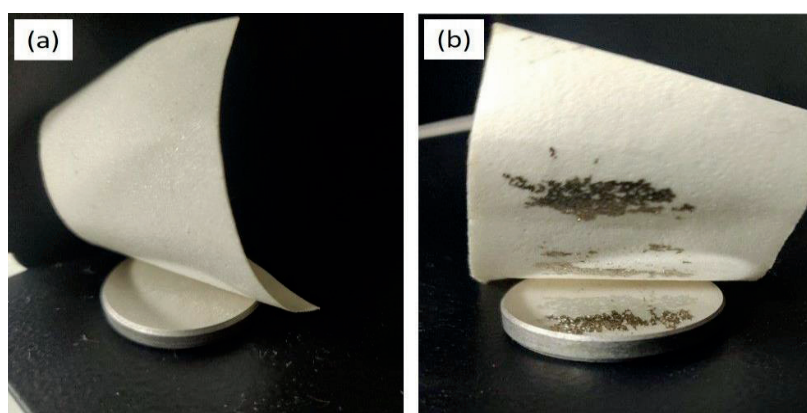

Figure 4. 15 Image of tape test images of thin film deposited on a Mo substrate, stripped off test was performed for five times (a) 40 W and (b) 200 W.

제주대학교 중앙도서관
JEJU NATIONAL UNIVERSITY LIBRARY

4.4 Conclusion

It can be concluded that a low power deposition has finer grain growth but a slightly larger grain size than the higher deposition rate of the film. The interlayer apparently reduced the problem of thermal expansion between the thin-film layers, provided the above experimental setup and deposition parameters. Reflectivity is higher than 70% which is expected in the fusion reactor but film deposited with the OAD process has poor reflectivity than the NAD process. Hence it can assume that NAD deposition is a better application for the FMs. Also, the adhesion property increased with an increase in the lifetime of the thin films coated FMs. It can prove that scratch results are comparable with the Rh-Mo thin-film experimented by the other laboratories. With the analysis results, Zr can be an excellent material bridging the thermal expansion coefficient between two primary FMs material; Mo and Rh for the fusion reactor optical diagnostics.

제주대학교 중앙도서관
JEJU NATIONAL UNIVERSITY LIBRARY

CHAPTER 5
Ion Assisted Oblique Angle Deposition of Interlayer Coated Metallic Mirror

5.1 Introduction

Film coating technology has been around with humankind for more than 2000 years[60]. Since human development, film technology also developed and grown into more significant industries, and this technology became essential for all kinds of functional coating and semiconductor industries [20], [52]. To produce novel optical properties of devices from a various film deposition techniques and available wide range of materials, the technology needs to adopt specific fabrication techniques, material deposition, processing, and optical characterization [52][51][61]. Thin film is generally used to improve the surface properties of materials on which it deposited. Thin-film deposition techniques are usually divided into two broad categories [3][6]; PVD (physical vapor deposition) and CVD (chemical vapor deposition) processes. Among these processes, sputtering is the most common way to fabricate thin films. It is a PVD process where atoms (ions) are ejected from a target material and deposited onto a substrate in a high vacuum condition.

In this study, film deposition was done by using DC magnetron sputtering (MS). Oblique angle deposition (OAD; 54° incidence) configuration was applied to obtain tilted columnar microstructures and dense film. This columnar microstructure depends on many experimental parameters affecting the growth mechanism, like substrate temperature, deposition power, deposition angle, target to substrate distance, process or working gas and flow rate, deposition pressure, and initial substrate roughness [7]. This initial substrate may strongly affect the shadowing and other particle relocation effects.

제주대학교 중앙도서관
JEJU NATIONAL UNIVERSITY LIBRARY

These parameters are critical to controlling the thin film microstructure [65]. To create different thin-film geometry by repeatedly coating with varying the parameters using oblique angle deposition is sometimes also called sculptured thin films [54], [66]–[68].

This thesis focuses on how oblique angle deposition (OAD) (tilt angle), hence the microstructure of thin-film (Rhodium and Zr), affect the reflectivity and adhesion between the substrate and deposited films for optical applications. Thin films were deposited by using DC MS at room temperature with fixed deposition conditions (deposition angle, target-sample distance, process gas pressure and flow rate, deposition power, ion-assisted current supply). We also used the ion beam assisted deposition (IBAD) on OAD and compared the characteristics of the films. This technique is an interest in sensor and electrochromic applications [69]–[71]. We expect the control of the microstructure and properties of these films will help the understanding of IAD and OAD for optical applications; thus, this technique can be used for fabricating high reflectance mirrors such as "First Mirror" for the fusion plasma diagnostics.

IBAD is the technique to enhance the coating quality by increasing the adhesion of thin films by physical and chemical vapor deposition in a low-temperature process. IBAD is mainly involved in the alteration of nuclei growth near the surface area of the substrate. Ions are embedded into the material by virtue of its high kinetic energy low temperatures.[54], [72].

Ion assisted deposition is the combination of two surface coating technologies, namely, ion implantation and vacuum deposition. Here we used DC MS and hollow cathode ion source for thin layer deposition, as shown in figure 5.1. The sputtered atoms from the target with the incident angle of α, (54°) with the vertical plane, and the

제주대학교 중앙도서관
JEJU NATIONAL UNIVERSITY LIBRARY

β angle between the ion implantation direction (vertical) and the film growth direction on the substrate surface. The ion beams provide a controlled energy supply into the thin films and substrate to improve film growth and adhesion in conjunction with DC MS deposition. IBAD, unlike conventional coating methods, the thin film is integrated into the surface, and develop a comprehensive interface, in turn, gives better adhesion and lessen the chance of peeling. However, it is not always necessary to mix the interface atoms to achieve an ion beam to improve film substrate bonding [73]. A thin layer can be bond to the substrate surface by lightly implanting, called ion beam stitching [63]. In this process, actual atoms will not be displaced by the incoming ions and atoms particles. Hence low doses of ions are enough for the good adhesion of the coating.

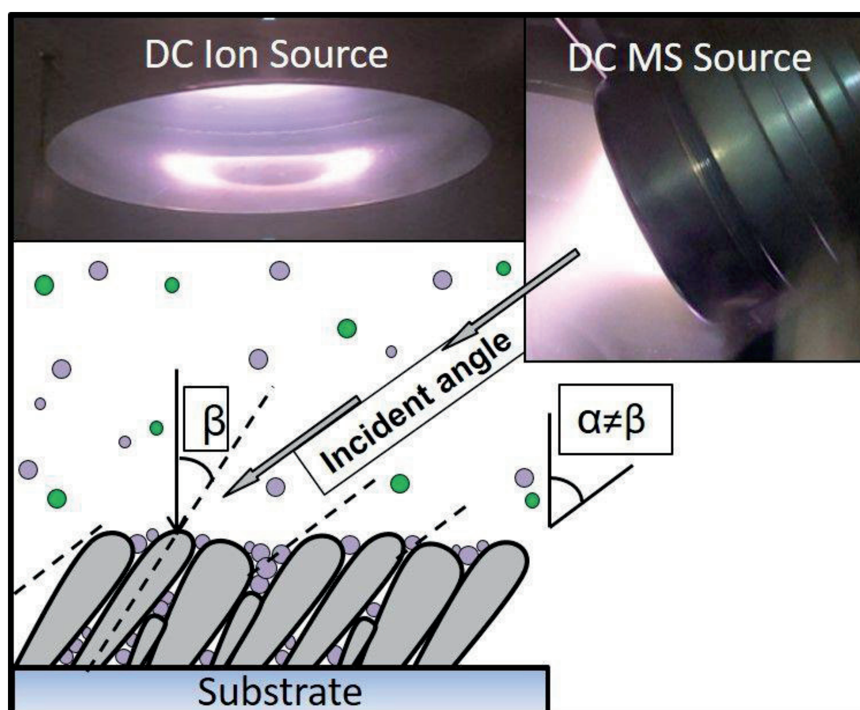

Figure 5. 1 IBAD on OAD process

제주대학교 중앙도서관
JEJU NATIONAL UNIVERSITY LIBRARY

5.2 Experimental Setup

As explained in the previous chapter, the experimental setup for the IBAD, OAD, and NAD are similar; the only difference is the addition of the ion source to the setup configuration, as shown in figure 5.2. Si (100) wafer was used for many repetitions of experimental deposition to prepare the samples that were used to confirm the thickness, growth structure before experimenting on the actual bulk Mo substrate. Mo mirrors with 20 mm diameters and 3 mm thicknesses were used for all experiments.

As in the experimental setup (figure 5.2), DC ion source is installed at the top of the reactor, and two MS guns are on the cylindrical wall at the 54^0 with the vertical plane as DCMS gun 1 (for Rh target sputtering) and DCMS gun 2 (for interlayer target materials). The high vacuum of 10 μTorr was created by using TMP and dry scroll pumps. The angle valve and line valves were used to control the pressure inside the vacuum. The Ar gas was used as a process gas during deposition, and gas flow was control by the MFC unit and readout unit. For better cooling and to keep the devices under controlled temperature, the chiller temperature was kept at 20 °C and the water flow rate was set about 5.5 L/min. In figure 5.2, the blue colored pipe is for circulating cold water and black/red pipes for hot water, flowing out of the devices.

In the entire experiment, substrates were prepared as explained in the previous chapter.

제주대학교 중앙도서관
JEJU NATIONAL UNIVERSITY LIBRARY

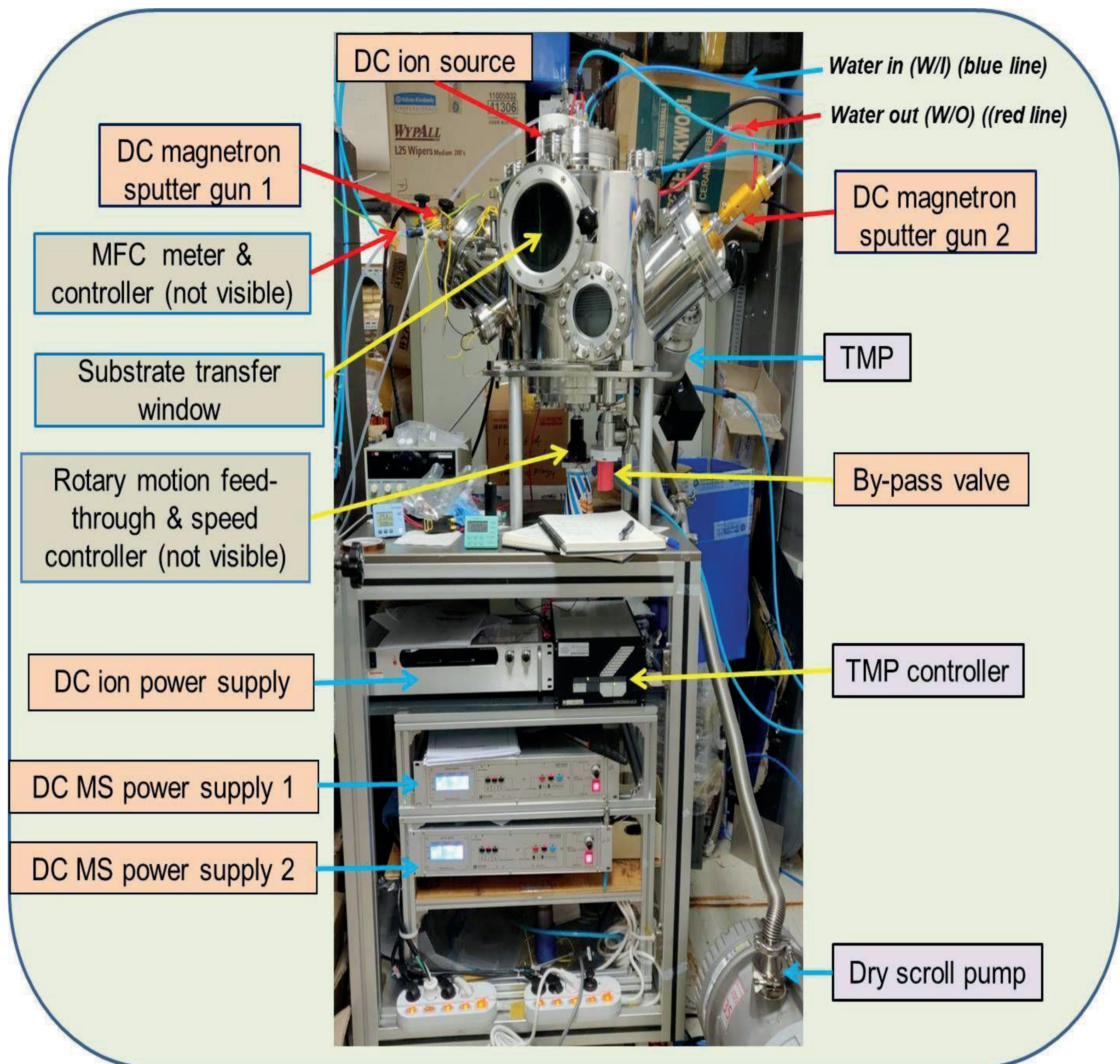

Figure 5. 2 Experimental setups for the OAD- ion beam assisted thin film deposition.

5.2.1 Film Deposition

The thin film samples were fabricated in a high-vacuum chamber by two different thin film deposition techniques. First, oblique angle deposition (OAD) and another one, ion-assisted-oblique angle deposition (IA-OAD) by using a DC magnetron sputtering source (magnetron sputter source, Korea Vacuum Technology) and a DC hollow cathode ion source, as shown in figure 5.3 (a &b). It is also called ion assisted

제주대학교 중앙도서관
JEJU NATIONAL UNIVERSITY LIBRARY

oblique angle deposition (IA-OAD), or Ion beam assisted deposition (IBAD). The oblique angle depositions are usually performed with a fixed substrate, but by manipulating the microstructure with a rotating substrate or changing the substrate position, OAD can produce multilayers art-like-sculpture design.

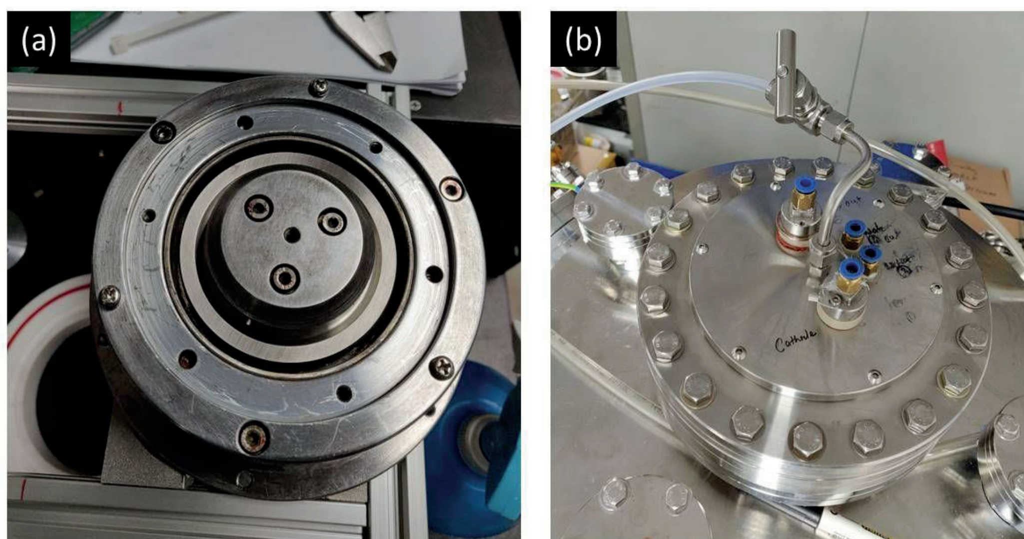

Figure 5. 3 photographic images of DC hollow cathode ion source, (a) revealing internal parts of the device (b) assemble view

DC magnetron sputtering can be achieved in the low pressure of several mTorr. However, for better deposition quality, the vacuum chamber should be maintained at high vacuum pressure. The right vacuum environment provides a longer mean free path of atoms for collision and has lesser collision before reaching the substrate surface[74]. To generate a high vacuum condition the chamber was pumped down to a base pressure of 10 μTorr by the turbo-molecular pump and a dry scroll pump, but Ar

제주대학교 중앙도서관
JEJU NATIONAL UNIVERSITY LIBRARY

gas pressure of 5 mTorr maintained as a working gas pressure during the deposition. Dual DC magnetron sputter guns were ignited one at a time (as shown in the figure5.4) with a power rating of 40 W, 100W, and 200 W by using power.

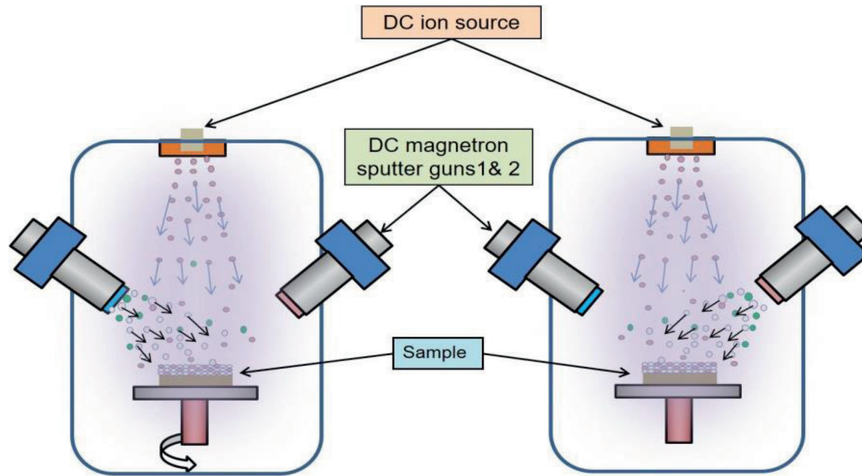

Figure 5. 4 Schematic diagram of dual DCMS gun sputtered material deposited one at a time by the IA-OAD process.

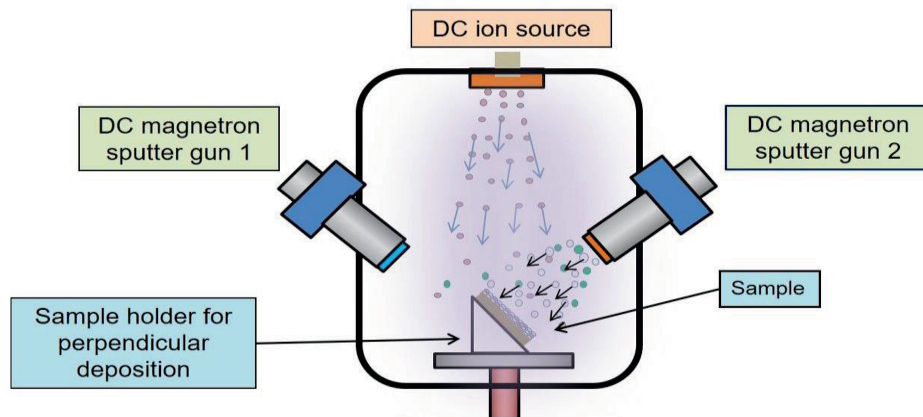

Figure 5. 5 Ion beam assisted deposition with slated substrate holder to have normal angle deposition.

제주대학교 중앙도서관
JEJU NATIONAL UNIVERSITY LIBRARY

Samples were prepared with keeping sample holder fixed sample holder and during deposition applied DC Ion source as well as DCMS at the different power supplies. The distance between the target interlayer material (Zr) and the Rh was at 120 mm, and at 70mm, respectively for the fixed sample holder deposition process that we used for all the characterization and analysis of this study. The targets purity of 99.95% were pre- sputtered for 30 mins at the beginning of the operation. However, after the first deposition, they were pre-sputter only for 5-10 mins each time to remove impurity remains on its surface[75]. To have a slanted film growth sample holder was kept fixed (stationary for the Zr deposition). The OAD was carried out by a DC sputter gun, which has a fixed angle in a vacuum chamber. An incidence angle α of the sputter gun is $54^{o,}$ with the normal to the substrate. Parameters such as the target-to-substrate distance, the working pressure of the Ar gas, and the flow rate were kept constant throughout the processes. The deposited thin film for Rh approximately kept about 150 nm, and interlayer material Zr was thickness of 40 nm throughout the fabrication and experimental process. The deposition parameters were summarized in Table 5.1. We choose the ion beam source that uses a supply voltage of 280V and current 200mA for our IBAD experiment (figure 5.7), as the lower power was very fluctuating and seems very low ion current impinging on the surface of the substrate. When using a higher power for the IBAD process, deposited films on the Mo mirror become rougher, and reflectively obtain below 50%. Fabricated interlayered thin film mirror samples were heat-treated in a vacuum oven in 10 Torr at 200 ^{0}C for 4 hours to reduce the internal stress of the film layers.

제주대학교 중앙도서관
JEJU NATIONAL UNIVERSITY LIBRARY

Figure 5. 6 Multilayer thin films of Zr and Rh on a Mo substrate

Table 5. 1 Experimental parameters for IA-OAD

Parameters	Values
Base pressure	10μTorr
Working pressure	5 mTorr
Ar gas flow rate	30 SCCM (20 SCCM from main Ar supply unit, 10 SCCM through DC Ion source)
Discharge power of the dual magnetron sputtering gun	40 W, 100 W, 200 W
Target-substrate distance	70 mm (Rh) and 120 mm (Zr)
Film thickness	Approx. 40 nm (Zr) – approx. 150 nm (Rh)
Target-substrate incidence angle	54°

제주대학교 중앙도서관
JEJU NATIONAL UNIVERSITY LIBRARY

<table>
<tr><td rowspan="4">Deposition rate nm/min</td><td>Power (W)</td><td>Zr (OAD)</td><td>Rh (OAD)</td></tr>
<tr><td>40</td><td>5</td><td>12</td></tr>
<tr><td>100</td><td>16</td><td>27</td></tr>
<tr><td>200</td><td>33</td><td>48</td></tr>
<tr><td>Ion beam supply at 280V and 200mA</td><td colspan="3">Approx. 4μA</td></tr>
<tr><td>Target dimensions</td><td colspan="3">50.8 mm diameter, 6.25 mm thickness</td></tr>
<tr><td>Substrate temperature</td><td colspan="3">Room temperature</td></tr>
<tr><td>Substrate spinning (revolving)</td><td colspan="3">0, 25rpm</td></tr>
<tr><td>Vacuum chamber inner dimensions</td><td colspan="3">320 mm cylindrical height,
370 mm diameter</td></tr>
</table>

제주대학교 중앙도서관
JEJU NATIONAL UNIVERSITY LIBRARY

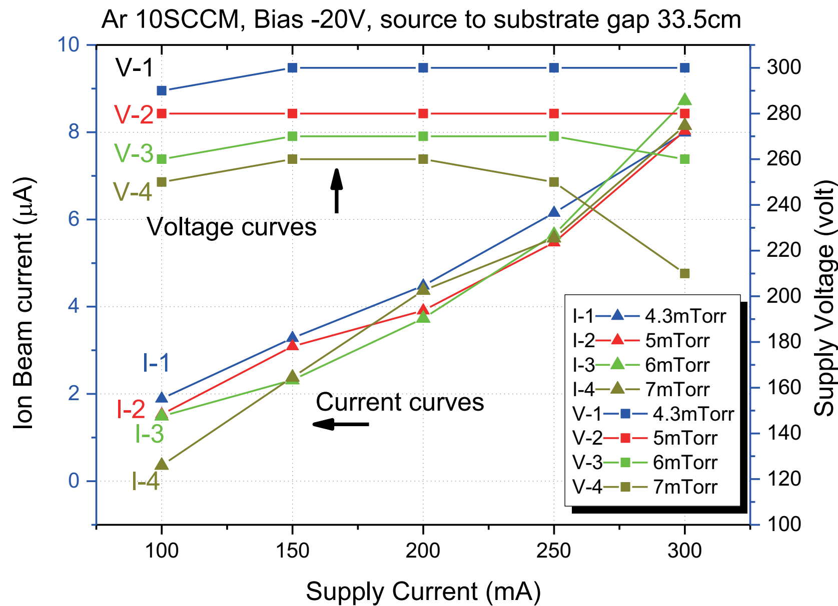

Figure 5. 7 Ion beam current at the different vacuum pressure and power supplies

5.2.2 Characterization

From as our previous analysis, thin film grown on low deposition power provided satisfactory results of reflectivity and adhesion strength. Hence, for the characterization of deposited thin films, we mostly compared the films that were deposited in 40 W power. Characterization of deposited thin films majorly differs from the previous experiments in terms of extensive use of SEM characterization and Si wafer as a substrate to study the tilted angle of grown films. DCMS oblique angle deposition provides the specific angle of incidence to grow the thin layer in a columnar microstructure. The cross-sectional measurement of the samples confirmed the tilted film grown by using field emission scanning electron microscopy (FESEM; TESCAN MIRA 3, Czech). While to confirm the chemical composition of Rh, Zr coated molybdenum mirror, and Si substrate, energy dispersive X-ray spectroscopy (EDS) was

제주대학교 중앙도서관
JEJU NATIONAL UNIVERSITY LIBRARY

used in conjunction with FESEM. The crystallinity and microstructure of the films were determined via X-ray diffraction (XRD; Empyrean, Malvern Panalytical, UK), using a Cu anode (Cu K-α= 1.54 Å) at room temperature. Columnar (Grain) size was found to be related to the electric power used in for sputtering of the target material and ion deposition source. Increased electric power gives a larger grain size [76].

The roughness of the films was analyzed by using a 3D Nano-profiler system (Optical surface profiler NV-2400). The images captured by using an objective lens on the area of 50 μm^2. The reflectivity of the deposited films was measured with a UV-VIS spectrophotometer (S-3100, SCINCO) in the range of 400-1000 nm.

The adhesions of the deposited films on the substrates were tested by using the tape and the scratch tests. Adhesive tape (ASTM D3359, Elcometer, USA) was used to test the strip off the strength of the deposited thin film after heat treatment while the scratch test was performed using a lab-made scratch tester, as schematically shown in fig. 5.20. The scratch tester has a DC motor, which drive the tungsten-carbide needle (tip radius: 250 μm) across the surfaces of the mirrors to create a scratch with applied vertical loads of 0.5, 1 and 2 N. The needle holder, which was connected to the driving shaft of the motor via a piece of yarn, was guided by using a sliding guide that traveled back and forth in the horizontal direction. The testing mirror was placed below the tip of the needle. The tip of the needle was cleaned carefully before and after the scratch test. The constant scratching speed of the tip was set to 37 mm/s, and the length of the scratch was approximately 10 - 20 mm along the surface of the mirror and the silicon wafer substrate. The wear tracks were observed with an optical microscope (2MP, 20x - 400x, 8 LED, USB Digital Microscope).

제주대학교 중앙도서관
JEJU NATIONAL UNIVERSITY LIBRARY

5.3 Results and Discussion

To check the ion beam assisted deposition on the oblique angle deposition (IBAD-OAD or IA-OAD) by DCMS, at first experiments were performed on the Si (100) wafers. Adopting proper substrate preparation procedure, we produce an excellent thin film (Rh-150nm, Zr-40 nm) on the Si substrate with an interlayer coating. As shown in figure 5.8, both films were coated by using a 40 W power. 1 (a-b) and 2 (a-b) show the film deposited on a Si substrate with OAD and with IA-OAD processes respectively. Both films have very fine surface roughness in the area of 50 µm. The average roughness of the films is (Ra_{Si1}) 0.79 and (Ra_{Si2}) 0.47 nm for OAD and IAOAD, respectively. Here results of the 3D nano profiler show the ion-assisted deposition has lesser roughness compare to the OAD.

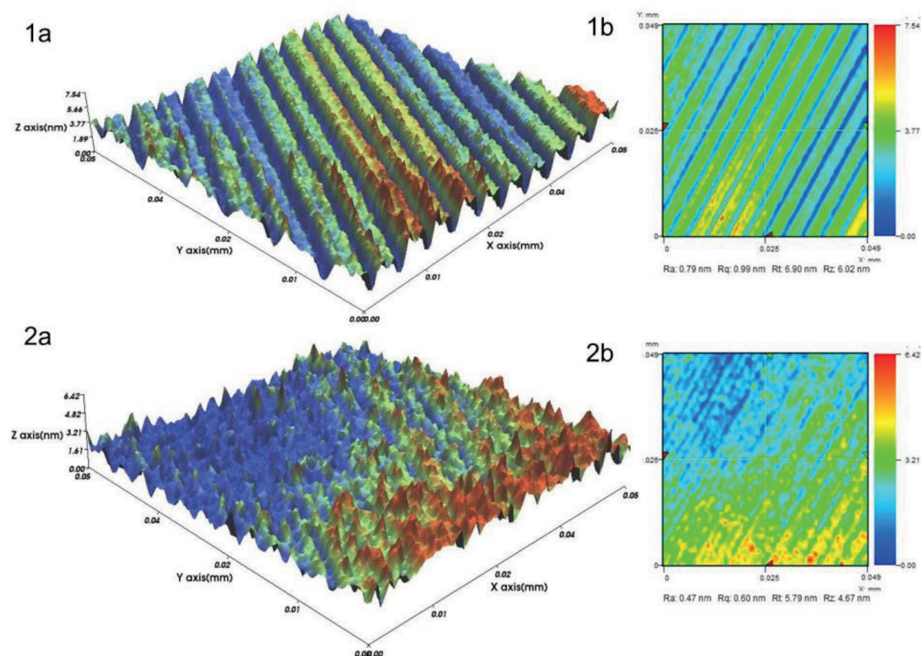

Figure 5. 8 Si wafer roughness images deposited by OAD (1a/1b) and IA-OAD (2a/3b) process at 40 W power.

제주대학교 중앙도서관
JEJU NATIONAL UNIVERSITY LIBRARY

Similarly, in figure 5.9, films were coated on the power of 100 W. Si wafer was used as a substrate to deposit the Rh and Zr. Figure 5.9 (1a-b); (2 a-b) are the film deposited by the OAD process and by IAOAD, respectively. Here we can notice some increase in the roughness but relatively small in number. Average roughness (Ra_{Si1}) 0.92 and (Ra_{Si2}) 0.63 nm for OAD and IAOAD respectively

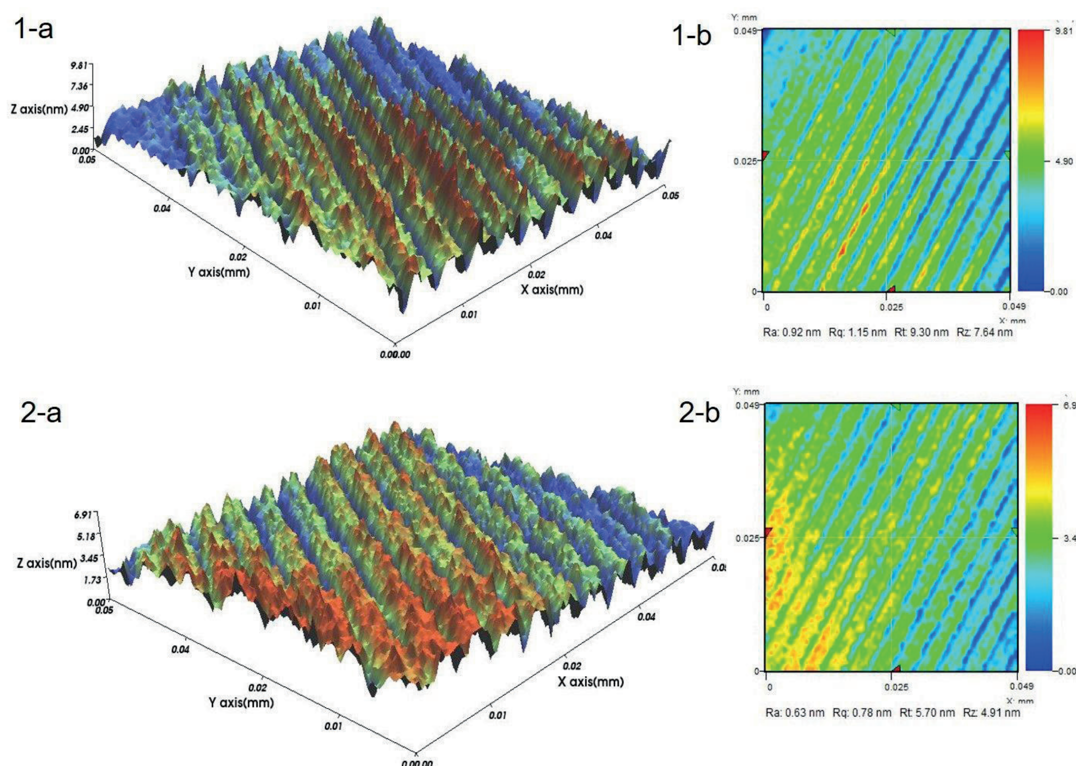

Figure 5.9 Si wafer roughness images deposited by OAD (1a/b) and IA-OAD (2a/b) process at 100 W power

Films deposited on 200 W power with ion source of 280 v and 200 mA has the highest roughness among the three different power. As in figure 5.10, average roughness

제주대학교 중앙도서관
JEJU NATIONAL UNIVERSITY LIBRARY

(Ra_{Si1}) is 1.13 nm for the OAD process and average roughness (Ra_{Si2}) 0.89 nm for the film, which was deposited by IAOAD.

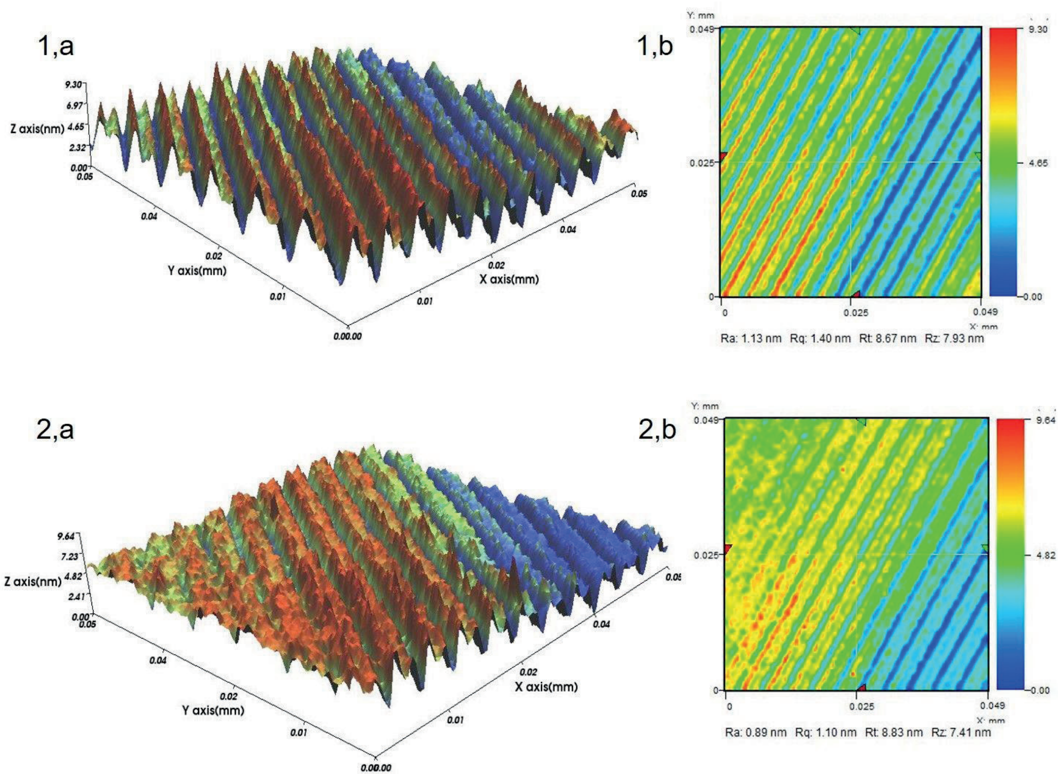

Figure 5. 10 Si wafer roughness images deposited by OAD (1a,b) and IA-OAD (2a,b) process at 200 W power

These 3D nano profiler results show the good surface morphology as the commercially purchased Si wafer itself has a very smooth surface. All the grain is orientated uniformly across the surface. There were no pinholes and cracks like in the Mo substrate. As seen in the previous chapter, the pristine Mo surface has 200 to 400

제주대학교 중앙도서관
JEJU NATIONAL UNIVERSITY LIBRARY

nm pinhole size and several small craters. growth in the surface roughness is associated with the increase in power [77] as an increase in the power increases the thermal heat and grain sizes of the deposited particle[78][79].

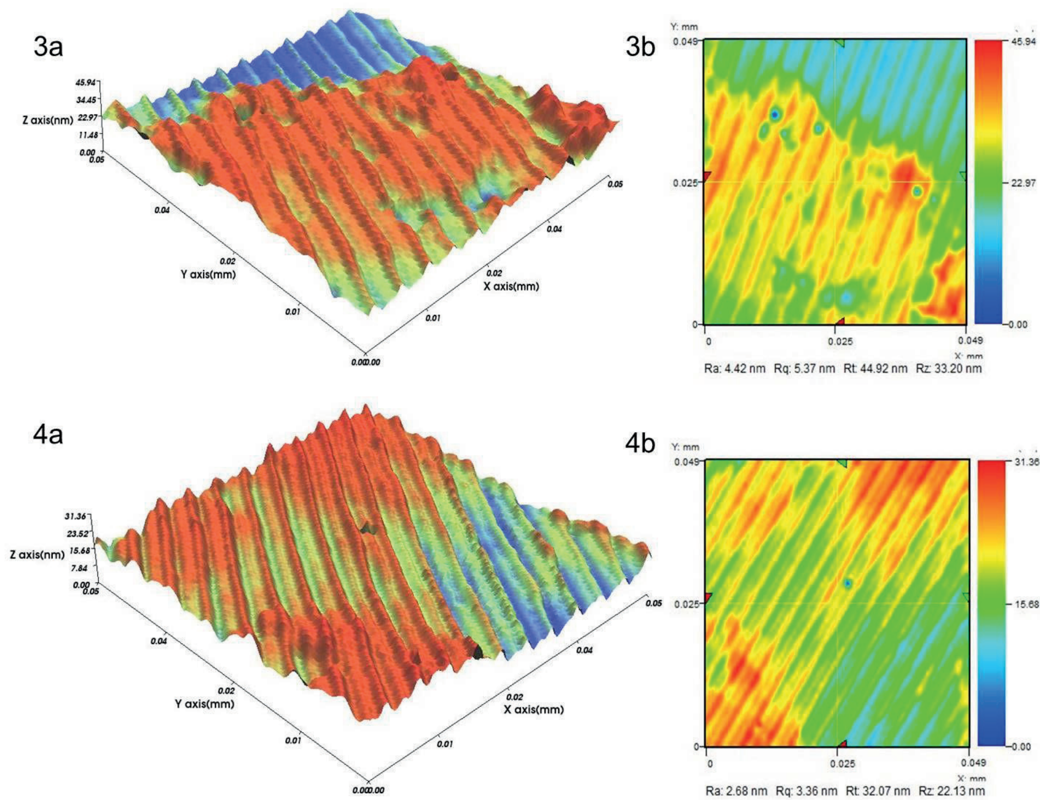

Figure 5. 11 3D nano surface roughness thin film deposited by (1-a,b) OAD and (2-a,b) with IA- OAD processes at 40 W

Due to the rougher Mo substrate surface than that of Si wafer, surface roughness also is seen rougher on the Mo substrate even after the deposition of films. In figure 5.11 (1a-b) and (2a-b), films that deposited on the Mo/Zr/Rh mirror using 40 W power has avg. Roughness values of Ra_{mo1} 4.42 nm (OAD) and Ra_{mo2} 2.68 nm (IAOAD),

제주대학교 중앙도서관
JEJU NATIONAL UNIVERSITY LIBRARY

respectively.

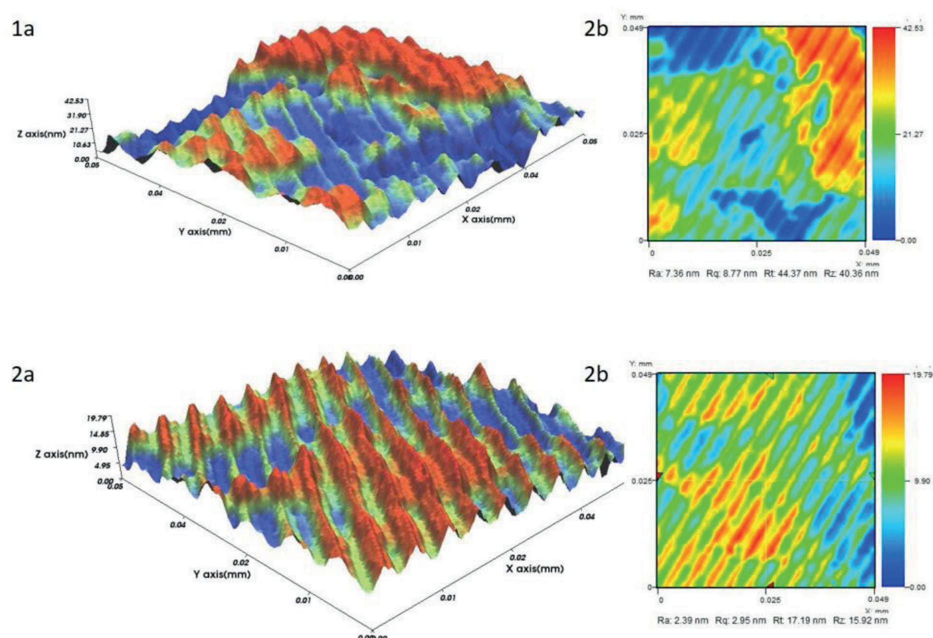

Figure 5. 12 Images of 3D nano surface roughness (5-a,b)OAD and (6-a,b) with IA-OAD processes at 200 W

As the power increased, film surface roughness also increases, in figure 5.13, 3D nano profiler result shows that oblique angle deposition at 200 W has higher roughness value of $Ra_{mo1a,b}$ 7.36 nm than that of the film deposited by ion beam assisted using same power $Ra_{mo2a,b}$ 2.39. Reduction of surface roughness can be, as ion bombard on the growing thin films, it leads to higher surface mobility and morphology of the film surface, thus becomes smooth, dense and continuous films [36], [61].

Further crystalline structure and elemental orientation were analyzed by using XRD, as shown in figure 5.13. The XRD diffraction patterns show crystallite formed in a different plane of crystal lattices of the Rh/Zr/Mo mirror corresponds to the plane (101) and (102) at peak at 2θ - 36.511° and 47.99° (JCPDF #00-005-0665) represents

제주대학교 중앙도서관
JEJU NATIONAL UNIVERSITY LIBRARY

the Zr interlayer of very weak diffraction. Diffraction spectrum at 2θ - 40.51°, 58.76° and 73.66° corresponding to the (110), (200) and (211) reflection planes of the body-centered cubic Mo substrate (JCPDF #00-004-0809). The Rh element shows the distinct reflection peaks at 2θ - 41.12° and 47.96°, corresponding to the (111) and (200) planes, respectively (JCPDF #00-005-0685)[80]. From this, XRD diffraction peaks show that there were no other impurities on the deposited film.

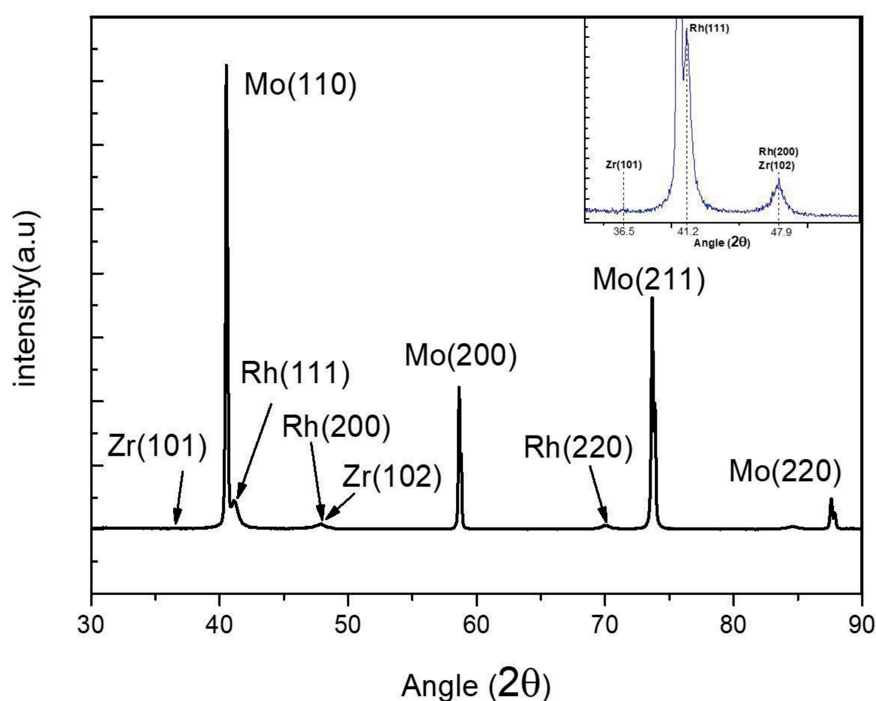

Figure 5. 13 Image XRD pattern of Mo-Zr-Rh thin

제주대학교 중앙도서관
JEJU NATIONAL UNIVERSITY LIBRARY

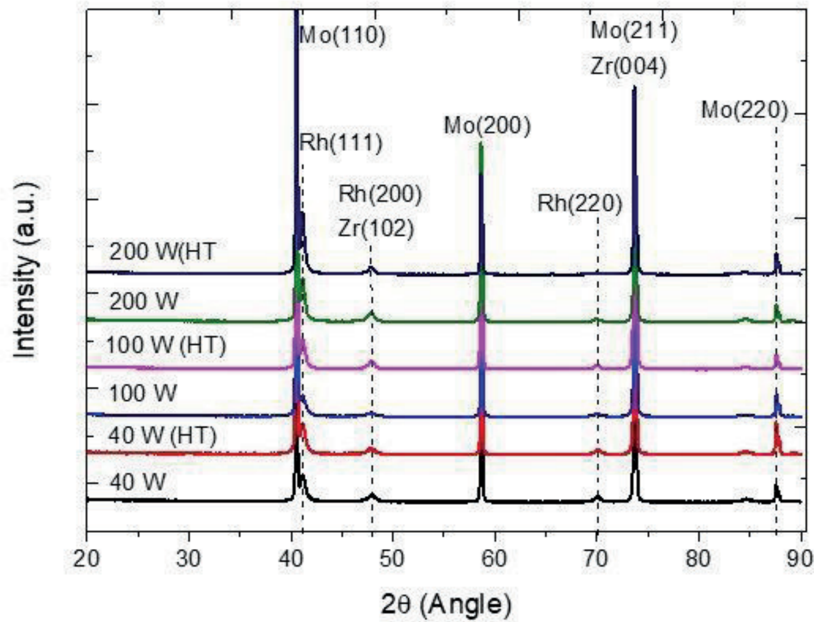

Figure 5. 14 XRD spectrum of 3 different samples (before and after exposure to high temperature) that prepared by 40, 100, and 200 W power.

Above figure 5.14 shows the comparisons of six different Mo-Zr-Rh samples that were fabricated by 40, 100, and 200 W power using the IAOAD process before and after the heat treatment process. The XRD patterns show that there was no shift of peaks. In the previous study, the heat-treated Mo samples at 200 °C for 6 hrs showed a slight shift of peaks and increased grain size [18]. In this experiment, samples were heat-treated for 4 hrs at the same temperature of 200 °C and left for natural cooling. The stable peaks might be of exposure to high temperature, and the time, that was just enough to rearrange the grain or columnar microstructure and to relieve the internal stresses of the films layer. The study also shows that the heat treatment time and temperature affect the optical properties of the film [81].

제주대학교 중앙도서관
JEJU NATIONAL UNIVERSITY LIBRARY

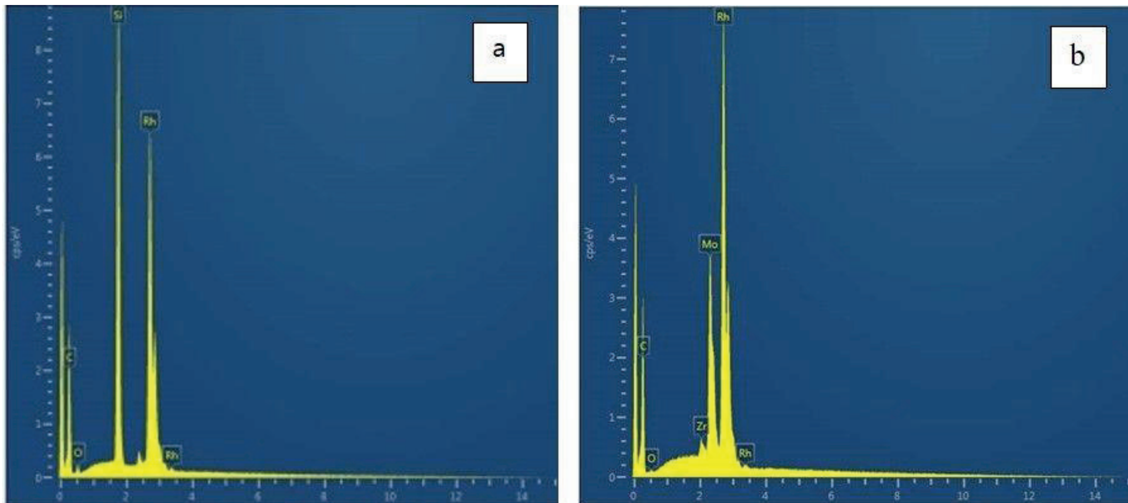

Figure 5. 15 EDS images of Si substrate (a) and Mo substrate (b)

EDS qualitative analysis of interlayer coated thin films on the silicon substrate (figure 5.15 a) and molybdenum (figure 5.15 b) revealed a significant presence of silicon (a), molybdenum (b) with rhodium, zirconium, carbon and oxygen peaks. These analyses results indicated carbon and oxygen peaks in the EDS could not be rid entirely due to using carbon tape to secure the sample on the holder, and some contaminants as oxygen atoms in the vacuum system are always present. Above both XRD and EDS analysis showed that film was deposited purely by target material of Zr and Rh, but substrate materials have dominant intensities.

제주대학교 중앙도서관
JEJU NATIONAL UNIVERSITY LIBRARY

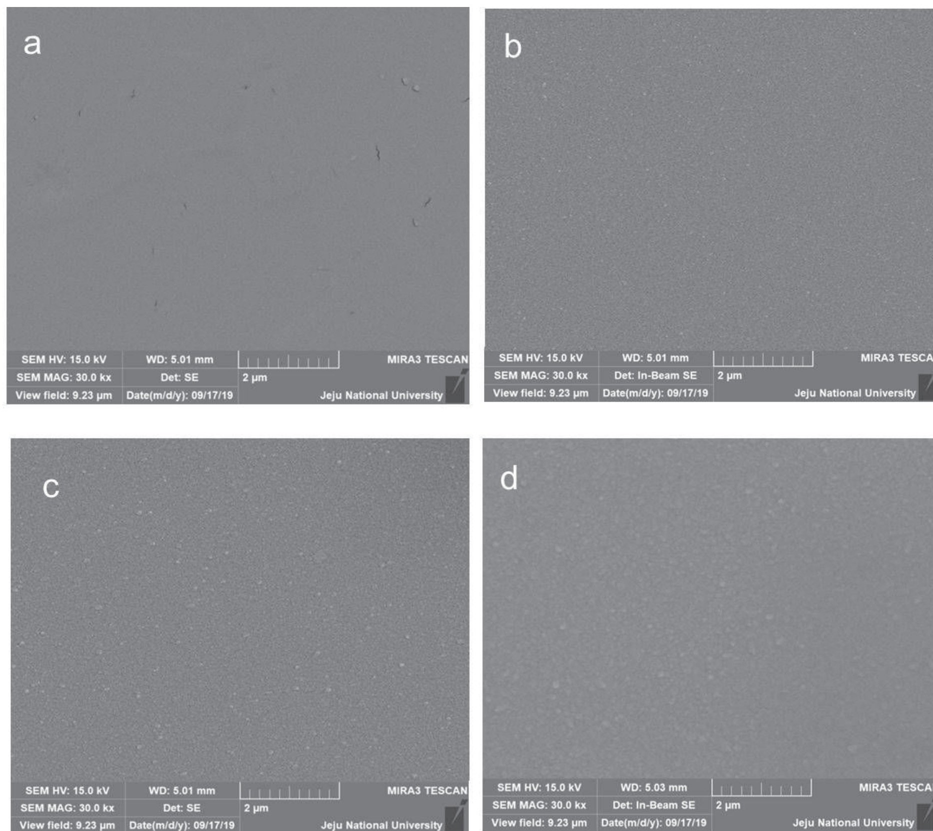

Figure 5. 16 SEM morphology of Rh surface deposited on Mo substrate at 40 W; (a) Mo pristine surface; (b) Zr-Rh thin film surface deposited by NAD; (c) Zr-Rh film deposited with IA-OAD; and (d) Zr-Rh OAD (fixed substrate)

Along with the EDS, FESEM analysis also performed on the Zr-Rh deposited surface. Figure 5.16 shows the SEM images of the Rh thin films deposited at 40 W power. Figure 5.16 (a) is the bare pristine Mo bulk material surface, where we can see clean surface with large crystalline boundary; (b) image is the surface coated with normal angle deposition process, (c) image shows the ion-assisted oblique angle deposition and (d) is the thin film of Rh coated with oblique angle deposition. With the visual inspection, we can say that grain size is more pronounced on the surface of the film, which was deposited by only the OAD (fixed substrate) process. The reason for the increase in the grain will be discussed in the next section.

제주대학교 중앙도서관
JEJU NATIONAL UNIVERSITY LIBRARY

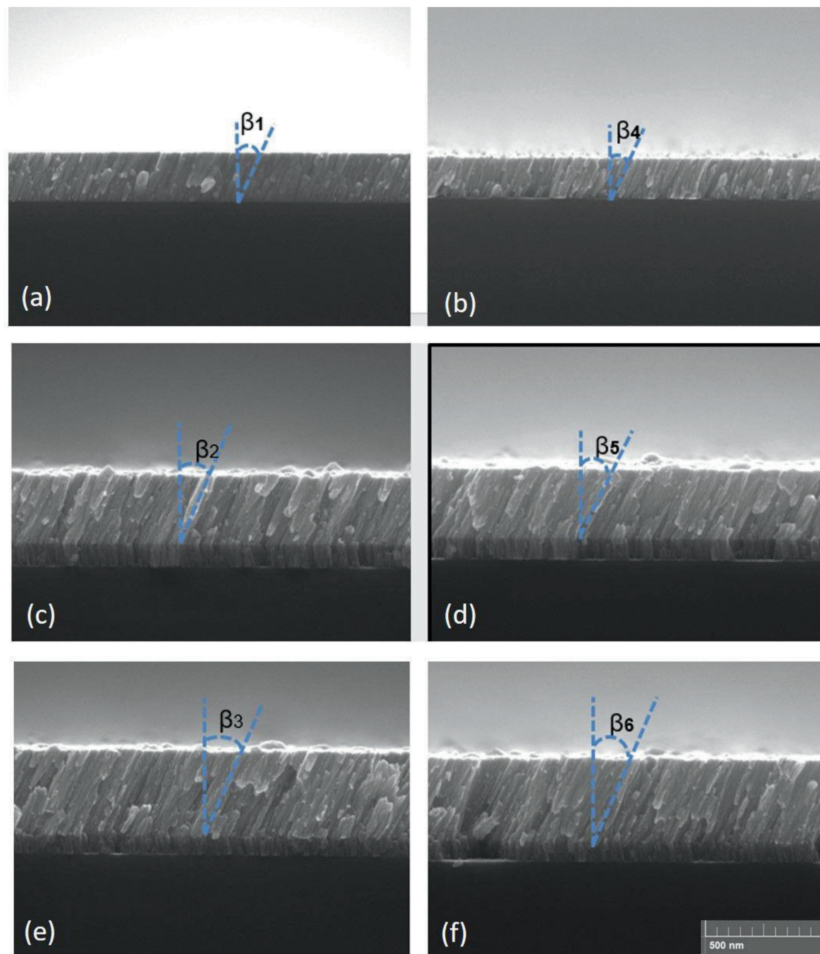

Figure 5. 17 SEM images of the thin-film OAD process at the power of 40, 100, 200 W.

Using Si wafer as a substrate is easy for handling, storing, and cleaning, hence we used Si wafers to deposit Zr and Rh films to check the thickness and the orientation of the film growth. Figure 5.17 reveals the orientation of the films. The columnar structure was clear and tilted away from the vertical. It is due to the oblique angle of deposition at 54° degree with the vertical plane. Dual DCMS and DC ion sources were used for the deposition. In the above figure, 5.17, (a) and (b) films were deposited at 40 W power with ion-assisted deposition and without ion assistance, respectively. The angle between the film growth direction and the vertical plane is termed as β. The angle of tilt approximately we calculate β- 25°. On the images (c) and (d) (figure 5.17)

제주대학교 중앙도서관
JEJU NATIONAL UNIVERSITY LIBRARY

films were deposited at the 100W, it has a tilt angle of β-26°.

Similarly, images (e) and (f) (figure 5.17) were the films deposited by the power of 200W and its columnar structure tilted to the β-30° degree. To analyzed the columnar microstructure, surface morphology optical and mechanical properties of the thin films, different power supplies were used. As the power increase, the columnar microstructure also increases with the increase in tilt angle because of the deposition rate and the temperature increase [82], [83]. This shadowing effect and limited surface diffusion can produce a higher tilted microstructure like sculpture when parameters were controlled [84].

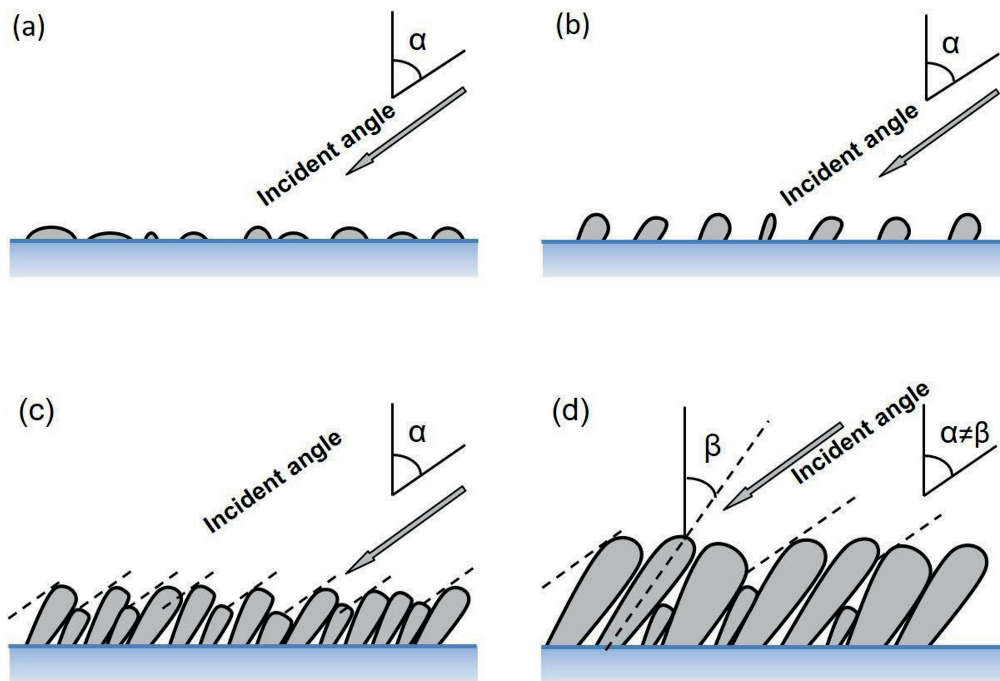

Figure 5. 18 Schematic view of OAD film growth; (a) initially few particles reaching at the substrate surface at an angle of α random;(b) nuclei grows with more ions and

제주대학교 중앙도서관
JEJU NATIONAL UNIVERSITY LIBRARY

atoms deposition; (c) columns growth develop as partially shadowing the neighboring columns and suppressing the growth and (d) columns grow with more tilting towards the incident angle and some columns completely stop growth, leaving void between two shadowing columns.

During the oblique angle deposition at an angle of α (incident angle) shown in figure 5.18 (a), at the initial stage of film formation, few particles of target material randomly form film nuclei when particles arrive at the substrate surface. As seen in figure 5.18 (b) nuclei grows into the column as more particles arrive and growth direction takes towards the source of the particles. As the particles distributed randomly, nuclei growth will vary as casting shadows to the neighboring nuclei from reaching the flux and suppress their growth (figure 5.18 c). With more extended time, smaller columns will be shadowed entirely and stop growing because of the shadowing effect of larger columns, as in figure 5.18 (d). The vanishing of the grown column is termed as column extinction[54]. This extinction of columns usually leaves a void between them, which might be the reason to have low adhesion of the films if they were not controlled properly. Nuclei grow towards the direction of the source with a deposit of flux on the top of one another, and self-reinforcing behavior develops, with the low surface mobility adatom growth will take into the form of columnar microstructure. Sometime this column size can be larger than the deposited film thickness [85]. The growth of the tilted columns depends on the shadowing between columns, deposition rate, temperature, pressure, substrate material, and it's surface, substrate preparation, and target materials [54]. It is found out that increasing substrate temperature has been shown to decrease column number density [86].

제주대학교 중앙도서관
JEJU NATIONAL UNIVERSITY LIBRARY

Introduction of the ion-assisted deposition (IAD), in a high vacuum condition the void left by the extinction of columns, can be filled, as ions will fall on that void space where the shadowing effect started due to outgrown of neighboring columns. Hence conjunction with the ion beam assisted deposition (IBAD) or IAD oblique angle deposition (IA-OAD) can be implemented to have a smoother and stronger surface of the film. This IA-OAD process might increase the optical properties too. We saw in figure 5.8- 5.12, 3D nano surface profiler observed the roughness decrease with the IA-OAD process on the films for the same parameters of the deposition.

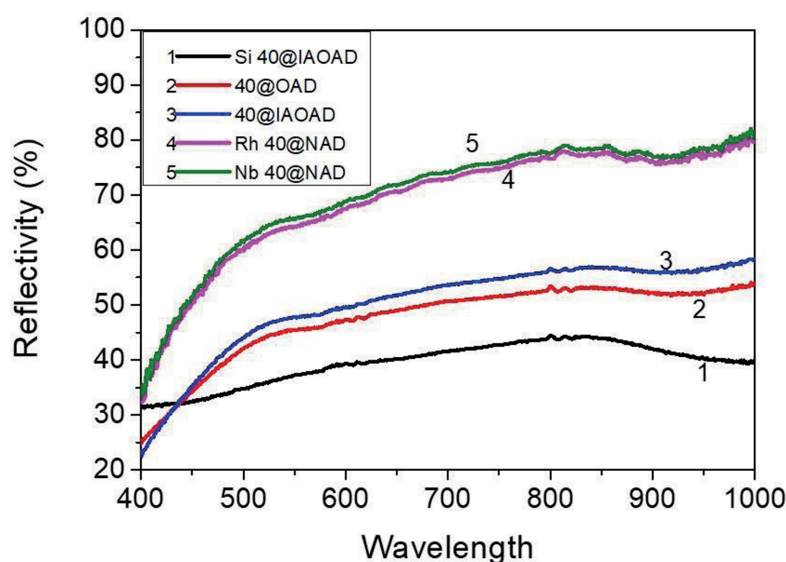

Figure 5. 19 Graph of reflectivity of the Zr-Rh fabricated thin-film coated mirrors at 40 W power; (1) Si substrate coated mirror has the lowest reflectivity (40%) as compared to all other Mo substrate coated mirrors; (2)OAD film has around 50% with tilted columnar structure on the Mo substrate; (3) mirror has nearby 55% of reflectivity due to ion-assisted deposition; (4 and 5) both mirror has highest among all almost 77% of total reflectivity, both were deposited normal angle of deposition

제주대학교 중앙도서관
JEJU NATIONAL UNIVERSITY LIBRARY

The reflectivity of the thin film surface is the vital parameter for the optical diagnostics, and reflectivity must be fair enough to reflect the signals. As in figure 5.19 (1), Zr-Rh coated Si substrate has very low reflectivity (40%) measured by the UV-Vis spectroscopy. Low reflectivity might be due to the translucent nature of the wafer and the possibility of light transmitted through the Si substrate is high. Figure 5.19 (2), OAD mirror has slightly more reflectivity than Si substrate, reason can be as the porosity of the films due to shadowing and column extinction. Hence the light might have been dispersed from the film surface even though the surface is smooth. In figure 5.19 (3) spectrum of IA-OAD has reflectivity around 55%. The ion deposition on it filled slight improvement in the reflectivity as the porous or void space. Nevertheless, as the column grows a continuous bombardment of energetic ions on the top of the column might rupture the surface, thus reflectivity of the film reduced, although adhesion strength of the films is reasonably stable. Figure 5.19 (4 and 5) both Nb and Zr interlayered coating was performed by normal angle deposition. SEM images show that the surfaces of the films are smoother and have a high reflectivity percentage. It is due to the uniform deposition of the particles with a concentrated flux of target material [87], [88]. The reason for the lower reflectivity of OAD and IA-OAD might be due to the porosity and the damage of the columnar microstructure [87]. The deposition power increase, the columnar microstructure also increases the microstructural damage or porosity of the films[89]. The tilt angle of measurement also affects the reflectivity of the surface. So, measuring from a different direction may have a different value of reflectance [90].

제주대학교 중앙도서관
JEJU NATIONAL UNIVERSITY LIBRARY

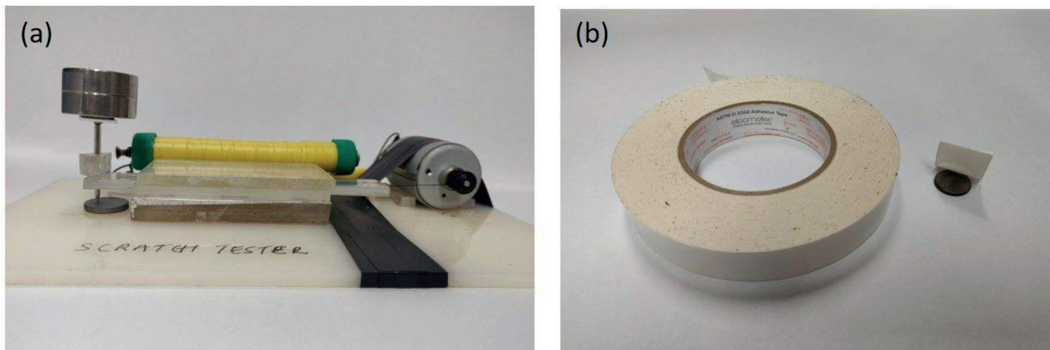

Figure 5. 20 Image of the lab-made scratch tester (a) and pressure-sensitive tape (b)

.

제주대학교 중앙도서관
JEJU NATIONAL UNIVERSITY LIBRARY

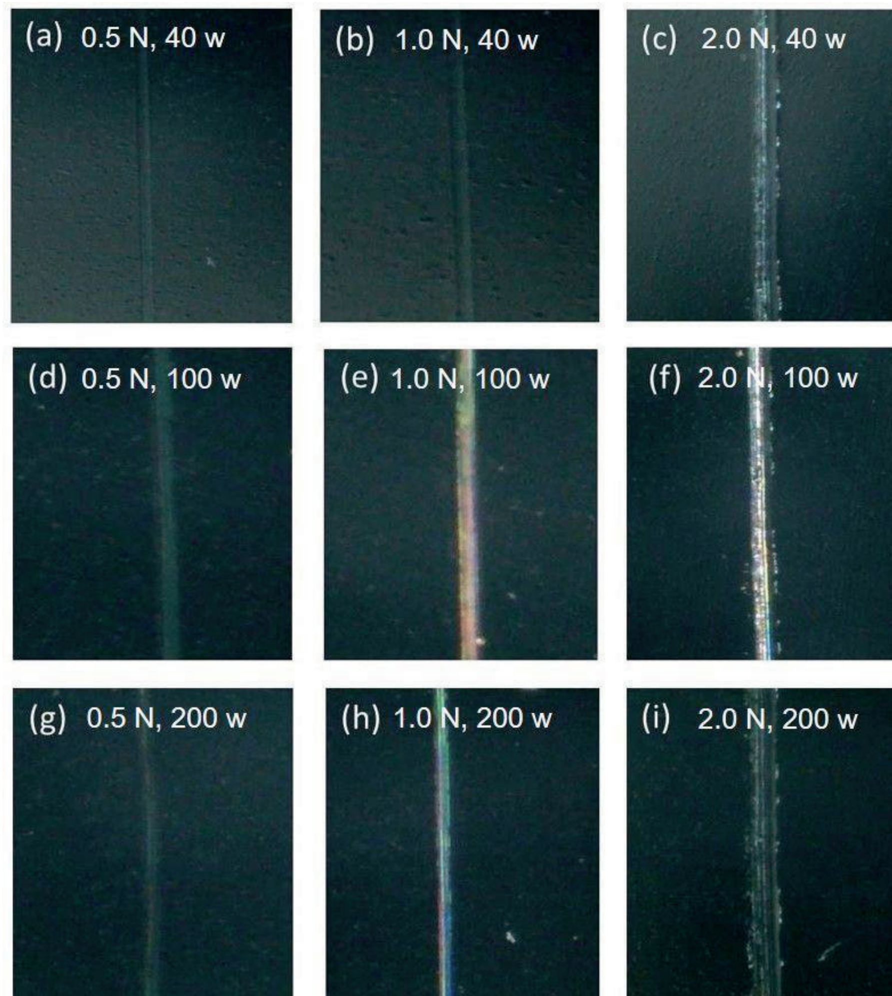

Figure 5. 21 Scratch test results of IA-AOD technique thin film surface deposited by three different power (a) ,(b) and (c) by 40 W; (d), (e) and (f) by 100 W; (g), (h) and (i) by 200 W.

For reliability and durability of films, surface adhesion must be good enough to sustain specific force and scratches. Surface film prepared by the process of IA-AOD by 40, 100 and 200 W powers were tested their adhesion strength by scratch test and pressure-sensitive test, as shown in figure 5.20. Lab-made scratch tester was used to scratch on the surface by applying a minimum vertical load of 0.5, 1, and 2 N. figure 5.21 shows the scratch marks made by sliding the needle along the surface of fabricated multilayers films. As in Figure 5.21 (a, d, and g) in all films, 0.5 N did not damage the

제주대학교 중앙도서관
JEJU NATIONAL UNIVERSITY LIBRARY

surface. The film deposited by 40 w power (figure 5.21 b) also has no apparent damage on the surface by the scratcher applied a vertical load of 1 N, but in the figure 5.21 (c, f and i) all have visible scratch marks by the 2 N load on the films. In all films. These results show that the IA-OAD technique has better film adhesion with the substrate; it is due to the compact deposition of film layers by filling up the void space by the extra ions from the ion source [91]. Another reason for stronger adhesion is due to relieving the internal stress by heat treatment and heating films might increase the column size to have tight-fitting between columns [92]. As per the Mie theory, small partials are absorbed higher than the bigger particles [58].

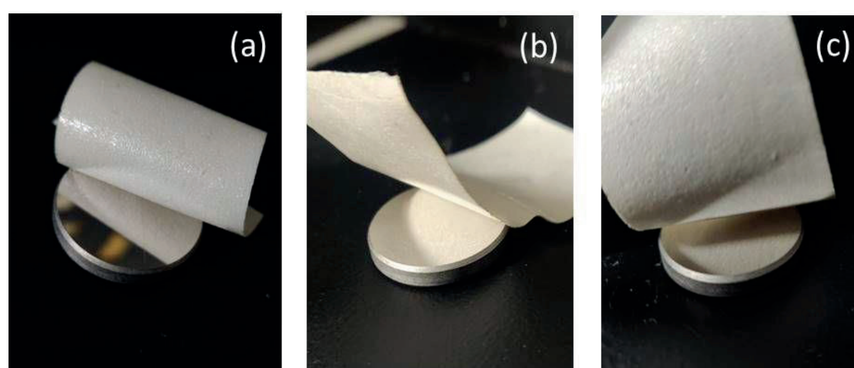

Figure 5. 22 photographic image of Zr-Rh coated Mo mirror; Mirror prepared by 40 w (a), 100 W (b) and 200 W (c) power with the Ion beam assisted OAD process

As in the figure 5.22, tape test was performed for thrice for all samples, giving pressure about of 20 N force, we thought this force was enough to test the pressure stripping of the coated film by the pressure-sensitive tape. In the 5.22. Figure (a), (b) and (c) are the mirrors fabricated by using the power of 40, 100 and 200 W; all the test result shows no stripping or peel of the thin films from the substrate surface.

제주대학교 중앙도서관
JEJU NATIONAL UNIVERSITY LIBRARY

All the above results show the scratch tests and tape tests show good adhesion of the films by IA-OAD techniques. Films become stronger by energetic ions bombardment on the surface of the substrate, which acts as the stitching of the nuclei. [61]

5.4 Conclusion

Ion beam assisted deposition on oblique angle deposition (IBAD-OAD) shows the excellent adhesion and durability of the film by compact and dense columnar microstructure film growth. However, adhesion strength comes with the loss of reflectivity. Thus, we can conclude that thin films fabricated by using IBAD-OAD might not have enough reflectivity to perform an optical diagnostic on the fusion reactors. Still, the Zr is a good candidate material that bridges the thermal expansion coefficient of two (Mo and Rh) choice materials. Therefore, with all the above results we can conclude that by using techniques of IA- OAD, film growth structure and its properties is more useful in other microelectronics and semiconductor application rather than optical diagnostics of the fusion reactor that needs higher reflectivity (above 70%).

.

제주대학교 중앙도서관
JEJU NATIONAL UNIVERSITY LIBRARY

CHAPTER 6
Summary, Future Work and Conclusion

6.1 Summary,

This chapter summarizes the overall view of this thesis work, possible future work, and the conclusion. The thesis is a comprehensive study of fabrication of metallic mirrors by the introduction of thin interlayer material between two choices of metals to produce "First Mirror" for the fusion reactor. Nuclear fusion power has been taken as the most attractive long-term production of clean energy solutions in the future. Although it was all started with the ambitious project, now it is proving as the scientific

The essential task of controlling and to know phenomena of the thermonuclear fusion plasma, requires a large number of optical diagnostic systems that are based on reflected, scattered plasma electromagnetic radiation by a chain of optical elements. The most important components of the optical diagnostic are the metallic mirrors that directly face the burning plasma. The exposure to the extremely high-temperature plasma environment FMs is subjected to erosion and re-deposition of the contaminants on the surface, affecting their reflectivity performance. This phenomenon of degradation of optical performance is the critical issue to FMs durability and longevity. There have been lots of research carried out to tackle this problem and to implements the best material and fabrication method. Considering the optical performances and properties of materials to withstand the harsh environment of fusion plasma, the Mo and Rh have been chosen for the FMs' material. However, the high production cost of bulk Rh mirrors and limited technical issues of producing large mirrors (up to 500 mm

제주대학교 중앙도서관
JEJU NATIONAL UNIVERSITY LIBRARY

diameter); instead, thin film deposition on the Mo substrate is seen as more feasible to fabricate Mo-Rh mirrors.

We understood that FMs are in different sizes and shapes that depend on the location and requirements of the fusion reactor. FMs subjected to high radiation, CXN particles, erosion, and redeposition on the surface and occurs gradual decrease of optical properties. Therefore, there has been developed various methods and techniques to fabricate the FMs according to the requirement and material choice.

FMs must satisfy some essential requirements to be used in the fusion reactor;

- It should high reflectivity as possible
- Reflectivity should not depend too much on the wavelength in the operating spectral range.
- Resistance to physical and chemical reactivity
- High thermal conductivity and resistance to high temperature.
- Low sputter yield.

Progressive degradation of optical properties is the primary concern of the FM application in the fusion reactor. In several choice materials that could be used for the fabrication of the mirror, we were motivated to improve the performance of the FMs and tried to reduce the thermal coefficient gap of different materials.

This thesis aims to fabricate a thin layer of Nb or Zr materials between Mo and the Rh material by using lab-scale equipment (experimental setup for DC magnetron sputtering system) and analyze with the available devices and instruments in the Jeju National University.

제주대학교 중앙도서관
JEJU NATIONAL UNIVERSITY LIBRARY

We can summarize our thesis as;

- A new technique for fabricating a rhodium (Rh) coated molybdenum (Mo) mirror with niobium (Nb) thin interlayer, can withstand high temperature and has excellent adhesion strength with acceptable reflectivity as compare to the other research articles (Usual reflectivity of FMs are above 70% is considered high reflectivity in the fusion plasma).
- Mimicking the plasma environment, we treat samples at high temperatures at 200°C for 6 hours and cooled down naturally to room temperature. This heat treatment increases the grain size and roughness of the surface, eventually reducing the reflectivity by 10-15%.
- Apparently, we can see from the scratch test till the 1 N dead load applied on the deposited film can resist scratch of tungsten carbide spherical tip radius of 250 μm under the scratching rate of 37 mm/sec by the lab-made scratch tester. We have compared this scratch test with the results of the standard CSM Micro Scratch tester instrument. which has a diamond stylus, a spherical tip radius of 200 μm. During the test, the load is applied 0-20 N progressively at a rate of 10 N/min for the scratch length of 10 mm. Our test result shows similar resistance but still, we think it is not fair to compare the results of both scratch tests as they are tested under different types of devices and testing processes. Nb interlayer reduces the thermal expansion problem of the deposited thin film by bridging between the Rh and Mo interfaces. From the experiment, we have seen the lower deposition power (40 W) has fine grain growth.
- Zr interlayer also shows the same bridging characteristics as that of Nb interlayer material between Mo and Rh. Tape test revealed that sufficient pressure

제주대학교 중앙도서관
JEJU NATIONAL UNIVERSITY LIBRARY

given to pressure-sensitive tape stick on the deposited film has good adhesion strength. Force applied to the tape by hand was approximately 20 N. 200 W deposited film failed after 5 or more continuous tape test processes.

- Zr and Nb interlayer coated Mo-Rh mirrors (40 W power) have the reflectivity around 75% after heat treatment at a temperature (at 200 ℃ for 6 hours). This reflectivity also comparable to the other research articles and claim acceptable reflectivity for the fusion reactor diagnostic system. Results also show that higher power deposition has higher reflectivity (80-85%, 200 W) but later appears thermal distortion on the thin film layers.

- Zr-Rh mirror fabricated by the Oblique angle deposition process (substrate rotating) has a lower reflectivity percentage than that of the normal angle deposition process. At 800 nm wavelength deposited thin films have 10% different (NAD and OAD) in reflectivity

- Exposed to high-temperature, the thin-film deposited substrate at 200o C for 4 hrs shows a slightly small growth of grain sizes than that of heat-treated samples for 6 hrs.

- Ion beam assisted deposition (Rh-Zr-Mo) on oblique angle deposition (IBAD-OAD) (fixed substrate) shows the good adhesion and durability of the film by compact and dense columnar microstructure film growth. Scratch test results show, better adhesion and scratch resistance compare with films deposited without ion-assisted deposition.

- Thin films fabricated by using IBAD-OAD have good scratch resistance and adhesion property but have low reflectivity (approx. 55%, 40 W power), it is much

제주대학교 중앙도서관
JEJU NATIONAL UNIVERSITY LIBRARY

lower reflectivity of the FMs that are tested for the in-situ for fusion reactor. acceptable performance for an optical diagnostic on the fusion reactor.

6.2 Conclusion

The focus of this thesis was to investigate the potential another new way of fabricating Rh thin films on the Mo bulk substrate with interlayer coating. Our characterization and analysis showed that the thin film of Rh-NB/Zr-Mo was fabricated successfully.

Deposited thin films are polycrystalline in nature and they have high reflectivity (about 75% for 40 W) even after high-temperature heat treatment (at 200 ℃ for 4-6 hrs) (for mimicking the fusion plasma) with the result we can conclude that reflectivity of the fabricated mirror is good enough (usually FMs reflectance test in-situ were above 70%) and fabricated FM can be used in a fusion plasma for the optical diagnostic.
Interlayer material both Nb and Zr, can be the good candidate materials if Mo and Rh material really needs the interlayer coat to reduce thermal stresses on the interface between two different materials.

With our experimental setup, a higher thickness coat can be fabricated due to technical and time constraints, and we deposited 190 nm of thin layers over the entire experiment. Even that thin layer scratch and tape test show the good adhesion strength with our lab-made scratch tester and pressure-sensitive tape. Results show 1 N of load with the scratch rate of 37 mm/sec, no apparent damage to the surface. But still recommended testing in standard scratch tester instrument which will give accurate and reliable results.

제주대학교 중앙도서관
JEJU NATIONAL UNIVERSITY LIBRARY

The roughness of the surface increases with the increased supplied power in the OAD process but decreases when the ion beam assisted the deposition. (IA-OAD). Average roughness is in the range of 2-5 nm for IA-OAD but reflectance drop-in can be due to void and porosity in the layer.

Hence, the experimental study can conclude that techniques of the IA-OAD process are more useful in other microelectronics and semiconductor applications than optical diagnostics of the fusion reactor due to its poor reflectivity.

6.3 Future Work

As far as the future work and future research areas are concerned, it is believed that there is a lot of room available to produce high quality of FMs with applying interlayer between Mo-Rh mirrors. The work in this thesis has been carried out with our available resources in our laboratory and university. It is important to the in-situ test of the fabricated mirror to know the exact optical performance and lifetime. It would be better to do a scratch test with a standard instrument than a lab-made device which might give accurate results.

The size of the mirror differs from location and position inside the reactor. Hence it is possible to fabricate larger and thicker films and tests in an actual plasma environment. There has been fast and continuous progress in the field of fusion power to realize in the near future, therefore continuously trying out with new innovative ideas, new technologies, and hard work can reach the goal successfully.

Future work can be included removable of contaminants re-deposited on the mirror surface. Polishing of IA-OAD films' surface to have higher reflectivity because

제주대학교 중앙도서관
JEJU NATIONAL UNIVERSITY LIBRARY

our experimental results show that the IA-OAD process has better adhesion strength but lower reflectance.

Therefore, continuously trying out with new innovative ideas, new technologies, and hard work can guarantee the high quality and better performance of the optical mirror as per the requirement of the fusion reactor application to realize the fusion energy in the near future.

제주대학교 중앙도서관
JEJU NATIONAL UNIVERSITY LIBRARY

REFERENCE

[1] Alexander Piel, *An Introduction to Laboratrory, Space, and Fusion Plasmas*. 2010.

[2] K. Nagaoka, M. Isobe, K. Shinohara, and M. Osakabe, “Energetic Ion Measurements Using a Directional Probe,” *Communications*, vol. 1, pp. 8–9, 2006.

[3] Jeffrey P. Freidberg, *Plasma Physics and Fusion Energy*. 2007.

[4] “https://en.wikipedia.org/wiki/Nuclear_fusion.”

[5] W. M. Stacey, *Stacey - Fusion Plasma Physics*. 2005.

[6] G. De Temmerman, “On the lifetime of the first mirrors in the diagnostic systems of the international thermonuclear experimental reactor,” p. 147, 2006.

[7] “https://www.sciencelearn.org.nz/resources/242-plasmas-and-nuclear-fusion.”

[8] A. Uccello, “Development of nanostructured rhodium films for diagnostic mirrors employed in nuclear fusion systems,” 2014.

[9] K. Seshan, *Handbook of Thin Film Deposition*. .

[10] “https://www.iter.org.” .

[11] “https://www.iter.org/mach/Tokamak.” .

[12] J. Wesson, *Tokamaks*, 2nd ed. 1997.

[13] “https://en.wikipedia.org/wiki/ITER.” .

제주대학교 중앙도서관
JEJU NATIONAL UNIVERSITY LIBRARY

[14] and P. T. T. Sugie, A. Costley, A. Litnovsky, "Update of First Mirror Table.12th Meeting of the ITPA Topical Group on Diagnostics," 2007.

[15] K. Y. Vukolov *et al.*, "Main challenges for ITER optical diagnostics," *AIP Conf. Proc.*, vol. 1612, pp. 164–170, 2014.

[16] T. SUGIE, A. COSTLEY, A. MALAQUIAS, and C. WALKER, "Spectroscopic Diagnostics for ITER," *J. Plasma Fusion Res.*, vol. 79, no. 10, pp. 1051–1061, 2003.

[17] S. Prunty, M. Spillane, and C. Walker, "Poloidal polarimeter for current density measurements in ITER," vol. 4694, no. November 2004, 2013.

[18] S. Rai, U. Shaislamov, J. K. Yang, S. Saud, W. A. Muhammed, and H. J. Lee, "Deposition and Characterization of a Rhodium Thin Films with a Niobium Interlayer on a Molybdenum Mirror for ITER First-Mirror Application," *J. Korean Phys. Soc.*, vol. 75, no. 8, pp. 644–651, 2019.

[19] M. Joanny *et al.*, "Engineering and manufacturing of ITER first mirror mock-ups," *Rev. Sci. Instrum.*, vol. 81, no. 10, pp. 1–4, 2010.

[20] K. Seshan, *Handbook of Thin Film Deposition*. 2002.

[21] P. M. Lloyd, J. R., and Smith, "Electromigration Lifetime of Al/Cu Thin Film Conductors," *J. Vac. Sci. Technol*, vol. 1, no. 12, p. 455, 1983.

[22] Solomon, P. M., "The Need for Low Resistance Interconnections in Future High Speed Systems," *SPIE, 947:104 (1988)*.

[23] Mastroianni S., "Multilevel Metallization Device Structures and Process Options," *Solid State Tech*, no. 155, 1984.

제주대학교 중앙도서관
JEJU NATIONAL UNIVERSITY LIBRARY

[24] V. Voitsenya *et al.*, “Diagnostic first mirrors for burning plasma experiments (invited),” *Rev. Sci. Instrum.*, vol. 72, no. 1 II, pp. 475–482, 2001.

[25] L. Marot *et al.*, “ITER first mirror mock-ups exposed in Magnum-PSI,” *Nucl. Fusion*, vol. 56, no. 6, 2016.

[26] L. Marot *et al.*, “Optical Coatings as Mirrors for Optical Diagnostics,” pp. 72–78, 2016.

[27] L. Moser *et al.*, “Plasma cleaning of beryllium coated mirrors,” *Phys. Scr.*, vol. 2016, no. T167, p. 14069, 2016.

[28] A. Litnovsky, V. S. Voitsenya, A. Costley, and A. J. H. Donné, “First mirrors for diagnostic systems of ITER,” *Nucl. Fusion*, vol. 47, no. 8, pp. 833–838, 2007.

[29] B. Eren *et al.*, “In situ evaluation of the reflectivity of molybdenum and rhodium coatings in an ITER-like mixed environment,” *J. Nucl. Mater.*, vol. 438, no. SUPPL, pp. S852–S855, 2013.

[30] Y. Krasikov, A. Panin, A. Litnovsky, P. Mertens, and M. Schrader, “Specific design and structural issues of single crystalline first mirrors for diagnostics,” *Fusion Eng. Des.*, vol. 124, pp. 548–552, 2017.

[31] B. Eren *et al.*, “Reflective metallic coatings for first mirrors on ITER,” *Fusion Eng. Des.*, vol. 86, no. 9–11, pp. 2593–2596, 2011.

[32] L. Marot, G. De Temmerman, P. Oelhafen, G. Covarel, and A. Litnovsky, “Rhodium coated mirrors deposited by magnetron sputtering for fusion applications,” *Rev. Sci. Instrum.*, vol. 78, no. 10, 2007.

제주대학교 중앙도서관
JEJU NATIONAL UNIVERSITY LIBRARY

[33] A. Litnovsky *et al.*, “First direct comparative test of single crystal rhodium and molybdenum mirrors for ITER diagnostics,” *Fusion Eng. Des.*, vol. 123, pp. 674–677, 2017.

[34] L. Moser *et al.*, “Investigation and plasma cleaning of first mirrors coated with relevant ITER contaminants: Beryllium and tungsten,” *Nucl. Fusion*, vol. 57, no. 8, 2017.

[35] Https://en.wikipedia.org/wiki/Thermal_expansion_coefficients_of_the_elements_(data_page), “Thermal expansion coefficients of the elements.” .

[36] H. Adachi, T. Hata, and K. Wasa, “Basic Process of Sputtering Deposition,” *Handb. Sputter Depos. Technol. Fundam. Appl. Funct. Thin Film. Nano-Materials MEMS Second Ed.*, no. Lcd, pp. 295–359, 2012.

[37] D.-J. Kwak, B.-W. Park, Y.-M. Sung, and M.-W. Park, “Effects of Gas Pressure and Discharge Power on Electrical and Optical Properties of Zno:Al Thin Film Deposited on Polymer Substrate,” *Japan Soc. Plasma Sci. Nucl. Fusion Res.*, vol. 8, pp. 1427–1430, 2009.

[38] “https://www.zebrapen.com (emailed).” .

[39] J. A. Thornton and J. Y. Thompson, “High rate thick film growth,” *Annu. Rev. Mater. Sci.*, vol. 7, pp. 239–60, 1977.

[40] B.-C. Luo, K. Li, J.-Q. Zhang, J.-S. Luo, W.-D. Wu, and Y.-J. Tang, “Effect of argon gas pressure on residual stress, microstructure evolution and electrical

제주대학교 중앙도서관
JEJU NATIONAL UNIVERSITY LIBRARY

resistivity of beryllium films," *J. Korean Phys. Soc.*, vol. 68, no. 4, pp. 557–562, 2016.

[41] Y. Shin, Y. Hwang, Y. Um, D. A. Tuan, S. Cho, and H. Park, "Structural and optical properties of polycrystalline NiO thin films prepared by using the oxidation of the metallic Ni," *J. Korean Phys. Soc.*, vol. 63, no. 6, pp. 1199–1202, 2013.

[42] X. Liu, H. Cui, X. Hao, S. Huang, and G. Conibeer, "Effect of vacuum thermal annealing on a molybdenum bilayer back contact deposited by radio-frequency magnetron sputtering for chalcogenide- and kesterite-based solar cells," *J. Korean Phys. Soc.*, vol. 71, no. 12, pp. 968–973, 2017.

[43] I. J. Kang, M. G. Ko, J. K. Yang, and H. J. Lee, "Plasma surface treatments by using a dielectric barrier discharge for the deposition of diamond films," *J. Korean Phys. Soc.*, vol. 63, no. 2, pp. 199–205, Aug. 2013.

[44] J. E. Nestell and R. W. Christy, "Reflectance and structure of evaporated chromium and molybdenum films," *J. Vac. Sci. Technol.*, vol. 15, no. 2, pp. 366–369, 2002.

[45] M. Nayak, G. S. Lodha, and R. V. Nandedkar, "X-ray reflectivity investigation of interlayer at interfaces of multilayer structures: Application to Mo/Si multilayers," *Bull. Mater. Sci.*, vol. 29, no. 7, pp. 693–700, 2006.

[46] L. Marot, G. Covarel, M. H. Tuilier, R. Steiner, and P. Oelhafen, "Adhesion of rhodium films on metallic substrates," *Thin Solid Films*, vol. 516, no. 21, pp. 7604–7608, 2008.

제주대학교 중앙도서관
JEJU NATIONAL UNIVERSITY LIBRARY

[47] A. Litnovsky *et al.*, "Diagnostic mirrors for ITER: Research in the frame of International Tokamak Physics Activity," *Nucl. Fusion*, vol. 59, no. 6, 2019.

[48] D. R. Baer and S. Thevuthasan, "Characterization of Thin Films and Coatings," *Handb. Depos. Technol. Film. Coatings*, pp. 749–864, 2010.

[49] F. Ding *et al.*, "Overview of plasma-material interaction experiments on EAST employing MAPES," *Journal of Nuclear Materials*, vol. 455, no. 1. pp. 710–716, 2014.

[50] J. C. Pivin, "An overview of ion sputtering physics and practical implications," *J. Mater. Sci.*, vol. 18, no. 5, pp. 1267–1290, 1983.

[51] S. Ebnesajjad, *Surface and material characterization techniques*. 2011.

[52] M. Henini, *Handbook of Thin-Film Deposition Processes and Techniques*, vol. 31, no. 3. 2000.

[53] J. Snyder, N. M. Markovic, and V. R. Stamenkovic, "Single crystalline thin films as a novel class of electrocatalysts," *Journal of the Serbian Chemical Society*, vol. 78, no. 11. pp. 1689–1702, 2013.

[54] M. T. Taschuk, M. M. Hawkeye, and M. J. Brett, *Glancing Angle Deposition*, Third Edit. Elsevier Ltd., 2010.

[55] M. Mayer *et al.*, "Tungsten erosion and redeposition in the all-tungsten divertor of ASDEX Upgrade," *Phys. Scr. T*, vol. T138, 2009.

[56] N. Hashimoto, Y. Yamamoto, and S. Niijima, "The Change of the Surface Morphology and Optical Properties During the Heat-Treatment for Silver Films

제주대학교 중앙도서관
JEJU NATIONAL UNIVERSITY LIBRARY

Deposited on Silicas," *e-Journal Surf. Sci. Nanotechnol.*, vol. 3, no. April, pp. 120–124, 2005.

[57] K. Bordo and H. G. Rubahn, "Effect of deposition rate on structure and surface morphology of thin evaporated al films on Dielectrics and Semiconductors," *Medziagotyra*, vol. 18, no. 4, pp. 313–317, 2012.

[58] A. . Fallis, *Hand Book of Printed Electronics Depositions*, vol. 53, no. 9. 2013.

[59] A. V. Rogov and K. Y. Vukolov, "Magnetron deposition of molybdenum mirrors and micrometer-thick mirror foil with an ordered columnar nanocrystalline structure," *Tech. Phys.*, vol. 51, no. 4, pp. 499–503, 2006.

[60] Jagannathan thirumalai, "Introductory Chapter: The Prominence of Thin Film Science in Technological Scale," *Intech*, vol. i, no. tourism, p. 13, 2016.

[61] J. J. Shea, *Handbook of thin film deposition - processes and technologies, 2nd edition [Book Review]*, vol. 18, no. 4. 2005.

[62] D. M. Mattox, *Handbook of Physical Vapor Deposition (PVD) Processing*, Second Edi. Elsevier Inc, 2010.

[63] H. Frey and H. R. Khan, *Handbook of Thin-Film Technology*. 2015.

[64] G. Bräuer, "Magnetron Sputtering," *Compr. Mater. Process.*, vol. 4, pp. 57–73, 2014.

[65] J. Gil-Rostra, F. J. García-García, F. J. Ferrer, A. R. González-Elipe, and F. Yubero, "Microstructure of mixed oxide thin films prepared by magnetron sputtering at oblique angles," *Thin Solid Films*, vol. 591, pp. 330–335, 2015.

제주대학교 중앙도서관
JEJU NATIONAL UNIVERSITY LIBRARY

[66] R. M. A Lakhtakia, *Sculpturd Thin film: Nanoengineered morphology and optics*. SPIE Press, 2005.

[67] K. Robbie and M. J. Brett, “Sculptured thin films and glancing angle deposition: Growth mechanics and applications,” *J. Vac. Sci. Technol. A Vacuum, Surfaces, Film.*, vol. 15, no. 3, pp. 1460–1465, 1997.

[68] Y. Zhao, D. Ye, G.-C. Wang, and T.-M. Lu, “Designing nanostructures by glancing angle deposition,” *Nanotub. Nanowires*, vol. 5219, p. 59, 2003.

[69] A. R. J. Gil-Rostra, M. Cano, J.M. Pedrosa, F.J. Ferrer, F.J. Garcia-Garcia, F. Yubero and Gonzalez-Elipe, “Electrochromic behaviour of WxSiyOz thin films prepared by reactive magnetron sputtering at normal and glancing angles,” *ACS Appl. Mater. Interfaces*, vol. 4, p. 628, 2012.

[70]] J. Gil-Rostra, F.J. Garcia-Garcia, F. Yubero, A.R. Gonzalez-Elipe, “Tuning the transmittance and the electrochromic behaviour of CoxSiyOz thin films prepared by magnetron sputtering at glancing angle,” *Sol. Energy Mater. Sol. Cells*, vol. 123, p. 130, 2014.

[71] A. R. G.-E.] F.J. Garcia-Garcia, J. Gil-Rostra, F. Yubero, “Electrochromism in WOx and WxSiyOz thin films prepared by magnetron sputtering at glancing angles,” *Nanosci. Nanotechnol. Lett*, vol. 5, p. 89, 2013.

[72] J. W. G. and S. M. Darina Manova, “Thin Film Deposition Using Energetic Ions,” pp. 4109–4141, 2010.

제주대학교 중앙도서관
JEJU NATIONAL UNIVERSITY LIBRARY

[73] K. H. Bäther, U. Herrmann, and A. Schröer, “Ion-beam-assisted deposition of magnetron-sputtered metal nitrides,” *Surf. Coatings Technol.*, vol. 74–75, no. PART 2, pp. 793–801, 1995.

[74] Y. P. Pershyn *et al.*, “Effect of working gas pressure on interlayer mixing in magnetron-deposited Mo/Si multilayers,” *Opt. Eng.*, vol. 52, no. 9, p. 95104, 2013.

[75] D. Toledano, R. E. Galindo, M. Yuste, J. M. Albella, and O. Sánchez, “Compositional and structural properties of nanostructured ZnO thin films grown by oblique angle reactive sputtering deposition: Effect on the refractive index,” *J. Phys. D. Appl. Phys.*, vol. 46, no. 4, 2013.

[76] J. Sotelo, J. Ederth, and G. Niklasson, “Optical properties of polycrystalline metallic films,” *Phys. Rev. B - Condens. Matter Mater. Phys.*, vol. 67, no. 19, pp. 1–8, 2003.

[77] S. R. Shekhtman and M. S. Migranov, “Influence of ion bombardment of a substrate on the quality of vacuum-plasma Ti-TiN coatings,” *J. Phys. Conf. Ser.*, vol. 872, no. 1, pp. 4–8, 2017.

[78] K. Davut and S. Zaefferer, “The effect of size and shape of austenite grains on the mechanical properties of a low-alloyed TRIP steel,” *Steel Res. Int.*, vol. 83, no. 6, pp. 584–589, 2012.

[79] W. L. Dang, Y. Q. Fu, J. K. Luo, A. J. Flewitt, and W. I. Milne, “Deposition and characterization of sputtered ZnO films,” *Superlattices Microstruct.*, vol. 42, no. 1–6, pp. 89–93, 2007.

제주대학교 중앙도서관
JEJU NATIONAL UNIVERSITY LIBRARY

[80] “Google search engine.” .

[81] I. Kondo, T. Yoneyama, and A. Kinbara, “Interface structure and adhesion of sputtered Ti-Ni layers on silicon,” *Mater. Res. Soc. Symp. - Proc.*, vol. 308, pp. 665–670, 1993.

[82] T. Hashimoto, K. Okamoto, K. Hara, M. Kamiya, and H. Fujiwara, “Columnar structure and texture of iron films evaporated at oblique incidence,” *Thin Solid Films*, vol. 91, no. 2, pp. 145–154, 1982.

[83] Tomoyoshi Motohiro and Y. Taga, “Thin film retardation plate by oblique deposition,” *Appl. Opt.*, vol. 28, no. 13, p. 2466, 1989.

[84] K. D. H. and D. Vick, “Column angle variations in porous chevron thin films,” *J. Vac. Sci. Technol.*, vol. 20, 2002.

[85] E. Petkucheva, G. Borisov, E. Lefterova, J. Heiss, U. Schnakenberg, and E. Slavcheva, “Gold-supported magnetron sputtered Ir thin films as OER catalysts for cost-efficient water electrolysis,” *Int. J. Hydrogen Energy*, vol. 43, no. 35, pp. 16905–16912, 2018.

[86] D. G. C.M. Zhou, “Surface patterning by nanosphere lithography for layer growth with ordered pores,” *Thin Solid Films*, vol. 516, p. 433, 2007.

[87] T. Market and M. Electronics, “Deposition Technologies: An Overview,” *Handb. Depos. Technol. Film. Coatings*, pp. 1–31, 2010.

[88] D. Depla, S. Mahieu, and J. E. Greene, *Sputter Deposition Processes*, Third Edit. Elsevier Ltd., 2010.

제주대학교 중앙도서관
JEJU NATIONAL UNIVERSITY LIBRARY

[89] G. F. Iriarte, J. G. Rodriguez, and F. Calle, “Effect of substrate-target distance and sputtering pressure in the synthesis of AlN thin films,” *Microsyst. Technol.*, vol. 17, no. 3, pp. 381–386, 2011.

[90] Z. Sun, Y. Lv, and Z. Tong, “Effects of particle size on bidirectional reflectance factor measurements from particulate surfaces,” *Opt. Express*, vol. 24, no. 6, p. A612, 2016.

[91] D. Manova, J. W. Gerlach, and S. Mändl, “Thin film deposition using energetic ions,” *Materials (Basel).*, vol. 3, no. 8, pp. 4109–4141, 2010.

[92] A. Barranco, A. Borras, A. R. Gonzalez-Elipe, and A. Palmero, “Perspectives on oblique angle deposition of thin films: From fundamentals to devices,” *Prog. Mater. Sci.*, vol. 76, pp. 59–153, 2016.

제주대학교 중앙도서관
JEJU NATIONAL UNIVERSITY LIBRARY